ELSEVIER

Journal of Fluids and Structures 19 (2004) 389–447

JOURNAL OF FLUIDS AND STRUCTURES

www.elsevier.nl/locate/jnlabr/yjfls

A critical review of the intrinsic nature of vortex-induced vibrations

T. Sarpkaya*

Department of Mechanical and Astronautical Engineering, Naval Postgraduate School, 700 Dyer Road, ME/SL, Monterey, CA 93943-5146, USA

Received 3 September 2003; accepted 26 January 2004

Abstract

This is a comprehensive review of the progress made during the past two decades on vortex-induced vibration (VIV) of mostly circular cylindrical structures subjected to steady uniform flow. The critical elements of the evolution of the ideas, theoretical insights, experimental methods, and numerical models are traced systematically; the strengths and weaknesses of the current state of the understanding of the complex fluid/structure interaction are discussed in some detail. Finally, some suggestions are made for further research on VIV.
Published by Elsevier Ltd.

1. Preliminary remarks

The highly specialized subject of vortex-induced vibrations (VIVs) is part of a number of disciplines, incorporating fluid mechanics, structural mechanics, vibrations, computational fluid dynamics (CFD), acoustics, wavelet transforms, complex demodulation analysis, statistics, and smart materials. They occur in many engineering situations, such as bridges, stacks, transmission lines, aircraft control surfaces, offshore structures, thermowells, engines, heat exchangers, marine cables, towed cables, drilling and production risers in petroleum production, mooring cables, moored structures, tethered structures, buoyancy and spar hulls, pipelines, cable-laying, members of jacketed structures, and other hydrodynamic and hydroacoustic applications. The most recent interest in long cylindrical members in water ensues from the development of hydrocarbon resources in depths of 1000 m or more. In fact, the depths reached during the past 55 years increased as $h \approx (1/540)N^{3.5}$, where h is the depth and N is the number of years, starting with $N = 0$ in 1949.

It cannot be emphasized strongly enough that the current state of the laboratory art concerns the interaction of a rigid body (mostly and most importantly for a circular cylinder) whose degrees of freedom have been *reduced from six to often one* (i.e., transverse motion) with a three-dimensional separated flow, dominated by large-scale vortical structures. A few exceptions in which a second degree of freedom is allowed (in the in-line direction) will be discussed later. The restrictions imposed on the physical and numerical experiments are a measure of the complexity of the self-regulated motion. It is not yet clear as to how the additional degrees of freedom will change some of the observations, measurements, numerical simulations, and the contemplated applications in all ranges of Reynolds numbers (subcritical, critical, transcritical, and supercritical).

Numerous contributions to flow-induced oscillations in general and to VIVs in particular have collectively defined the objectives of the current VIV research and have guided the acquisition of design data through physical and numerical

*Tel.: +1-831-656-3425; fax: +1-831-656-2238.
E-mail address: sarp@nps.edu (T. Sarpkaya).

0889-9746/$ - see front matter Published by Elsevier Ltd.
doi:10.1016/j.jfluidstructs.2004.02.005

experiments, theoretical analyses, and physical insight. The ultimate objective is, of course, the understanding, prediction, and prevention of VIVs (preferably without drag penalty), partly through the direct numerical simulations (DNS with spectral methods) of fundamental as well as industrially significant fluid–structure interactions, by obtaining as many Navier–Stokes (N–S) data points as possible (in the desired range of the controlling parameters) and, partly, through the use of Reynolds-averaged Navier–Stokes equations (RANS), large eddy simulations (LES) (with improved sub-grid scale models), vortex element methods (VEM), and their various combinations. As most aptly noted by Fischer and Patera (1994): "Fluid dynamics is, of course, not simply the solution of the Navier–Stokes equations for a particular configuration. Most broader problem statements, applied or fundamental, involve a vector of physical and technology-related parameters, which must be averaged over, eliminated by optimization, or varied. In all these examples, the typically rather large parameter space precludes a purely numerical solution; analytical, heuristic, and experimental data, as well as intuition, must be brought to bear if the final goals are to be achieved." In other words, the numerical simulations are to be guided and inspired by ground-breaking measurements and flow visualization, mostly with nonintrusive techniques: digital particle image velocimetry (DPIV), laser-Doppler velocimetry (LDV), time resolved PIV, pressure-sensitive paints, and other means which will surely emerge in the years to come. These must be augmented with large-scale benchmark experiments to guide the numerical simulations at very large Reynolds numbers.

Much progress has been made during the past decade, both numerically and experimentally, toward the understanding of the kinematics (vice dynamics) of VIV, albeit in the *low-Reynolds number regime*. The fundamental reason for this is that VIV is not a small perturbation superimposed on a mean steady motion. It is an inherently nonlinear, self-governed or self-regulated, multi-degree-of-freedom phenomenon. It presents unsteady flow characteristics manifested by the existence of two unsteady shear layers and large-scale structures. There is much that is known and understood and much that remains in the empirical/descriptive realm of knowledge: What is the dominant response frequency, the range of normalized velocity, the variation of the phase angle (by which the force leads the displacement), and the response amplitude in the synchronization range as a function of the controlling and influencing parameters? Industrial applications highlight our inability to predict the dynamic response of fluid–structure interactions. They continue to require the input of the in-phase and out-of-phase components of the lift coefficients (or the transverse force), in-line drag coefficients, correlation lengths, damping coefficients, relative roughness, shear, waves, and currents, among other governing and influencing parameters, and thus also require the input of relatively large safety factors. Fundamental studies as well as large-scale experiments (*when these results are disseminated in the open literature*) will provide the necessary understanding for the quantification of the relationships between the response of a structure and the governing and influencing parameters.

The difficulties experienced in describing the nature, identifying the occurrence, and predicting the characteristics of vortex-induced oscillations of bluff bodies and galloping (to a lesser extent) have been reviewed by Parkinson (1974), Sarpkaya (1979), Griffin and Ramberg (1982), Bearman (1984), Parkinson (1989), Pantazopoulos (1994), Sarpkaya (1995), and in a number of books (Chen, 1987; Blevins, 1990; Naudascher and Rockwell, 1994; Sumer and Fredsøe, 1997; Au-Yang, 2001; Zdravkovich, 1997, 2003, just to name a few) and, less formally, in practically every doctoral thesis, as part of the obligatory 'previous studies' section.

This review is not a flat chronology of scientific/engineering developments in VIV and does not attempt to refer to every work that has ever been published, but one that seeks to provide physical insight. It makes no promises that are either excessively pessimistic or unreasonably reassuring. It encourages cross-stimulation between relatively idealized physical and numerical experiments and far more complex technological applications, often found in books and numerous conference proceedings [see, e.g., Ziada and Staubli (2000) and Molin (2002)].

A separate section is not devoted to the discussion of flow about *fixed* bluff bodies. Reference is made only to specific fixed-body observations, measurements, computations, and deductions, as needed. The flow about bluff bodies (*fixed* or *in motion*) require and/or give rise to circumstances (influencing parameters) mostly beyond the capacity of the experimenter to control. Some of these are the finiteness of the body or the aspect ratio (as in the case of aircraft wings and ensuing end conditions), mobile separation points on curved surfaces, three-dimensional behavior over two-dimensional bodies, unpredictable (or difficult to predict) spanwise correlation, nonquantifiable growth of the disturbances in the wake, in the shear layers, and in the boundary layers (before and after separation). Furthermore, one may need to consider the distribution of the ambient velocity and turbulence (intensity and integral length scales), blockage ratio, surface roughness, yaw, body deformation, temperature gradients, stratification, bottom and free-surface effects, and the impossibility (at the start of this century) to perform direct numerical simulations at Reynolds numbers larger than about 3000.

In spite of most of these complex circumstances, the Strouhal number [$\mathrm{St}=f_{st}D/U$, after Cének (Vincent) Strouhal (a Czech scientist), where f_{st} is the vortex shedding frequency (or the Strouhal frequency) *of a body at rest*, D is the diameter of the circular cylinder, and U is the velocity of the ambient flow] emerges as the most robust parameter. It is followed by the mean base pressure whose instantaneous values can be as high as -0.2 and as low as -3.5,

(Zdravkovich, 1997, p. 133). Even the crudest numerical simulations or experiments predict the Strouhal number with sufficient accuracy. However, as noted by many researchers over the years, this is as much an advantage as it is an obvious shortcoming because the robust parameters do not serve as unique identification cards for the integrated effects of the individually nonquantifiable parameters. In fact, one or two parameters into which we can lump our inability to account for all the *influencing* parameters do not seem to exist. This is partly because some of the influencing parameters can become governing when they exceed certain critical values. For example, ambient turbulence may change the transition in the wake, in the separated shear layers, in *the boundary layers in the vicinity of the separation zone* (leading to possible reattachment of the flow), and in the boundary layers upstream of the mobile separation points. Thus, ambient turbulence (possibly quantifiable in terms of its four integral length scales and eddy-dissipation rate) may significantly affect the flow around the VIV suppression devices, and hence, may affect their performance. Then the question naturally arises as to what are a handful of parameters that could possibly serve (albeit imperfectly) as unique identification cards for the intended purpose. The most obvious candidates are those that exhibit large scatter in every experiment (confining ourselves to steady flow about smooth circular cylinders).

Measurements during the past century identified the fluctuating lift in steady flow about a cylinder at rest as the most likely quantifier of the combined effect of the influencing parameters; e.g., see Norberg (2003) and references cited therein. Thus, having a representative time record of the lift force and its complex demodulation analysis, in addition to the spectra and the r.m.s. (root-mean-square) value of lift, would be most desirable. As noted above, it would be equally desirable to have a measure of the turbulence distribution, eddy-dissipation rate, and the integral length scales (x, y, z, and t) of the ambient flow. As to the flow around the cylinder, the extension of the current understanding of the Gerrard–Bloor transition waves and their disappearance in the range of Reynolds numbers from about $\mathrm{Re} \cong 2 \times 10^4$ to 5×10^4 (Bloor, 1964; Bloor and Gerrard, 1966; Gerrard, 1978; Zdravkovich, 1997; Norberg, 2003) to unsteady flows would be quite valuable.

Measurements similar to those noted above are equally desirable for a VIV body (see Section 3) undergoing forced or self-excited oscillations in steady uniform or sheared flows. It appears that for such flows the fluctuating lift and the phase angle (between the total force and the displacement) or the 'in-phase' and 'out-of-phase' components of the transverse force could serve as suitable identification cards for the integrated effects of some of the important parameters, e.g., to assess the effects of Reynolds number on the correlation length along the cylinder, on the wake modes, and on the state of transition-to-turbulence in the free-shear layers emanating from a cylinder undergoing VIV at a given A/D for a range of Re or at a given Re for a range of A/D. However desirable, the sensitivity of the transition waves to VIV has not yet been investigated. Apparently, direct measurements will be a formidable task. Evidence, albeit indirectly, must be gathered to identify, for example, wake and response phenomena which occur only at relatively small Reynolds numbers.

The character of the separation, more specifically the excursions of the separation point (the mean angle plus fluctuations), their dependence on surface conditions, the upstream turbulence, the motion of the cylinder, the frequency spectrum of the fluctuations of the separation angle require serious investigation, particularly for comparison with direct numerical simulations of VIV *using simulated ambient turbulent flow*. In summary, it is interesting to note that a phenomenon as robust as vortex shedding gives rise to forces as unpredictable as the lift force whose power can be fully appreciated only when one tries to eliminate VIV without excising the after body. In fact, it may be more advantageous to predict and thereby to avoid the VIVs than to attempt to eliminate them. After all, the fluctuating lift will always be there, with or without VIV, and the pure circular cylinder will always be the preferred shape.

2. Nomenclature

As all disciples of VIV know, the literature is rife with too many f's. It is not unusual to find papers in which as many as three different symbols are used to denote one specific frequency. The reading of many papers is made difficult partly because the subscripts do not help one to immediately recognize what they represent and partly because the same author uses a new set of f's in his follow-on paper. The major parameters should be equally applicable to both forced and self-excited oscillations in physical and numerical experiments. The use of parameters that are part of the problem (rather than part of the solution) further complicates the matter and does not allow one to make comparisons with numerical simulations. The advent of powerful computers has increasingly forced the formulation of the VIV problems in mathematical and CFD terms. With these thoughts in mind, we purposely choose two- or three-letter subscripts to enhance the instant recognition of the most important symbols:

f_{vac}: the frequency measured in vacuum, as the only natural frequency [$f_{\mathrm{vac}} = (1/2\pi)(k/m)^{1/2}$], where k denotes the linear spring constant and m the mass of the oscillating body. Its relation to the frequency measured in air and water will be discussed later.

f_{com}: the common frequency at which *synchronization* or lock-in occurs at a given velocity, i.e., $f_{ex} = f_{com}$.

f_{ex}: the frequency of oscillation of a (forced or self-excited) body, meaning *the excitation frequency*, regardless of whether there is lock-in or not. At lock-in $f_{ex} = f_{com} = [(1/2\pi)[k/(m + \Delta m)^{1/2}]$, where Δm is the added mass.

f_{st}: the vortex shedding frequency (or the Strouhal frequency) *of a body at rest*. It is uniquely related to the velocity of the flow and the characteristic size of the body through the Strouhal number $St = f_{st}D/U$, where U is the steady ambient velocity of the uniform flow.

f_{vs}: the vortex shedding frequency of *a body in motion* (forced or self-excited). In the lock-in range, f_{vs} becomes increasingly smaller than f_{st} until the lock-out.

A cylinder may be *forced* to oscillate at any frequency and amplitude within reason. Furthermore, one is at liberty to change the frequency and/or the amplitude content of the oscillations. Outside the synchronization region(s) the force experienced by the body will have both the Strouhal and body oscillation frequencies. In other words, it is understood that in the periodic- and quasi-periodic non-lock-in regions, the two frequencies (f_{st} and f_{ex}) will appear for awhile, and then, at a slightly higher frequency, the synchronization will occur, leaving only one frequency, i.e., $f_{com} = f_{ex}$. However, one must hasten to note that in self-excited oscillations one should not expect perfect synchronization because of the continuous interaction between the body and the fluctuations of added-mass, separation line, amplitude, correlation-length, and the phase angle. This is distinct from the *beating motion* of a cable undergoing amplitude-modulated oscillations by excitation at two or more frequencies wherein the vortex shedding frequency alternates between the imposed frequency and the Strouhal frequency.

The following are identified as the most important dimensionless parameters: f_{com}/f_{st}, f_{ex}/f_{st}, f_{ex}/f_{vac}, $V_r = U/f_{ex}D$, and $Re = UD/\nu$ where ν is the kinematic viscosity . Finally, f_{wtr} and f_{air} will be introduced for those in dire need of a frequency in still water or in still air. Additional parameters, controlling and influencing VIV, will be discussed later.

3. Introduction

An all-inclusive definition of a self-exciting or, better, self-regulating 'Bluff Body' does not exist. It can be described only in general terms by relying on the readers' imagination. It is an elastic or elastically mounted fore-and-aft body of proper mass, material damping, and shape whose cross-section facing the ambient flow at high-enough Reynolds numbers gives rise to separated flow and hence to two shear layers, which interact with each other and bound an unsteady wake. A body with no aft section (e.g., a D section with a flow from *right to left*) behaves like a bluff body but does not present an aft profile on which the alternating lift force can act. For the purposes of this review, a body capable of giving rise to VIV will be called a 'VIV-Body.'

Numerous experiments have shown that a VIV-body (e.g., a circular- or square-section cylinder) with material damping ζ, (determined in vacuum, especially for sharp-edged bodies) and proper reduced mass $m^* = (m/L)/(\rho_f \pi D^2/4)$, or $m^* = \rho_m/\rho_f$ with $\rho_m = (m/L)/(\pi D^2/4)$ as the 'mean mass density,' may be excited by the vortices it sheds if it is mounted on springs and exposed to a steady uniform flow. When the prevailing vortex shedding frequency f_{vs} (not always close to f_{st}) and the excitation frequency f_{ex} of the body approach a common frequency f_{com}, the body begins to experience relatively small vortex induced oscillations. These are controlled by the spring constant, body mass, structural damping, the density and the motion of the fluid surrounding the body, plus a number of difficult-to-quantify influencing parameters Sp, to be called Schewe (1983) parameters (see Section 5). This is followed by a substantial increase of the coherence length (Koopmann, 1967a; Ferguson and Parkinson, 1967; Toebes, 1969; Ramberg and Griffin, 1976 (for oscillating cylinders); Mansy et al., 1994 (for stationary cylinders); and Novak and Tanaka, 1975 (in smooth flow).

The vortex-excited oscillations increase the vortex strength (Davies, 1976; Atsavapranee et al., 1998) when the amplitude in the transverse direction exceeds a threshold value of about $0.1D$, (it is about $0.02D$ for the in-line oscillations, see e.g., Mandini, 1961; Sainsbury and King, 1971; Dickens, 1979; Okajima et al., 2002; Sugimoto et al., 2002, and the references cited therein). The ratio of the circulation of the nascent vortex to that of the shed vortex is about $\Gamma/\Gamma_0 = 0.51 \pm 0.08$ for the stationary cylinder (Atsavapranee et al., 1998) in agreement with those reported in the literature (Berger and Wille, 1972). For the cylinder oscillating in the lock-in range ($V_r = U/f_{ex}D \approx 4$ to 8), the ratio of the vortex strength to the total supply of circulation in one shedding period Γ/Γ_0 is found to be 0.66 ± 0.09. This conforms Sarpkaya's (1963) findings in accelerating flow about cylinders.

If the velocity U and hence the amplitude are increased (gradually) to new values, the diameter 'seen' by the flow (or the spacing between the shear layers defining the virtual body) increases initially, *at least for small amplitudes* [see, e.g., Di Silvio (1969)]. The apparent 'increase' in D is compensated by the real increase in velocity U, thus keeping the vortex shedding frequency nearly constant. This represents a departure from the vortex shedding frequency of the fixed

cylinder at the new (increased) ambient flow velocity. In other words, the self-excitation begins with a *real decrease in the frequency of vortex shedding* to a value close to f_{com}, which may be close to but not equal to that obtained from pluck tests in still water. The vortex-shedding mode and frequency change most to match f_{com}. Apparently, the body motion is dominant (but not invariant) in the sense that it accommodates somewhat the changes in vortex shedding by letting the flow change its virtual mass and hence its frequency and acceleration as both the flow and the body arrive at a common frequency to which the body responds with exuberance: the matching of the frequency of the prevailing dynamics of the vortical wake with the frequency of the body oscillation.

Figs. 1 and 2 show two interesting examples. The first [Fig. 1, after Feng (1968)] was conducted in air with a single-degree-of freedom flexible cylinder with a relatively large mass ($m^* = \rho_m/\rho_{air} = 248$, $\zeta = 0.00103$, $m^*\zeta = 0.255$) and relatively large Re, *varying with* $V_r = U/f_{air}D$, from 10^4 to 5×10^4. The second, Fig. 2, compares Feng's data with those obtained by Khalak and Williamson (1999, hereafter referred to as K–W) in water with a single-degree-of freedom flexible cylinder with a relatively small mass ($m^* = \rho_m/\rho_{wtr} = 10.1$, $\zeta = 0.0013$ and $m^*\zeta = 0.013$) and smaller Re. In both self-excited cases, the Reynolds number increases along the V_r axis because f_{air}, f_{wtr}, and D are kept constant and only U or Re is allowed to vary as prescribed. This is unlike the forced oscillation experiments in which Re *is kept constant* and the frequency of excitation is varied. K–W (1999) stated that "our studies here and in Govardhan and Williamson (2000), for Re = 3500–10 000, indicate that it is principally the parameter ($m^*\zeta$), which influences whether the Upper branch (see Fig. 2) will appear or not." The existing facts do not support their assumption. For *steady flow about a stationary* cylinder, Basu (1986) noted that "the Re number range 1350–8000 overlaps the Re number range in which the principal feature of the flow field is the upstream movement of transition in the free shear layer with increasing Re number." The 'eddy formation length,' L_f, shrinks from $L_f \approx 1.9D$ at $\mathrm{Re} = 5 \times 10^3$ to $L_f \approx 1.1D$ at $\mathrm{Re} = 14 \times 10^3$, and the distance to the center of the transition region (transition from a laminar to a turbulent free shear layer) decreases from about $L_t \approx D$ to $L_t \approx 0.4D$ (Zdravkovich, 1997). These change the character of the free shear layers and hence that of the vortices emanating from them. In fact, Zdravkovich (1990) was the first to suggest that the occurrence of a jump to an Upper branch in the Meier-Windhorst experiments (1939) might be a Reynolds number effect. Clearly, the physics of the shear layers, in general, and that of the unsteady shear layers, in particular, is very complex. For this reason the sensitivity of the transition waves due to VIV (even for a single degree of freedom) has not yet been directly investigated. However, the experiments of Carberry (2002) and Carberry et al. (2002) with oscillating cylinders (with Reynolds numbers in the same range as that of K–W) provide direct evidence to show that the phase angle φ and, in particular, the lift coefficient C_L, significantly increase (as much as 100%) with increasing Reynolds number (Re = 2300, 4400, and 9100) for a given A/D, and with A/D for a given Reynolds number (up to A/D values of about 0.5).

Feng's data (A/D and phase φ versus $U/f_{air}D$), at higher Reynolds numbers (10^4 to 5×10^4), have only two branches (Initial and Lower). The K–W (1999) data (A/D versus $U/f_{wtr}D$), at lower Reynolds numbers (3500–10 000) have three branches (Initial, Upper, and Lower), a much larger peak amplitude, and a broader synchronization range. It must be emphasized that the horizontal axis in both figures denotes $U/f_{air}D$ and $U/f_{wtr}D$, as well as the increasing Reynolds number, $\mathrm{Re} = UD/\nu$. In all such free VIV experiments the frequency f_{air} (or f_{wtr}) and D are kept constant (along with m^* and ζ) and the variation of A/D with U or with the Reynolds number is plotted from a minimum to a maximum Re. Evidently, Re may be kept constant by maintaining U, D, L/D, k, ζ, ρ_f and ν constant and varying only m in $\rho_m = 4m/(\pi LD^2)$ and hence f_{vac} in $V_r = U/f_{vac}D$ or in f_{ex}/f_{vac}. Such experiments, which constitute the essence of our on-going VIV research, will define a three-dimensional space showing A/D versus f_{ex}/f_{vac} in each plane of constant Re. This will enhance the understanding of the various regimes and their dependence on Reynolds number, shear layer instability, mass ratio or ρ_m/ρ_{wtr}, material damping, aspect ratio, modes of vibration, modes of vortex shedding, abrupt as well as gradual changes in the phase, and the degrees of freedom, along with several other parameters, to be discussed later.

As noted by Huerre (2002), "vortex shedding is represented by a *global mode*, i.e., a self-sustained time-periodic state characterized by a specific spatial structure and a frequency, which is the same throughout the flow domain." The freedom provided to a body through elastic mounting is capable of modifying the character of the global mode, i.e., modifying both the frequency and the spatial structure of the *near wake*. In any case, the body vibrates neither at f_{wtr} (for VIVs in water), nor at f_{air} (for VIVs in air), nor at f_{st} of the fixed body. Surprisingly, synchronization (sometimes referred to as the lock-in, lock-on, vortex capture, or frequency capture) occurs not only near f_{st}, but also over a wide range of flow velocities. It appears that 'lock-in' or 'lock-on,' 'vortex capture', or 'frequency capture' are misnomers. In fact, one needs to redefine VIV to make a distinction between the two distinct roles, *excitation and driving*, played by vortices.

Excitation means that the vortices can and do excite the body, even when the out-of-phase component of their lift force is relatively small (in comparison to mechanical restoring force), provided that their shedding frequency f_{vs} is close to the prevailing frequency of the body. This is like a single-degree-of-freedom system with small (but nonzero) viscous

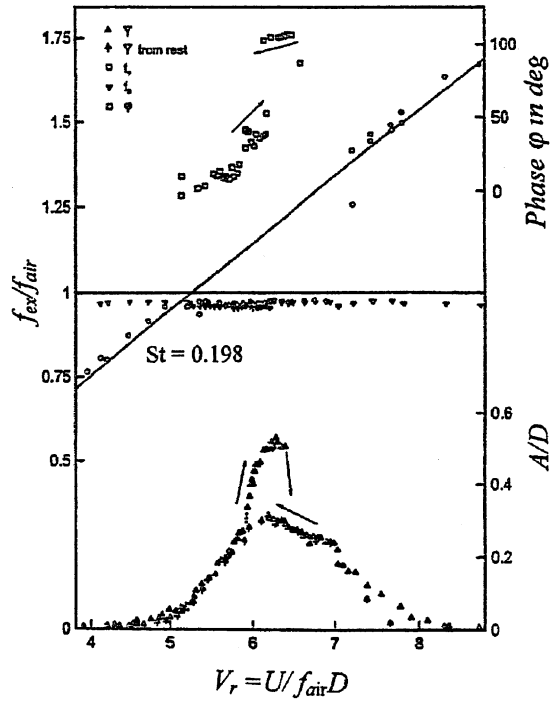

Fig. 1. Response and wake characteristics of a spring-mounted cylinder freely oscillating in air: $m^* = 248$, $\zeta = 0.00103$, $m^*\zeta = 0.255$), and Re (varying with $V_r = U/f_{\text{air}}D$) from 10^4 to 5×10^4 (Feng, 1968).

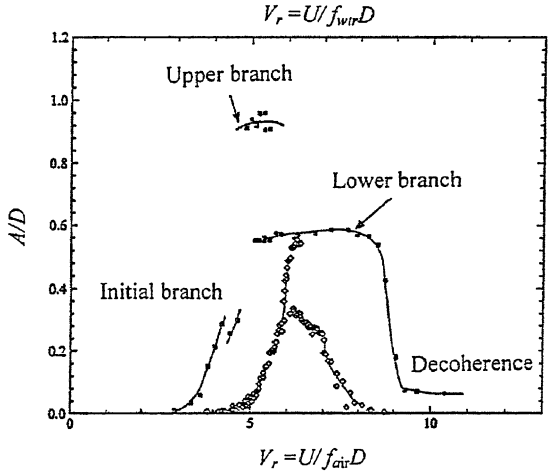

Fig. 2. A comparison of Feng's amplitude data (maximum A/D versus f_{ex}/f_{air}, the lower axis), with those obtained by Khalak and Williamson (1999) in water (the upper axis) with a single-degree-of-freedom flexible cylinder ($m^* = 10.1$, $\zeta = 0.0013$, $m^*\zeta = 0.013$, and Re varying from 3×10^3–10^4). Feng's data at higher Re has only two branches (Initial and Lower, as in Fig. 1). The Khalak and Williamson data (A/D versus $U/f_{\text{wtr}}D$) have three branches (Initial, Upper, and Lower), a larger peak amplitude, and a broader synchronization range.

damping. Thus, even weak vortices in some regions of f_{ex}/f_{st} can excite a body to large amplitudes when the body and the vortices arrive at a common frequency f_{com}, (in the region of f_{ex}/f_{st} from about 0.5 to 0.9).

The driving ability of the vortices ensues from their particular modal dynamics to give rise to a sufficiently large out-of-phase lift component in certain regions of f_{ex}/f_{st} (from about 0.9 to 1.0). Thus, the excitation function of the vortices

is a mandatory requirement for the inception and maintenance of VIV. However, the effectiveness of their driving function depends on a number of parameters (the range of f_{ex}/f_{st}, Reynolds number, damping, virtual mass of the oscillating system, and some influencing parameters).

It is clear from the foregoing that, to sustain a self-excited, self-limiting resonant response, the motion of a freely vibrating VIV–body interferes at proper amplitudes and frequencies with the mutual interaction of the shear layers and becomes a dominant part of the overall instability mechanism: shear-layer interaction leading to vortex shedding, leading to alternating transverse and modulated in-line forces, leading to body motion, leading toward the common frequencies of the excitation and response in respective directions. Thus, the interaction of the body and the flow under proper conditions serves as the magnifier, organizer, and synchronizer of the phenomenon. It is not ever likely to happen at a *constant* amplitude and *frequency* for the freely oscillating bodies, because of the significant amplitude/frequency/added-mass modulations. In the words of one of the pioneers (Koopmann, 1967a) "when the wind velocity approaches the boundaries of the resonant region, the shedding frequencies are close enough to the natural frequency of the system to cause the system to respond in short bursts of periodic motion in the plane to the direction of the wind. If the motion during one of these bursts is large enough to correlate the vortex wake along the span, the cylinder jumps to a higher displacement amplitude than before and a steady-state oscillation follows. Once inside this instability boundary, the cylinder motion controls the wake frequency, and the resulting oscillation takes place at the natural frequency of the system." In addition, "as the wind velocity is slowly increased in the resonant region, the displacement amplitude of the cylinder steadily increases until at some definite velocity, a peak displacement amplitude is reached."

Cheng and Moretti (1991) conducted a series of experiments with a circular cylinder subjected to forced transverse vibration in a uniform cross-flow at Reynolds numbers of 1500 and 1650. They have measured the prevailing *vortex shedding frequency* f_{vs} with hot-film probes, placed $4D$ downstream and $2.5D$ across from the center of the cylinder. They have varied f_{ex}/f_{st} (driving frequency/Strouhal frequency for a stationary cylinder) from zero to 4.5 and the amplitude A/D from zero to 0.75. The driving frequency was monotonically increased to avoid hysteresis effects. Fig. 3 (for $A/D = 0.05$, $\mathrm{Re} = 1500$ and for $A/D = 0.235$, $\mathrm{Re} = 1500$) shows representative data identifying the relevant subharmonic, nonharmonic, and superharmonic wake frequencies. When f_{vs} is near f_{st}, on a horizontal line given by $f_{vs}/f_{st} = 1$, f_{vs} is unaffected by the excitation. However, when f_{vs} falls on a line from the origin with a slope of unity, the vortex structure in the wake locks onto the excitation frequency ($f_{ex}/f_{st} \approx 0.5$ to 1.6). A further observation is made that f_{vs} tends to decline with increasing excitation, possibly due to the widening of the wake. A more recent set of data (Fig. 4) by Krishnamoorthy et al. (2001) shows the wake frequencies as a function of the oscillation frequency, vortex shedding frequency, and remaining wake frequencies for $A/D = 0.22$ and $\mathrm{Re} = 1500$. Cheng and Moretti (1991) found that the lock-in range exhibits an onion-shaped region as shown in Fig. 5(a). At small amplitudes, this dependence is essentially the same as that found by Koopmann (1967b) and Bublitz (1972). The center frequency of the lock-in is slanted toward lower frequencies, and the Reynolds number has a strong effect on the upper frequency lock-in boundary.

Vickery and Watkins (1962), Hartlen et al. (1968), Blevins and Burton (1976), and Pantazopoulos (1994) have provided extensive data for A/D versus the lift coefficient C_L for a variety of conditions. Fig. 5(b) shows that C_L increases with A/D up to $A/D \approx 0.5$ and then decreases rapidly with increasing A/D.

For long, rigid or flexible structures (e.g., a cable), the phenomenon is further complicated by the fact that the structure tends to respond at a variety of frequencies over its entire length. This, in turn, gives rise to additional and omni-directional fluid forces whose prediction is at best approximate [see, e.g., Vikestad (1992), Vandiver and Li (1994), Larsen and Halse (1995), Triantafyllou and Grosenbaugh (1995), Halse (1997), and the references cited therein]. When there is no synchronization (lock-in), the driving fluid force and the structure oscillate at their own frequencies. In field tests, a locked-in condition or a standing wave profile may not occur on long wires towed in the ocean (Alexander, 1981). There is no total spanwise correlation along very long structures placed in the ocean environment partly because cooperating instabilities prevent such coherence, even in well-controlled laboratory experiments, and partly because larger amplitude disturbances and omni-directional waves and currents surely prevent anything other than short coherence lengths [an extensive table is given by Pantazopoulos (1994)]. Only the relatively short test cylinders or cables result in well-separated modal frequencies, reducing the effects of modal interaction and enabling single-mode lock-in to be studied in some detail (Iwan and Jones, 1987). A fitting summary of the foregoing is given by Kim et al. (1986): "Multimoded non-lock-in response did occur when the mean shedding frequency fell between natural frequencies. At these times, three or four modes were present in the cross-flow response. The in-line response would at the same time have several modes. Under lock-in conditions, the excitation bandwidth is very narrow. Under non-lock-in conditions, even with very uniform flow, the excitation bandwidth broadens substantially. Under such circumstances, the lift force is best characterized as a narrow band random process with sufficient bandwidth to excite two or more adjacent modes. Lock-in occurs if and only if the separation of the natural frequencies of the cylinder are large compared to the

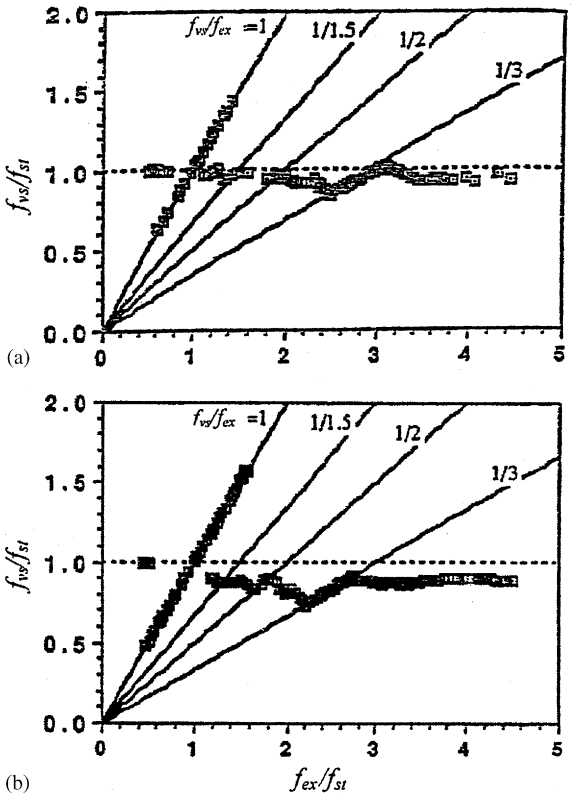

Fig. 3. Variation of the shedding frequency with driving frequency of a single cylinder in uniform flow: (a) $A/D = 0.05$, Re = 1500; and (b) $A/D = 0.235$, Re = 1500 (Cheng and Moretti, 1991).

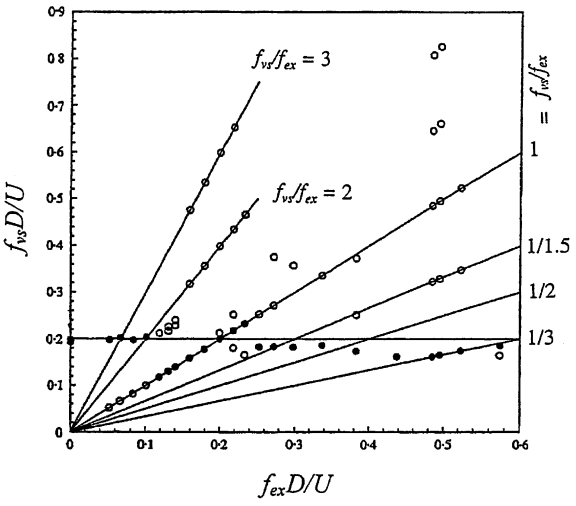

Fig. 4. The normalized wake frequencies as a function of the normalized oscillation frequency, vortex shedding frequency, and remaining wake frequencies for $A/D = 0.22$ and Re = 1500 (Krishnamoorthy et al., 2001).

bandwidth of vortex-induced forces.'' Clearly, the vortex shedding, the character and timing of the vortices and the amplification of the driving force are inextricably related. Also, self-excitation without lock-in is common but self-regulated lock-in without self-excitation is impossible.

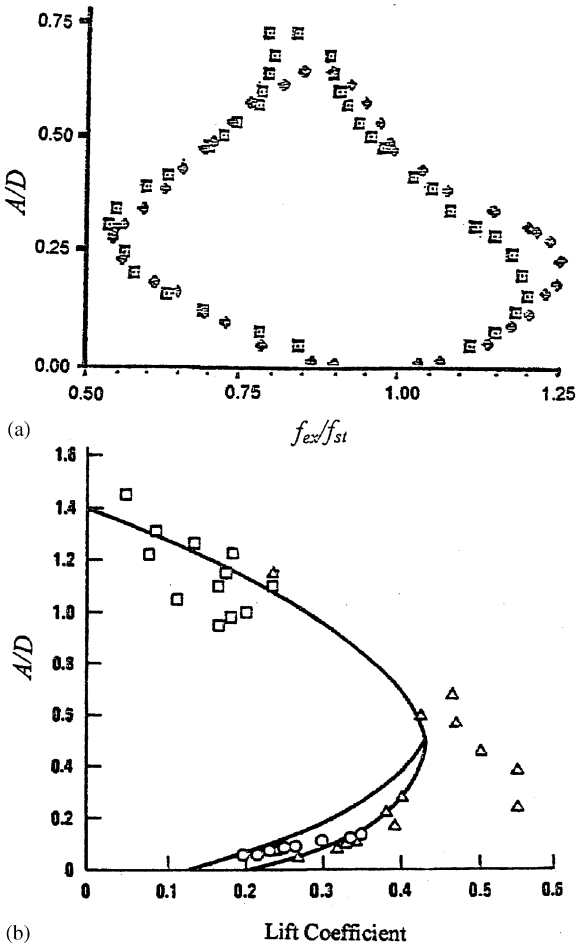

Fig. 5. (a) The lock-in range exhibits an onion-shaped region ($A/D = 0.22$, Re = 1500). The center frequency of the lock-in is slanted towards lower frequencies (Cheng and Moretti, 1991). (b) Lift coefficient for a pivoted rod at resonance: □, $L/D = 48$, and △, $L/D = 15$, Vickery and Watkins (1962); ○, $L/D = 13.8$, Hartlen et al. (1968). Curve-fit by Blevins and Burton (1976). More extensive C_L data for spring-supported cylinders and cantilevers are tabulated by Pantazopoulos (1994).

If a cylinder is free to oscillate in both the transverse and in-line directions, the common frequencies of the body and the driving forces in their respective directions may lead to lock-in and the axis of the body traces the path of figure *eight* (Moe and Wu, 1990; Moe et al., 1994; Sarpkaya, 1995). The figure-eight loop is caused by the considerable variation of drag force during large amplitude oscillation. Dye (1978) tested a cantilevered cylinder in water and made the following observations: "During the swing of a cylinder from a dead-end, the wake is tilted and the projected drag in the velocity direction is reduced. Once the dead-end is reached, the wake realigns with the velocity and the drag force is increased. The cylinder is pushed back along the maximum amplitude line before the wake becomes tilted again." Zdravkovich (1990) noted that "the two-degree-of-freedom response is the interaction of the streamwise synchronization at $V_r = U/f_{ex}D \approx 2.5$ with the transverse synchronization at $V_r \approx 5$". It is a well-known fact that [see, e.g., Sarpkaya (1979)] for $1.7 < V_r < 2.3$ (the so-called first instability region) oscillations occur in the in-line direction and the vortices are shed symmetrically. In the interval $2.8 < V_r < 3.2$, (the second instability region), the vortices are shed alternately. Chen and Jendrzejczyk (1979), working with a cantilevered tube in water, varied the reduced velocity from 1.92 to 4.92. They found a 'beating' mode, typical of the pre-synchronization at $V_r = 4.53$, as shown in Fig. 6. A single-degree-of-freedom system is inhibited from exhibiting these intricate variations.

The mobility of the separation points is important but not necessary for synchronization (e.g., for a square or rectangular cylinder). The separation points on a smooth *stationary* circular cylinder trace an arc whose magnitude depends on Re and the frequency and amplitude of the flow oscillation (Sarpkaya and Butterworth, 1992; Sarpkaya,

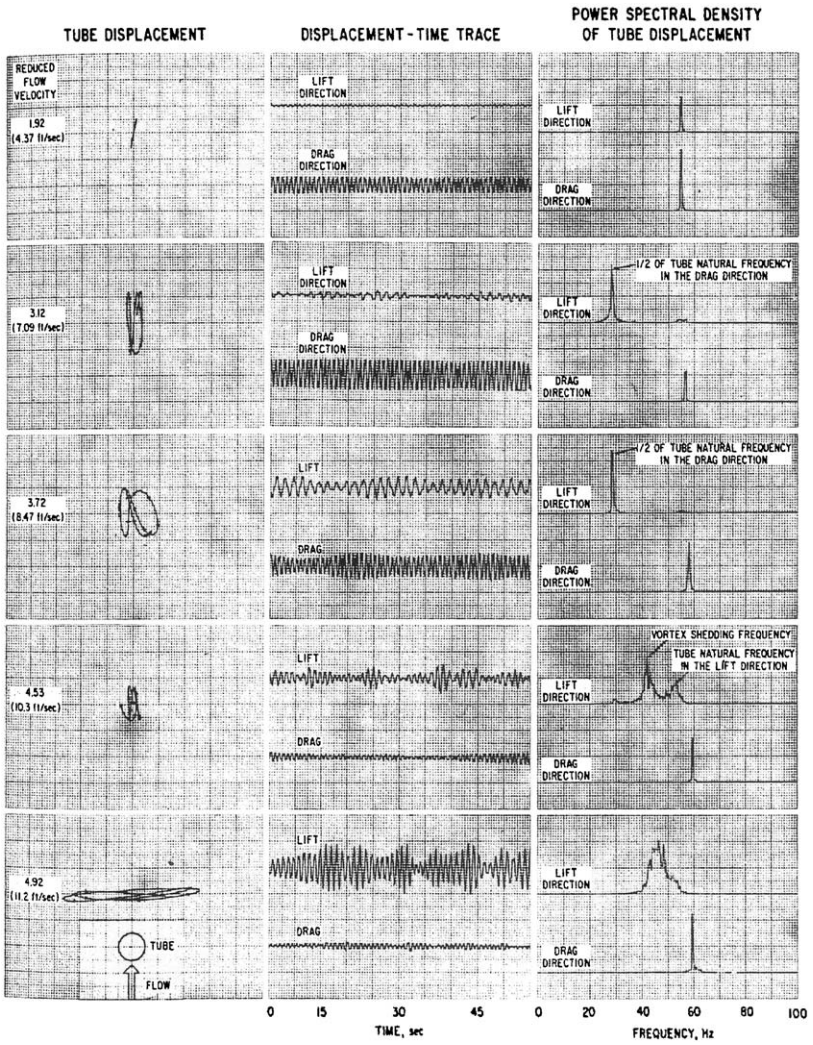

Fig. 6. A cantilevered tube in water with reduced velocities from 1.92 (top) to 4.92 (at the bottom). The left, middle, and right columns show, respectively, the tube displacement, the displacement-time trace, and the power spectral density of the tube displacement. The 'beating' mode is typical of the pre-synchronization at $V_r = 4.53$ (second frames from the bottom). A single-degree-of freedom system is inhibited from exhibiting these intricate variations (Chen and Jendrzejczyk, 1979).

2002). It is understood that the characteristics of turbulence of the approaching flow at each cycle depends on the energy stored in the fluid and is not independently controllable. In general, the point of separation on a cylinder depends not only on the pressure gradient but also on the type of unsteadiness of the ambient flow (e.g., sinusoidal), turbulence upstream of the separation points, roughness of the surface or other excrescences, symmetry or the asymmetry of the cylinder, taper along the rod, presence of salient edges, and the mode of vortex (or vorticity) shedding. For a cylinder undergoing VIV, the actual instantaneous value of the wake angle is greater than that between the ambient flow velocity and the relative fluid velocity (Mei and Currie, 1969; Raudkivi and Small, 1974) and the oscillation of a cylinder enhances both the strength of the vortices and the excursions of the separation points. Detailed discussions of the oscillation of bodies with salient edges may be found, for example, in Öngören and Rockwell (1988a, b), Lotfy and Rockwell (1993), Deniz and Staubli (1997, 1998), and in the numerous references cited therein.

The lock-in also occurs at excitations that are superharmonics of the shedding frequency (see Figs. 3 and 4). Furthermore, the lock-in regions for the odd-number superharmonics appear to differ from those for the even-number superharmonics (Olinger and Sreenivasan, 1988; Cheng and Moretti, 1991; Rodriguez and Pruvost, 2000). This is undoubtedly related to the nature of the shedding of the vortices.

In the following, we shall discuss a number of fundamental topics which are inextricably related to VIV and which are of major importance to understanding the intricate relationships between the governing parameters and the observed or predicted dynamics of the oscillating system.

4. Added mass and virtual mass

Added mass is one of the best known, least understood, and most confused characteristics of fluid dynamics. It exists in all flows about bluff bodies. However, it *manifests its existence*, like all masses, only when it is accelerated. It depends on the type of motion of the body or the fluid about the body and its wake, proximity of other bodies, free surface, and time. It can be positive, it can be negative, depending on the relative direction of the *drift*. Its inviscid-flow values (tabulated in books and special reports) often give the impression that they are applicable to all unsteady *viscous* flows at all Reynolds numbers (Leonard and Roshko, 2001). Such an impression is so prevalent that one often encounters general force expressions or force decompositions for viscous flows using a velocity-square-dependent drag force plus an *ideal inertial force* (or frequency expressions using the mass of the body plus the ideal added mass [with C_a = (added mass/displaced mass) = 1 for a cylinder] (Maull and Milliner, 1979; Lighthill, 1986; Leonard and Roshko, 2001). This is in spite of the fact that Stokes (1851) showed over 150 years ago that viscosity does affect the added mass (even in simpler flows) and that if the ideal inertial force is subtracted from the total force it still leaves some inertial force in the so-called 'vortex force.' In other words, *in unsteady flows, neither is the drag equal to its steady state value nor is the added mass equal to its inviscid flow value*; both are affected by viscosity and acceleration (Stokes, 1851; Basset, 1888; Sarpkaya, 2001).

The effect of the smooth evolution of the unsteady viscous flow is expressed by Basset (1888) with a 'history term,' which yields exactly the same result as the viscosity-dependent terms in Stokes' solution, but draws attention to the fact that unsteady flow is not a juxtaposition of instantaneous steady states. Only if the body is started from rest in a fluid otherwise at rest, the initial value of the added mass is in agreement with its ideal value because the vorticity is still confined to a thin sheet on the boundary. Sometimes this very special case is used to 'prove' that the added mass coefficient C_a for a circular cylinder is 'always' equal to unity (Leonard and Roshko, 2001). There is, of course, nothing wrong with the proof, as long as it is not generalized to viscous flows for times greater than an infinitesimally small Δt. Even though Stokes' solution is valid only for unseparated laminar flows at small Reynolds numbers and amplitudes, the fundamental concepts gleaned from it are universally applicable to all unsteady flows about bluff bodies and to all 21 independent components of the added mass coefficient.

The added mass has several applications besides those of the problem of acceleration from rest. As examples of such applications, the following may be cited: correcting the measured drag coefficient in wind tunnels with diverging walls (due to convective or both convective and local acceleration), estimating the aerodynamic forces in cases of buffeting and flutter, calculating the periods of heaving, pitching, and rolling motions of a ship, and, in general, in calculating forces and accelerations wherever the kinetic energy imparted to the fluid by the body is not negligible relative to the kinetic energy of the body itself.

The added mass may be quantified in other ways besides the use of kinetic energy. Riecke (1888) surmised and, subsequently, Sir Charles Darwin (1953) made his celebrated discovery that the added mass for a body translating uniformly in an infinite expanse of perfect fluid equals the drift-volume times the density of the fluid. The drift mass (similar to the drift mass in Stokes waves) is displaced permanently in the direction of motion of the body. Darwin and, subsequently, Benjamin (1986) showed that the individual fluid particles, which are pushed aside by the body in its forward motion, do not return to their former positions. The paths of the individual particles are not closed curves but open-ended elasticas. Hence, besides pushing the particles aside temporarily in passing, the cylinder also displaces the fluid particles permanently in the direction of its motion. This permanently displaced fluid mass, enclosed between the initial and final positions of the fluid particles, is in fact the added mass itself for the inviscid flow. The calculation of the drift mass for a separated viscous flow is exceedingly difficult. It can be achieved only for special unsteady flows (as in the case of Stokes' solution) or experimentally, as will be seen later. Interestingly, the drift mass is associated with the name of the grandson of the creator of the theory of evolution.

It follows from the foregoing that the added mass is not a concentrated mass attached to the centroid of the body. It is distributed throughout the fluid set in motion by the body. Thus, its magnitude and centroid change with time as the intensity and distribution of the kinetic energy of the fluid change with time. For the numerical experiments, one does not need to know the added mass since the pressure and the viscous contributions are explicitly incorporated into the solutions of the N–S equations. However, one does not have a larger range of Reynolds numbers from which to choose. Furthermore, VIV is not a small perturbation superimposed on a mean steady motion. It

presents strong unsteady flow characteristics manifested by the existence of large-scale structures for which the use of standard turbulence models in RANS, LES, and DVM simulations is highly questionable; (see Section 13 for further discussion).

The cycle-averaged added mass coefficient C_a ($= \Delta m/\rho_f V_b$), where ρ_f is the density of fluid and V_b is a suitable reference volume, can be negative, with far-reaching consequences for freely vibrating cylinders with low mass ratio m^* ($= \rho_m/\rho_f$), because

$$C_a/m^* = (\Delta m/m) = C_a\rho_f/\rho_s \tag{1a}$$

may approach –1 and the *normalized virtual mass*

$$(m + \Delta m)/m = (1 + C_a/m^*) \tag{1b}$$

may approach zero, resulting in an oscillating cylinder with no apparent or virtual mass. It has been noted, e.g., by Feng (1968), Bishop and Hassan (1964), and Sarpkaya (1979), among others, that *the transverse force needed to excite a cylinder to large amplitude oscillations is far greater than that exerted by vortex shedding*. It was not clear in the 1970s that the virtual mass of the body may decrease to very small values. The high-mass ratio cylinders are obviously less affected by the added mass and its variations. In fact, the significance of several parameters stands out only at lower mass ratios. These issues will be discussed in more detail later.

It follows from the foregoing that in separated time-dependent flows (such as VIV), the common frequency (between the body and the vortices) at lock-in cannot remain constant throughout the synchronization range because the added mass is a function of time, the shape of the body and its surroundings, and the type of motion and orientation of the body through the fluid. For example, the added mass of a cylinder tracing the path of figure *eight* is not the same as that of a cylinder constrained to move only in the transverse direction.

The negative added mass has been previously discussed a number of times [see, e.g., Keulegan and Carpenter (1958), Sarpkaya (1963, 1976a, b, 1977a, 1986a, b), Vandiver (1993), Vikestad et al. (2000)] and will be discussed again in Section 9. The negative added mass occurs mostly in the approximate range of $0.5 < f_{ex}/f_{st} < 0.85$ where $f_{\rm com}/f_{\rm vac} > 1$, the phase angle and amplitudes are relatively large, and two pairs of vortices are shed per cycle (to be discussed later). A similar occurrence of negative added mass in transverse vortex shedding, from a cylinder undergoing sinusoidal oscillations in a fluid otherwise at rest, has been evaluated and discussed in great detail by Sarpkaya (1977a).

Subsequently, it will become clear that the fluctuations of the added mass hold the key to understanding the similarities and differences between the forced and self-excited vibrations. The fluctuations of the amplitude of self-excited oscillations (about $\pm 10\%$) impose higher-order harmonics on the cyclic variation of the added mass. This, in turn, leads to fluctuations in frequency. Their combined effect leads to further changes in amplitude, added mass, frequency, coherence length, phase angle and so on. Clearly, if one can eliminate the modulations superimposed on the cyclic variation of the added mass in self-excited vibrations, one will maintain its amplitude and frequency constant and thus make the motion behave more like a forced vibration. When no two cycles are alike, one should expect a large variety of wake states as the motion transitions from a *high lift-phase state* to a *low lift-phase state* (sometimes called 'low-frequency' and 'high-frequency' states, even through the frequency changes only slightly between the two states). What is of course remarkable in VIV is that a small change in frequency (say, f_{ex}/f_{st} or $f_{\rm com}/f_{st}$) may cause rather large changes in phase, in wake structure, and thus, in all the attendant consequences of VIV in or out of lock-in.

5. Governing and influencing parameters

5.1. Parameter space

A simple dimensional analysis shows that the parameters 'controlling' the transverse vortex-induced oscillations of a cylinder are the density of fluid ρ_f, dynamic viscosity μ_f, velocity of the ambient flow U, diameter of the cylinder D, length of the cylinder L, spring constant k, mean roughness height of the cylinder k_s, *structural* damping factor ζ, mass of the body m (with no added mass), mean shear $\mathrm{d}U/\mathrm{d}y$, taper $\mathrm{d}D/\mathrm{d}y$, characteristic turbulence intensity ε_t and the integral length scales $I_{\rm ils}$ of the ambient flow, and Schewe parameters Sp. Then the normalized amplitude may be

written as

$$\frac{A}{D} = F\left\{\begin{array}{l}\zeta, \dfrac{\rho_f UD}{\mu_f}, \dfrac{L}{D}, \dfrac{4m}{\rho_f \pi L D^2}, \dfrac{D}{U}\left(\dfrac{k}{m}\right)^{1/2}, \mathrm{Re}_{sl}, \\ \mathrm{Re}_{cr}, \dfrac{D}{U_o^2}\dfrac{\mathrm{d}U}{\mathrm{d}t}, \dfrac{D}{U}\dfrac{\mathrm{d}U}{\mathrm{d}y}, \dfrac{\mathrm{d}D}{\mathrm{d}y}, \varepsilon_t, \dfrac{k_s}{D}, \dfrac{I_{\mathrm{ils}}}{\mathrm{D}}, \mathrm{Sp},\end{array}\right. \tag{2}$$

where Re_{sl} is the Reynolds number beyond which the transition eddies in the free shear layers disappear ($\mathrm{Re}_{sl} \cong 2 \times 10^4$ for steady flow), and Re_{cr} is the critical Reynolds number beyond which the Strouhal number of the *vibrating* cylinder exhibits a *smooth transition* to a higher value (about 0.24), unlike its steady-flow counterpart. The material damping ζ is composed of grain friction, dislocation friction (rather small), and the presence of vacancies (microscopic voids). When a material is deformed, say by a VIV event, the structure moves against itself, causing the above phenomena (one or more depending on the structure of the material) to consume some of the energy of the motion. Thus, this gives rise to damping. Clearly, there are no materials or structures without some damping and 'the undamped natural frequency' does not exist.

The shear parameter $(D/U)(\mathrm{d}U/\mathrm{d}y)$ has been suggested by Vandiver (1993) after consideration of several other possibilities. Humphries and Walker (1988) defined the shear parameter in terms of a characteristic velocity U_r (often as the mid-span velocity) as $(D/U_r)(\mathrm{d}U/\mathrm{d}y)$. It is not unique and does not define all the dynamics of shear, as noted by Vandiver. However, the use of a larger number of shear parameters is not practicable. The current objective is to use as few parameters as possible, experimental data obtained from rigid cylinders, and strip theory in conjunction with approximate correlation-length models, as suggested by Triantafyllou et al. (2003). Clearly, when the shear parameter is small (say, less than 0.01), one would expect longer correlation lengths and cells. Additional parameters such as the number of excited modes, wave characteristics, cable properties, axial-end conditions (i.e., free or constrained to move in the axial direction as the test pipe flexes) may have to be considered but are not included in Eq. (2). This is primarily because of the fact that there are no programmable means to quantify some of them (or their interaction with other parameters) at any Reynolds number. The most important facts about shear are the following:

(a) there should be no fear as far as safety is concerned (assuming no complications due to proximity effects to free-surface, bottom- and/or other pipe lines, stratification, and the strong nonlinearity of the shear);
(b) it reduces and broadens the peak amplitude at all Reynolds numbers (from subcritical to supercritical); and
(c) at high shear parameters (e.g., 0.03), the vortex excitation range usually extends over a larger reduced-velocity range, but at reduced peak amplitudes (Humphries and Walker, 1988). These will be discussed in Section 12 in connection with VIV at high Reynolds numbers.

The ratio of the longitudinal integral length scale to the diameter, I_{ils}/D gives a good insight into the effect of turbulence. As shown by Basu (1985), the larger the I_{ils}/D, the smaller is the interaction between the free-stream turbulence and the cylinder boundary layer and wake. The intensity of turbulence of the ambient flow plays an important role (within reason) in establishing the critical and supercritical regimes (with or without the help of distributed roughness) and on the effectiveness (often degradation) of some singular VIV suppression devices at sufficiently large Reynolds numbers (Zdravkovich, 1981).

The parameter $(D/U_0^2)(\mathrm{d}U/\mathrm{d}t)$, with U_0 as a reference ambient velocity (say, prior to the start of the acceleration or deceleration), or in more general terms, the parameter $(D^n/U^{n+1})(\mathrm{d}^n U/\mathrm{d}t^n)$, must be considered in assessing the significance of the local acceleration to the convective acceleration. If it is small (Sarpkaya, 1991, 1996a) the flow may be approximated by a juxtaposition of steady states, i.e., by flows with negligible or no history effects. If large, it is not sufficient to define the changes in flow velocity with more or less arbitrary or qualitative measures such as 'increasing velocity,' 'progressive change of velocity,' 'velocity with large steps,' or 'decreasing velocity.' It is a well-known fact that, depending on its magnitude, the rate of change of velocity (plus or minus), as defined by the subject parameters, gives rise to very interesting response characteristics, even for an isolated cylinder or cable [see, e.g., Sumer and Fredsøe (1988), Brika and Laneville (1993), and Frédéric and Laneville (2002)]. Thus, $(D/U_0^2)(\mathrm{d}U/\mathrm{d}t)$ must be quantified during both the acceleration and deceleration periods to assess the effect of the rate of change of velocity on the inception of the transient states (e.g., hysteresis, intermittent jumps) in both numerical and physical VIV experiments. Sarpkaya (1991) has shown that the rate of deceleration at the end of the acceleration period is just as important as the acceleration period. Obviously, it is not only the rate of change of velocity that can precipitate hysteresis effects. The rate of change of amplitude and the rate of change of frequency can produce equally interesting forms of hysteresis and can help to explain some puzzling observations. Thus, it is necessary to consider and quantify the following additional parameters in assessing the history effects: $(1/U)(\partial A/\partial t)$ and $(D/U)^2(\partial f_{ex}/\partial t)$. Such studies will help to resolve the

consequences of a specific unsteady input of given type and duration on the subsequent stages of the fluid/structure interaction.

The parameter $(D/U)(k/m)^{1/2}$, or its inverse, may be written as $V_r = U/f_{\text{vac}}D$ using the 'natural frequency' f_{vac} obtained in a vacuum because it is the *only natural frequency*. All other frequencies represent unsolved or partially solved fluid/structure interaction problems of the type pioneered by Stokes (1851) and Basset (1888). Nevertheless, a number of other reduced velocities have been used in the literature for a variety of reasons, including the need to emphasize the importance of the variation of one or the other parameter (added mass, phase, in-phase and out-of phase components of the lift force): $V_r = U/f_{\text{air}}D$, using f_{air}, obtained from pluck tests in *still* air, or $V_r = U/f_{\text{wtr}}D$, using f_{wtr} obtained from pluck tests in a *still* test fluid (e.g., water), or $V_r = U/f_{\text{com}}D$, using the actual (or common) frequency f_{com} at which the lock-in occurs at a given velocity. Here a clear distinction must be made between forced and self-excited oscillations. In forced oscillations, $f_{\text{com}} = f_{ex} = 1/T$ (where T is the period of oscillation), and it was used by Sarpkaya (1978) to define $V_r = UT/D$ against which the force-transfer coefficients were plotted. Thus, f_{com} or f_{ex} vary as the period of oscillation is varied. Furthermore, one is at liberty to change the frequency and/or the amplitude content of the oscillations.

5.2. Schewe parameters

All but the last parameter in Eq. (2) can be controlled (some directly, some indirectly) if one were to dedicate the time and equipment necessary to uniquely qualify the investigation. However, the Schewe parameters Sp encompass all the circumstances (influencing parameters) mostly beyond the capacity of the experimenter to control or to vary systematically. They are unknowable facility-related constraints or a consequence of *unsteady facility-interference coupling*. Some of these are the end conditions, parameters controlling the mobility of the separation points on curved surfaces, three-dimensional behavior of flow over two-dimensional bodies, unpredictable (or difficult to predict/control) spanwise correlation and its possible dependence on the forced or free nature of the vibrations, consequences of restraining the in-line oscillations, the strong facility-and-amplitude dependence of the lift coefficient, spectral bandwidth of lift force, shedding frequency bandwidth, nonquantifiable growth of the various disturbances in the unsteady shear layers, effects on VIV of the distribution of the ambient velocity and turbulence across the test section, blockage ratio, size and shape of the end plates, nonuniformity of the surface roughness, yaw, body deformation, unwanted secondary vibrations of the body and its support system, noise, temperature gradients, and other parameters influencing a given experimental setup. Often a number of small (presumed innocuous) assumptions in analysis and experiments or both may make the interpretation of the results rather difficult. However, we must also heed Stokes' (1851) words of wisdom: "Such extreme precision in unimportant matters tends, I think, only to perplex the investigator, and prevent him from entering so readily into the spirit of an investigation." Obviously, all the dimensionless parameters cannot replace the physical insight that springs from experience and knowledge.

5.3. Mass and structural damping

Returning to the discussion of m^* $[= \rho_m/\rho_f]$ and ζ versus $m^*\zeta$ $[= \zeta\rho_m/\rho_f]$, it is noted that there is no compelling reason to combine m^* with ζ. In fact, Sarpkaya (1978, 1979, 1995, 1996a, 1997) and Zdravkovich (1990) suggested over the years that they should not be combined to form a new parameter (or to eliminate an independent parameter). Nevertheless, it has almost become a common practice, at least until recent experiments with small m^* (large ρ_f and small ρ_m) to combine the two parameters into a so-called 'mass-damping' parameter $m^*\zeta$ (with $\delta = 2\pi\zeta$). This will be discussed in more detail later in connection with the consequences of free- or self-excited oscillations where the structural-damping-dependent response may not necessarily be a sinusoidal or stationary random process. Suffice it to note that m^* and ζ play very important roles in VIV. According to K–W (1999), the range of synchronization is controlled primarily by m^* (when $m^*\zeta$ is constant), whereas the peak amplitudes are controlled principally by the product of $m^*\zeta$ in the range of Reynolds numbers $(3.5 \times 10^3$–$10^4)$ encountered in their experiments. However, the dependence of A/D on ζ, ρ_f/ρ_m, $U/f_{\text{vac}}D$, $f_{\text{vac}}/f_{\text{com}}$, the lift coefficient C_L, the phase angle φ, and the Reynolds number remains to be resolved.

As to the role of the damping factor, it is rather unfortunate that no systematic experiments have been reported in vacuum to determine ζ. During the second half of the past century, the word 'damping' has been used at various times to mean 'damping in vacuum', 'damping in still air', 'damping in still water', and 'damping in flowing test fluid'. Furthermore, some experiments were reported without the damping factor and they were subsequently obtained from tests on pipe or cable samples by Griffin et al. (1976). To the best of our knowledge, only Koopmann (1967a; also reported in Griffin et al., 1976) conducted limited experiments to determine the 'structural to the still-fluid damping' of an elastically supported 6-mm cylinder by oscillating it in both air and vacuum. He found that the actual structural

contribution was only 15% of the still-air damping. Based on this experiment, Griffin et al. (1976) concluded that "the decay of the system in still air was predominantly *due to fluid resistance*, and the common assumption of negligible 'in-air fluid loading' was not valid." The consequences of this conclusion are: (a) it is difficult to compare amplitude data from various sources because of the potential variations in the relative contributions of fluid and structural damping to *still fluid damping* ζ_f used in the so-called mass-damping parameter $m\zeta_f/\rho D^2$; and (b) at relatively small mass-damping ratios, the comparison of the data obtained in air and water is further complicated. It is often assumed that one could calculate the mass-damping either with the damping in air or water. This is not quite accurate because the actual structural contribution may be only a small fraction of the still-air damping, whereas the ratio of the same structural-plus-air damping to that brought about by the out-of-phase component of the transverse force in water is negligible. In any case, 'damping in still water', like 'added mass in still water', is only another manifestation of an unsolved fluid-interaction problem (i.e., the VIV itself), and it is not an independently controllable parameter [for further discussion, see Batchelor (1967, p. 357) and Blevins (1990)]. However, for VIVs in water, the structural damping term in the equation of motion may be negligibly small relative to the out-of-phase component of the transverse fluid force. It may even be assumed zero in numerical simulations of VIV in dense fluids.

The concern regarding the reliability of the much-reproduced graph showing the maximum A/D versus the so-called response parameter S_G $(= 2\pi^3 \mathrm{St}^2 \zeta \rho_m/\rho_f)$, [see, e.g., Sarpkaya (1978)] provided us with a strong impetus to carry out a series of experiments with circular rods and tubes in air and in the vacuum chamber of an existing electron microscope. The ends of the cantilevered (smooth and roughened) rods were rounded and the free ends of the cantilevered tubes were fitted with semi-spherical caps. The supporting ends were imbedded in a solid wall (a small hole allowed the complete vacuuming of the inside of the tubes). The oscillating mass of each test element was varied by changing L. The mass was varied from 0.072 to 0.72 kg/m. The results have conclusively shown that the ratio of the actual structural contribution to the still-air damping varied from 0.990 to 0.995, depending on the frequency of vibration and the shape of the cantilevers. For any one test tube, the frequencies of vibration in air and in vacuum were identical. It is on the basis of this conclusion that we have replotted the data compiled by Griffin et al. (1976) and subsequently by Skop and Balasubramanian (1997) in Fig. 7(a) using a linear axis for A/D. Several attempts were made in the past (Sarpkaya, 1979; Griffin and Ramberg, 1982; and Skop and Balasubramanian, 1997) to devise semi-empirical relationships or least-squares fits to the data shown in Fig. 7(a). The shortcomings of the previous A/D versus S_G relationships were that they were mostly curve-fits [except the one proposed by Sarpkaya (1979)] and none was able to represent the data satisfactorily at higher S_G values. We have devised (in spite of our long-standing dislike for curve-fits) a new and relatively simple curve-fit given by

$$\left(\frac{A}{D}\right)\frac{1}{\gamma} = 1.12\mathrm{e}^{-1.05S_G}, \tag{3}$$

which may also be written as $(A/D)/\gamma = 1.12 \times 0.35^{S_G}$, which conveys the unrigorous but plausible suggestion that $\ln(A/D/\gamma)$ may be, to a first order of approximation, a linear function of S_G. The dimensionless mode factor γ is 1.0 for a rigid cylinder, 1.291 for a uniform pivoted rod, 1.155 for a taut string or cable, and 1.305 for a cantilevered uniform beam. However, as pointed out by one of the reviewers, "the energy balance, e.g., between a cantilever and a rigid cylinder on springs, may lead to another ratio between the cantilever-end-displacement amplitude and the rigid cylinder amplitude than 1.305 since the force coefficients are strongly nonlinear functions of A/D." Clearly, such nonlinearities may account for some of the scatter in the A/D versus S_G plots. Additional mode factors are tabulated in Blevins (1990).

Figs. 7(b)–(d) show the linear–log, log–log, and log–linear plots of $(A/D)/\gamma$ versus S_G and the corresponding curve fits using the above equation. The scatter in the data, particularly for S_G less than about 0.5 (i.e., mostly for experiments in water), is of practical as well as research interest and is not entirely due to experimental errors. It is partly due to the use of relatively small Reynolds numbers (less than 10^4) for which the transition to turbulence on the free shear layers does not move sufficiently upstream, magnification of the uncertainties in the damping factors, the end conditions (i.e., the restraint applied to the ends of the cables for or against *axial* motion), the history of the motion [e.g., whether a particular steady flow velocity has been arrived at from a lower or higher value (Brika and Laneville, 1993)], and, most importantly, from the particular behavior of the wake and the lift coefficient C_L, leading to strongly nonlinear dependence of the force coefficients on A/D.

5.4. f_{vac},f_{com}, *and added mass*

In 1995, Sarpkaya denoted f_{com} by f_{ny} (prevailing frequency) to include the self-excited oscillations. Moe and Wu (1990), working with self-excited as well as forced oscillations, introduced f_{true}, the frequency "at which the cylinder is

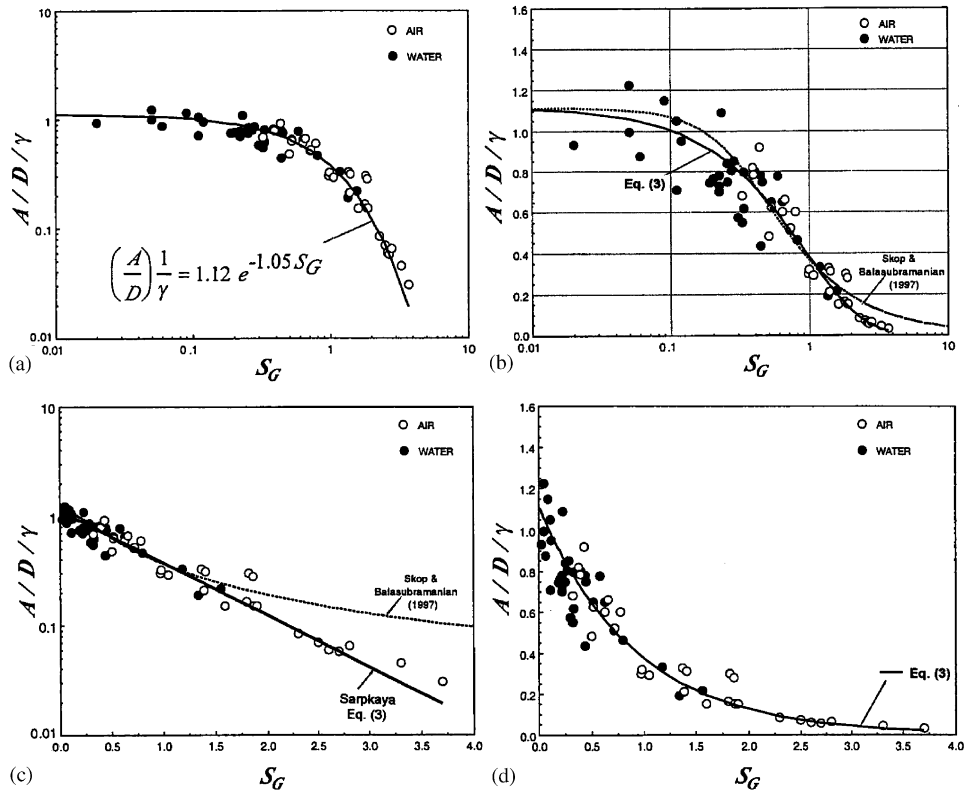

Fig. 7. Experimental measurements of the modally normalized maximum amplitude versus the response parameter S_G and the proposed curve-fit: Eq. (3). The data is tabulated in Skop and Balasubramanian (1997). The above figures show: (a) a log–log plot; (b) a linear–log plot, (c) a log–linear plot, and (d) a linear–linear plot. In each case Eq. (3) represents the data reasonably well and makes an unrigorous but plausible suggestion that $\ln(A/D/\gamma)$ may be a linear function of S_G.

actually vibrating." Here it is denoted by f_{com} to cover both the forced and self-excited oscillations. It does not remain constant throughout the synchronization range because the added mass coefficient C_a in viscous flow is not only a function of the shape, orientation, and the physical surroundings of the body, but is also a strong function of the resulting viscous fluid motion. In fact, f_{com} (either from experiments or from DNS) can be used together with f_{vac} to determine *a posteriori* the actual added mass,

$$\Delta m = m[(f_{\text{vac}}/f_{ex})^2 - 1], \tag{4a}$$

or the added mass coefficient,

$$C_a = m^*[(f_{\text{vac}}/f_{ex})^2 - 1]. \tag{4b}$$

Clearly, the cycle-averaged value of Δm is zero for $f_{\text{com}} = f_{\text{vac}}$, and Δm (and C_a) are negative whenever $f_{\text{com}} > f_{\text{vac}}$, *regardless of the viscous medium in which the synchronization occurs at the common frequency* f_{com}. For experiments conducted in a dense fluid (say, water), the contribution of the air to the added mass may be neglected, i.e., $f_{\text{air}} \approx f_{\text{vac}}$. Then one has, for the added water mass, $\Delta m_{\text{wtr}} \approx m[(f_{\text{vac}}/f_{\text{com}})^2 - 1]$. In any case, C_a for a circular cylinder oscillating in water is not equal to its ideal value of unity. Rewriting the above expression as

$$C_a/m^* = \Delta m/m = (f_{\text{vac}}/f_{ex})^2 - 1, \tag{4c}$$

it is seen that for a given m^*, C_a is strongly dependent on the accuracy of $f_{\text{vac}}/f_{\text{com}}$. Also, re-writing the normalized total mass or 'virtual mass' as

$$(1 + C_a/m^*) = (1 + C_a\rho_f/\rho_m) = (f_{\text{vac}}/f_{ex})^2, \tag{4d}$$

and noting that C_a may have negative as well as large positive values for a circular cylinder [see, e.g., Sarpkaya (1977b, 1978), Gopalkrishnan (1993), Vikestad et al. (2000)], one observes that the role of the added mass at high mass ratios is minimal or that f_{com} *approaches* f_{vac}. However, for small mass ratios, C_a becomes increasingly important as the mass ratio m^* becomes smaller, i.e., for a large (positive) C_a and small m^*, the *virtual mass* (added mass plus m) may acquire very large values. More importantly, however, for a relatively large *negative* C_a (say, -0.7) and small m^* (for example, 0.6), the *virtual mass becomes negative*, a result that is unacceptable. Thus, one must have $C_a/m^* > -1$ or $(m^* + C_a) > 0$. It is clear that bodies of very small m^* will have rather large in-vacuum natural frequencies (f_{vac}). Thus, under the circumstances in which C_a has a large negative value and the out-of phase component of the lift force is positive (energy transfer from the fluid to the body), the system can develop rather large amplitudes. It must be emphasized that the positive as well as the negative values of the added mass strongly depend on A/D, as first shown by Sarpkaya (1977b, 1978), and, to a lesser extent, on the Reynolds number, provided that the Reynolds number is larger than about 1.5×10^4 to 2×10^4.

Eq. (4d) may also be written as

$$\frac{m^*}{m^* + C_a} = \frac{(f_{\text{com}}/f_{st})^2}{(f_{\text{vac}}/f_{st})^2}, \tag{4e}$$

which emphasizes the role of f_{ex}/f_{st} and f_{vac}/f_{st} in determining the ratio of the normalized mass of the oscillating body to its virtual mass. Only when $C_a = 0$, one has $f_{ex} = f_{\text{vac}}$. For all values of $C_a < 0$, $f_{ex} > f_{\text{vac}}$, and, conversely, for all values of $C_a > 0$, $f_{ex} < f_{\text{vac}}$. Forced vibration experiments show that C_a for $A/D = 0.5$, for example, goes through zero at $f_{ex}/f_{st} \approx 0.85$ (for $A/D = 0.5$, for example) and abrupt changes occur in phase and the energy transferred to the cylinder from the fluid as f_{ex}/f_{st} decreases, say from, $f_{ex}/f_{st} \approx 0.88$ to $f_{ex}/f_{st} \approx 0.80$. For cylinders with relatively *large* m^*, f_{ex}/f_{vac} remains close to unity, the shedding mode changes from a Karman-type of vortex shedding (two single vortices per cycle) to two pairs of vortices per cycle (to be discussed in more detail later). However, for cylinders with *small* m^*, the mode of vortex shedding remains essentially the same. The importance of these interesting phenomena, leading to a strong connection between the forces, masses, VIV suppression, and mode and phase changes will become apparent later.

6. Linearized equations of the self-excited motion and their limitations

The equation of motion for a body of single-degree-of-freedom with linear springs and damping has been known for a long time and constitutes one of the classic examples in most vibration texts. Briefly, it may be written as

$$m\ddot{y} + c\dot{y} + ky = \tfrac{1}{2} C_y \rho D L U^2, \tag{5a}$$

in which m is the mass of the cylinder, c the linear material damping coefficient, k the linear spring constant, ρ_f the density of fluid, D and L are the diameter and length of the cylinder, U is the 'steady' ambient velocity, and C_y [$= F(t)/\frac{1}{2}\rho U^2 D$] is the strongly amplitude-dependent lift coefficient. The amplitude of the exciting force, denoted by C_L, and the phase angle φ (between the total force and the displacement) embody the essence of all that is needed for the *dynamics* of VIV. Introducing $y_r = y/A$ and following Parkinson (1974), Eq. (5a) may be reduced to

$$\ddot{y}_r + 2\zeta\dot{y}_r + y_r = (\zeta/S_G)(f_{\text{com}}/f_{\text{vac}})^2 C_y, \tag{5b}$$

in which time is normalized by $\omega_{\text{vac}} t$. This is a nonlinear equation because of the strong dependence of C_y on the amplitude of the cylinder displacement. However, at lock-in, the displacement y and the transverse fluid-force coefficient C_y are usually expressed, to an unknown order of approximation, by sinusoidal functions (known as the harmonic model approximation) in which the force leads the displacement (the horse leads the cart) by a phase angle φ,

$$y_r = (A/D) \sin 2\pi f_{\text{com}} t, \tag{6}$$

$$C_y = C_L \sin(2\pi f_{\text{com}} t + \varphi) \tag{7a}$$

or

$$C_y = (C_L \cos\varphi) \sin(2\pi f_{\text{com}} t) + (C_L \sin\varphi) \cos(2\pi f_{\text{com}} t). \tag{7b}$$

The displacement and acceleration are zero at $y = 0$ (the mean position) and the absolute values of the displacement and acceleration are maximum at $y = A$. The cylinder decelerates as it moves toward larger $|y|$ and accelerates as it moves

towards smaller $|y|$ values. It is a well-known fact that in *steady flow* the angle that the shear layer separates from a cylinder is affected by the Reynolds number. A shear layer on a body undergoing VIV is expected to be strongly affected by whether the relative flow past the cylinder is accelerating or decelerating. Thus, the variations of the total relative velocity about the cylinder and the alternating nature of the accelerations and decelerations of the cylinder could lead to highly complex excursions of the separation points and shear layer transitions. Krishnamoorthy et al. (2001) observed that "both shear layers develop abrupt double roll-ups as the cylinder accelerates from the top-dead-center to its mean position."

The substitution of Eqs. (6) and (7) into Eq. (5b) yields the following well-known expressions for the frequency and amplitude in terms of ρ_m/ρ_f rather than m^*:

$$\frac{f_{\text{com}}}{f_{\text{vac}}} = \left[1 - \frac{C_L}{2\pi^3}\frac{D}{A}\frac{\rho_f}{\rho_m}\left(\frac{U}{f_{\text{vac}}D}\right)^2 \cos\varphi\right]^{-1/2} \tag{8}$$

and

$$\frac{A}{D} = \frac{1}{2} C_L \sin\varphi \frac{\text{St}^2}{S_G}\left(\frac{U}{f_{\text{vac}}D}\right)^2 \frac{f_{\text{vac}}}{f_{\text{com}}} \tag{9a}$$

or

$$\frac{A}{D} = \frac{1}{2} C_L \sin\varphi \frac{1}{2\pi^3\zeta}\frac{\rho_f}{\rho_m}\left(1 + C_a\frac{\rho_f}{\rho_m}\right)^{1/2}\left(\frac{U}{f_{\text{vac}}D}\right)^2. \tag{9b}$$

Thus, the linear equations of motion show that A/D is dependent on C_L, the phase angle φ, ζ, ρ_f/ρ_m, $(U/f_{\text{vac}}D)$, and $(1 + C_a\rho_f/\rho_m)^{1/2}$ or $f_{\text{vac}}/f_{\text{com}}$. There is no mathematically derivable direct dependence on such parameter combinations as $(m^* + C_A)\zeta$, where C_A is the potential flow added mass coefficient ($C_A = 1.0$ for a circular cylinder), or on yet another parameter $f^* = [(m^* + C_A)/(m^* + C_{EA})]^{1/2}$ where "C_{EA} is an 'effective' added-mass coefficient that includes an apparent effect due to the total transverse fluid force in phase with the body acceleration," introduced by Khalak and Williamson (1999), (in our notation, $C_{EA} = C_a$). Furthermore, numerical solutions of the 'exact' equations of motion do not need, do not depend on, and do not give rise to such arbitrary parameters as $f^* = [(m^* + C_A)/(m^* + C_{EA})]^{1/2}$.

Equating A/D from Eqs. (8) and (9a), one has the tangent of the phase angle,

$$\tan\varphi = \frac{2\zeta f_{\text{vac}} f_{\text{com}}}{f_{\text{vac}}^2 - f_{\text{com}}^2}. \tag{10}$$

Recalling that $C_a = m^*[(f_{\text{vac}}/f_{\text{com}})^2 - 1]$, one has for $f_{\text{com}} < f_{\text{vac}}$, i.e., for a positive added mass, $\tan\varphi > 0$ and for $f_{\text{com}} > f_{\text{vac}}$, i.e., for a negative added mass, $\tan\varphi < 0$. Thus, at $f_{\text{com}} = f_{\text{vac}}$, the phase angle shifts by 180°. Conversely, a 180° phase shift corresponds to a change in the sign of the added mass from positive to negative or vice versa, depending on the direction of the change of f_{com}. It must be emphasized that any change in C_a, and thus in phase, is not sudden. The reorganization of the wake occurs over a finite frequency range.

The foregoing analysis shows that A/D is a function of C_L (see Fig. 5b), C_a depends on A/D and $U/f_{\text{vac}}D$, $f_{\text{com}}/f_{\text{vac}}$ varies with $U/f_{\text{vac}}D$, and φ depends on ζ and $f_{\text{com}}/f_{\text{vac}}$, and they all depend on the Reynolds number. Nevertheless, one can reasonably conclude by inserting once $\rho_f = \rho_{\text{air}}$ and then $\rho_f = \rho_{\text{wtr}}$ in Eqs. (8) and (9b) that:

(a) $(f_{\text{com}}/f_{\text{vac}})_{\text{air}}$ approaches unity because the second term in the bracket in Eq. (8) becomes negligibly small and A/D in Eq. (9a) may be simplified to

$$\frac{A}{D} = \frac{1}{2}\frac{\text{St}^2}{S_G}\left(\frac{U}{f_{\text{vac}}D}\right)^2 C_L \sin\varphi; \tag{11}$$

(b) $(f_{\text{com}}/f_{\text{vac}})_{\text{wtr}}$ becomes smaller than one;

(c) $(A/\gamma D)_{\text{wtr}}$ becomes larger than $(A/\gamma D)_{\text{air}}$ with decreasing S_G (see Fig. 7 and Eqs. (4) and (9b));

(d) The suppression of $(A/\gamma D)_{\text{wtr}}$ is more difficult compared to $(A/\gamma D)_{\text{air}}$ partly because of the much larger ρ_f (for water) leading to a much smaller S_G ($= 2\pi^3\text{St}^2\zeta\rho_m/\rho_f$), particularly for small mean mass densities, and partly because of a number of other issues such as the variation of C_L, the width of the lock-in range, and the coherence length with A/D, discussed in connection with Figs. 5(a) and (b). Thus, one needs suppression devices which could successfully reduce C_L in water for *amplitude ratios smaller than about* 0.5, without excessive drag penalty. As appropriately noted by Bearman and Brankovic (2002), "it is more difficult to suppress any resulting VIV in water compared to air because of the much smaller $m^*\zeta$." Evidently, the entire suppression issue is relatively more involved than that posed by S_G or $m^*\zeta$ alone.

The foregoing analysis is predicated on the assumption that the frequency and the amplitude of the oscillations remain constant, as assumed in Eqs. (6) and (7) for the displacement and force. Oddly enough, this is more so for the 'forced' oscillations than for the free oscillations. As noted by Schewe (1983), in connection with stationary cylinders in steady flow, "The time functions of the lift, drag and amplitude look like sine functions, which are randomly modulated in amplitude and frequency. The instantaneous total force acting on the cylinder is then the result of the more or less cooperative behavior of these individual subsystems, which differ slightly from each other in frequency and amplitude." Cylinders undergoing VIV exhibit similar nonstationary, nonergodic, randomly modulated amplitudes. As noted by Moe et al. (1994), nearly harmonic oscillations occur for self-excited vibrations in the lock-in region. The displacement spectra have narrow bandwidths, yet 10% variation in peak amplitudes is common and the associated force amplitudes are strongly irregular. Therefore, the average lift force for the self-excited case cannot be assumed equal to the lift force for the forced-vibration case, even though the average motion amplitudes for both cases may be equal. The assumption that the displacement and force must depend respectively only on $\sin\omega t$ and $\sin(\omega t+\varphi)$ renders the problem more manageable but conveniently avoids the issue as far as the nature of the random fluctuations of lift, drag, and amplitude are concerned. In fact, it might be said that the analysis of free oscillations on the basis of a single frequency as in Eqs. (5b), (6), and (7), without the inclusion of higher order harmonics, may be unwarranted.

7. Unsteady force decomposition

The lift coefficient in Eqs. (5a) or (7a) or its in-phase component with the cylinder velocity must be determined analytically, numerically or experimentally if any progress is to be made toward solving industrially significant VIV problems. It is much easier and more reliable to quantify the lift coefficient using forced vibrations (because of the constancy of the desired amplitude and frequency) in spite of the fundamental differences between the self-excited and forced oscillations. It is a well-known fact that the force-transfer coefficients used in designs (say, that of risers) do not come from the free VIV tests or from numerical simulations. They come from forced oscillation experiments [e.g., Sarpkaya (1977a, b, 1986a, 1995), Moe and Wu (1990), Gopalkrishnan (1993), just to name a few].

7.1. Drag and inertia coefficients and phase angle

Sarpkaya (1978), using $y=-A\sin\omega_{\text{com}}t$ and $U(t)=-U_m\cos\omega_{\text{com}}t$, expressed C_L as

$$C_L = C_{mh}\sin\omega_{\text{com}}t - C_{dh}\cos\omega_{\text{com}}t, \tag{12a}$$

where $\omega_{\text{com}}=2\pi f_{\text{com}}$ and the coefficients C_{mh} and C_{dh} are the Fourier averages, over many cycles of oscillation (about 100), of the transverse component of the normalized force acting on the cylinder. They are assumed to depend on A/D and the Reynolds number. Eq. (12a) may also be written as

$$C_L = -C_a\sin\omega_{\text{com}}t + C_d\cos\omega_{\text{com}}t, \tag{12b}$$

using $y_r=(A/D)\sin 2\pi f_{\text{com}}t$ as in Eq. (6) and $U(t)/U_m=\cos\omega_{\text{com}}t$. Here, C_a is the added mass coefficient and C_d is the drag coefficient. If the body were at rest and the fluid oscillated about it, C_a needs to be replaced by $1+C_a$ to account for the effect of the imposed pressure gradient. The genesis of the above equations is the so-called "Morison–O'Brien–Johnson–Schaaf" equation or the "MOJS" equation (1950), according to which the time-dependent force exerted on a body moving with the velocity $U(t)$ in a fluid otherwise at rest is assumed to be a linear sum of an acceleration-dependent inertial force and a velocity-square-dependent drag force, i.e.,

$$F(t)=\frac{1}{2}\rho C_d D|U|U+\rho C_a\frac{\pi D^2}{4}\frac{\mathrm{d}U}{\mathrm{d}t}. \tag{13}$$

The coefficients of the two forces are determined experimentally by measuring the force and calculating their Fourier or least-squares averages (Sarpkaya, 1976a, b, 1977a, 1986a, b, 1987). More intricate formulations of the time-dependent force at the price of complexity turned out to be arguably not beneficial (Sarpkaya, 1981, 1985, 2000, 2001).

For a cylinder oscillating sinusoidally with $U=U_m\sin\omega_{\text{com}}t$, the first term on the right-hand side of the above equation has often been *linearized* (provided the circumstances be such that the nonlinearity of the square of the velocity may be neglected) to yield Eq. (12b) (Sarpkaya, 1978). Rewriting Eq. (7b),

$$C_y=(C_L\cos\varphi)\sin(2\pi f_{\text{com}}t)+(C_L\sin\varphi)\cos(2\pi f_{\text{com}}t), \tag{7b-R}$$

and comparing it with Eq. (12b), one has

$$C_a=-C_L\cos\varphi \quad\text{and}\quad C_d=C_L\sin\varphi, \tag{14}$$

from which one can find $C_L=(C_a^2+C_d^2)^{1/2}$ and the phase angle $\varphi=\tan^{-1}(-C_d/C_a)$. The maximum of C_L, from Eq. (12b), occurs at $\theta_m=\tan^{-1}(-C_a/C_d)=\pi/2-\varphi$. In other words, the following holds true for the linear approximation of the sinusoidal VIV, regardless of whether it is obtained from the assumptions leading to the sinusoidal displacement and a sinusoidal force with a phase of φ or from a *linearization* of the MOJS equation,

$$\varphi=\tan^{-1}\left(-\frac{C_d}{C_a}\right)=\frac{\pi}{2}-\tan^{-1}\left(-\frac{C_a}{C_d}\right)=\frac{\pi}{2}-\theta_m, \tag{15}$$

or, combining it with Eq. (10), one has

$$\varphi=\tan^{-1}\left(-\frac{C_d}{C_a}\right)=\tan^{-1}\left(\frac{2\zeta f_{\rm vac}f_{\rm com}}{f_{\rm vac}^2-f_{\rm com}^2}\right). \tag{16}$$

As far as forced oscillations are concerned, the linearized version of Eq. (13) is no more or no less empirical than the Eq. (7a). However, for *the self-excited vibrations*, the original nonlinearized form of the MOJS equation is certainly more representative of the prevailing state of the flow, particularly at industrially significant Reynolds numbers.

The linearization represents a considerable simplification for both the ocean and the laboratory environment. The transverse as well as the in-line force for more complex oscillations (e.g., beating phenomena, oscillations with irregular or modulated amplitudes) cannot be represented by a two-coefficient model and certainly cannot be analyzed on a cycle-by-cycle basis in search of a new phenomenon. One needs to determine the Fourier averages of the said coefficients, deduced from many cycles (say, 100) to obtain representative results. There will always be considerable uncertainty stemming from the ambient flow environment and the Schewe parameters. This, in fact, is one of the fundamental reasons for the difficulty of dealing with fluid-structure interactions in a nonlaboratory environment and with self-excited vibrations in both nature and in the laboratory environment.

If the motion contains amplitude—as well as frequency—modulated fluctuations (as in the case of free or self-excited oscillations), one must perform a *complex demodulation analysis* to capture the basic features of the data [see, e.g., Bloomfield (2000)]. In such cases, the assumption of a mean frequency and/or amplitude may lead to less accurate force components and phase angles. One need not be reminded that the single most important parameter in VIV is φ and its dependence on all the parameters given by Eq. (2). To emphasize the point, we rewrite Eq. (2) as

$$\varphi=F\begin{cases}\zeta,\dfrac{\rho_f UD}{\mu_f},\dfrac{L}{D},\dfrac{4m}{\rho_f\pi LD^2},\dfrac{D}{U}\left(\dfrac{k}{m}\right)^{1/2},\mathrm{Re}_{sl},\\ \mathrm{Re}_{cr},\dfrac{D}{U_0^2}\dfrac{\mathrm{d}U}{\mathrm{d}t},\dfrac{D}{U}\dfrac{\mathrm{d}U}{\mathrm{d}y},\dfrac{\mathrm{d}D}{\mathrm{d}y},\varepsilon_t,\dfrac{k_s}{D},\dfrac{I_{\rm ils}}{D},\mathrm{Sp}.\end{cases} \tag{17}$$

Clearly, φ is destined to exhibit large scatter, particularly in tests with self-excited oscillations and in numerical simulations employing, for example, LES. An orbicular leaf attached to a tree responds with exuberance to droplets of uniform shape, weight, and frequency falling on it from a pipette when the frequency and the phase angle relative to the motion of the leaf are set precisely. When the phase angle is a few degrees off, the leaf comes to a dead stop even if the frequency is kept the same.

7.2. Lighthill's force decomposition

Lighthill (1986) asserted that the viscous drag force and the inviscid inertia force acting on a bluff body subjected to unsteady motion in a viscous fluid otherwise at rest operate independently. Accordingly, he expressed the MOJS equation, Eq. (13), as

$$F=C_a^*\rho(\mathrm{d}U/\mathrm{d}t)V_b+\tfrac{1}{2}\rho A_pU^2C_d, \tag{18}$$

where C_a^* is the ideal inviscid flow value of the added mass coefficient. It is obvious from the form of Eq. (18) that Lighthill (1986) meant by "viscous drag force" a force, which contains *no inertial force* due to the motion of vortices. Thus, his second term on the right-hand side of Eq. (18) is only a *velocity-square-dependent drag* force. A few years earlier, Maull and Milliner (1979) made a similar suggestion to simplify the use of the Morison equation, but without the arguments of Lighthill (1986). Sarpkaya (2001) has shown conclusively that the above assertion is invalid. This is rather obvious from the fact that the subtraction of the ideal inertial force from the total force leaves behind a *vortex-motion force* or, just simply, *a vortex force* which necessarily contains both a 'velocity-square-dependent' force and an 'acceleration-dependent' inertial force. In other words, the remainder of the total force (the second term) cannot be expressed as a velocity-square-dependent force alone (with a simple drag coefficient). Lighthill (1986) stated that "I want to argue that, as we necessarily move to more refined

methods of estimation, we can appropriately continue to separate hydrodynamic loadings (as Morison's equation does) into vortex-flow forces and potential-flow forces ... as Taylor (1928a) did … .'' This created the impression that the 'vortex-flow forces' and 'viscous drag forces' were one and the same: a velocity-square-dependent drag force, devoid of inertial forces. A careful reading of Taylor's papers (1928a, b) shows that they deal with the use of distributed sources and sinks to calculate the added mass of airfoils immersed in an inviscid fluid and the determination of the effect of *convective acceleration* on bodies immersed in converging or diverging wind/water tunnels (the so-called horizontal buoyancy) in *steady* inviscid flow. They do not deal with unsteady flows, vortex motion, or ''separation of hydrodynamic loading into vortex-flow forces and potential-flow forces'' contrary to Lighthill's (1986) assertions. However, we must emphasize that there is nothing wrong in separating the ideal inertial force from the total force (as done in the industry for many years) *as long as one recognizes the fact that the remainder of the force is still comprised of both drag and inertial forces*, which require a number of additional terms for their correct representation in a model equation.

Stokes' 153-year old solution (Stokes, 1851) of oscillating viscous flow about a sphere is given by

$$F(t)=\left(\frac{1}{2}+\frac{9}{2}(\pi\beta)^{-1/2}\right)\frac{\rho\pi D^3}{6}\frac{\mathrm{d}U}{\mathrm{d}t}+\left(1+\frac{1}{2}(\pi\beta)^{1/2}\right)(3\pi\mu DU). \tag{19a}$$

Clearly, both the inertial and drag components of the force are modified by the effect of viscosity [so called, Basset's (1888) history terms] as seen from the following version of the above equation:

$$F(t)-\left(\frac{1}{2}+\frac{\rho\pi D^3}{6}\frac{\mathrm{d}U}{\mathrm{d}t}\right)=\frac{9}{2}(\pi\beta)^{-1/2}\frac{\rho\pi D^3}{6}\frac{\mathrm{d}U}{\mathrm{d}t}+\left(1+\frac{1}{2}(\pi\beta)^{1/2}\right)(3\pi\mu DU). \tag{19b}$$

7.3. Total force less ideal inertial force

The subtraction, from the total force, of an 'ideal mass force' (generated by the displacement of the fluid as the body accelerates) leaves on the right-hand side of the equation a β-dependent *in-phase* inertial force and a β-dependent *out-of-phase* drag force.

Together these two are the unsteady flow forces [the so-called 'vortex-forces' in separated time-dependent flows (Sarpkaya, 1996a, 2001)]. The history of the motion (particularly in hysteresis) manifests itself in both the in-phase and the out-of-phase components of the force.

In vortex-induced oscillations, the phenomenon is far more intricate. However, the extraction of the ideal inertial force from the total force Govardhan and Williamson (2000), hereafter referred to as G–W] necessarily leads to a net force still comprised of an acceleration-dependent inertial force and a velocity- or velocity-square-dependent drag force, as in Eqs. (13) and (19b).

Let us now reconsider Eq. (7b) in a slightly different form and denote the phase angle between the total force and displacement as φ_{total}, for reasons which will become clear shortly,

$$C_L(t)=[C_L\cos\varphi_{\text{total}}]\sin(2\pi f_{\text{com}}t)+[C_L\sin\varphi_{\text{total}}]\cos(2\pi f_{\text{com}}t) \tag{20a}$$

and separate the in-phase (inertia) component of the force into two parts: the ideal inertial force IF (to be quantified later), plus the remainder,

$$[C_{L\text{vortex}}\cos\varphi_{\text{vortex}}+IF]\sin(2\pi f_{\text{com}}t). \tag{20b}$$

Now, inserting Eq. (20b) into Eq. (20a), one has

$$C_L(t)=[C_{L\text{vortex}}\cos\varphi_{\text{vortex}}+IF]\sin(2\pi f_{\text{com}}t)+[C_L\sin\varphi_{\text{total}}]\cos(2\pi f_{\text{com}}t). \tag{20c}$$

Obviously, the first term in the first bracket is modified by the addition of the word 'vortex' in the subscripts in order to compensate for the second term so that the total (in phase) inertial force remains unchanged, i.e., *only the forces, that are in phase with each other, can be subtracted from each other*. The out-of-phase component of the force ($C_L\sin\varphi_{\text{total}}$) does not change. However, both C_L and $\sin\varphi_{\text{total}}$ must individually change in order to render the out-of-phase component of C_L equal to $C_{L\text{vortex}}$ and $C_L\sin\varphi_{\text{total}}=C_{L\text{vortex}}\sin\varphi_{\text{vortex}}$. This leads to

$$[C_L(t)-IF\sin(2\pi f_{\text{com}}t)]=C_{L\text{vortex}}\cos\varphi_{\text{vortex}}\sin(2\pi f_{\text{com}}t)+C_{L\text{vortex}}\sin\varphi_{\text{vortex}}\cos(2\pi f_{\text{com}}t), \tag{20d}$$

where the amplitude of the ideal inertial force is given by

$$IF=2\pi^3\mathrm{St}^2\left(\frac{f_{\text{com}}^2}{f_{st}^2}\right)\frac{A}{D}. \tag{20e}$$

Furthermore, it is seen that $\tan\varphi_{\text{total}}$ and $\tan\varphi_{\text{vortex}}$ are related by

$$\frac{\tan\varphi_{\text{total}}}{\tan\varphi_{\text{vortex}}} = 1 - \frac{IF}{C_a}, \tag{20f}$$

which shows that large differences may occur between the two phase angles when strong changes occur in C_a and/or A/D due to rapid changes in vortex shedding, hysteresis, or intermittent jumps at some particular values of f_{com}/f_{st} (e.g., between the Lower and Upper branches in φ_{total} or between the Upper and Initial branches in φ_{vortex}) for a given St *at relatively small* Reynolds *numbers*. The foregoing is predicated on the assumption that the frequency and amplitude modulations are negligible to allow one to make precise *determinations* of the subject phase angles. In self-excited oscillations, this is not always the case. This will be discussed in more detail later.

8. Limitations of forced and free vibrations

8.1. General discussion

The motivation of this section is not to assess how the forced oscillations can be used to predict the free VIVs under otherwise similar conditions, but rather to examine in depth their similarities, differences, and limitations. Obviously, the two cases are not identical: one is driven internally by the wake at an *average* frequency f_{ex} (dictated by the past and the prevailing state of the motion and the periodic forcing arising from it) as the Reynolds number increases with increasing U in $U/f_{\text{wtr}}D$ as in K–W (1999) and G–W (2000). Furthermore, some or all of the Reynolds numbers in the synchronization range may not necessarily be larger than Re_{sl}, making the response dependent on both Re (i.e., on the state of the shear layers) and $U/f_{\text{wtr}}D$. Forced oscillations are driven externally at an *exact* frequency f_{ex} at a desired amplitude A/D and Reynolds number throughout the range of f_{ex}/f_{st} or $V_r = U/f_{ex}D$. One is limited largely by the lock-in regions and the other to a large range of reduced velocities and amplitudes. Forced oscillations help to regularize and idealize almost every aspect of the vortex-induced oscillations, leading to nearly pure sinusoidal oscillations, forces, and almost repeatable wake states. Thus, one has an exact knowledge of the frequency of motion and of the magnitude and shape of the displacement (and hence, of the velocity and acceleration). Even then, however, one expects and finds differences in the structure of the wake from cycle to cycle, for example due to changes in the motion of the separation points and the coherence length.

The bodies undergoing VIV in nature are neither constrained (except by their supports) nor forced to oscillate at a constant amplitude and frequency. Their reduced amplitude (A/D) and Reynolds number vary with the reduced velocity and the accurate determination of their individual effects on the remaining governing parameters in general and on the lock-in phenomenon in particular becomes difficult particularly when some or all Re values are below Re_{sl}. The extraction and interpretation of reliable force information from free oscillations are more difficult. This is particularly true when the body responds very rapidly to changes in reduced velocity as in Feng's (1968) or in Brika and Laneville's (1993) experiments in certain ranges of their reduced velocity $V_{rb} = (V_r/2\pi) = U/(2\pi f_{ex}D)$. Thus, neither the instantaneous center of gravity nor the cycle-averaged value of the virtual mass, nor the force acting on the body, nor the acceleration of the body is known, except for the fact that the virtual mass, the force, and the acceleration are nonlinearly related. This is analogous to deducing information from $F = (\text{virtual mass}) \times (\text{acceleration})$ without knowing *any one of the three elements of the most fundamental equation of motion*. In spite of this, it should be the ultimate objective of the VIV research to predict, to the extent possible, the kinematics and dynamics of self-excited vibrations from forced vibration (physical/numerical) experiments and, equally important, the dynamics of forced oscillations (say, e.g., drag, lift, and inertia coefficients and the phase angle) from the physical/numerical experiments with self-excited oscillations. However, perfect synchronization is not 'perfect' and 10% variation in peak amplitudes of force (in both forced and self-excited oscillations) is quite common, as shown in Fig. 8 (Moe and Wu, 1990). Griffin (1972) carried out both self-excited and sinusoidally forced oscillations under nearly similar conditions. At the same average amplitude, the free oscillations exhibited amplitude (and, most certainly, phase) modulations, similar to those noted above. The average velocities in the wake were quite similar, but their instantaneous values exhibited the expected discrepancies. The numerical simulations of Al-Jamal and Dalton (2003) and Blackburn et al. (2001), among many others, have shown that the computed lift (after sufficient transition time) exhibits 'quite large variability' as in Fig. 9, and the wave form exhibits interesting 'double peaks' as in Fig. 10, "likely to be related to the shedding of four concentrated regions of vorticity per motion cycle," as noted by Blackburn et al. (2001).

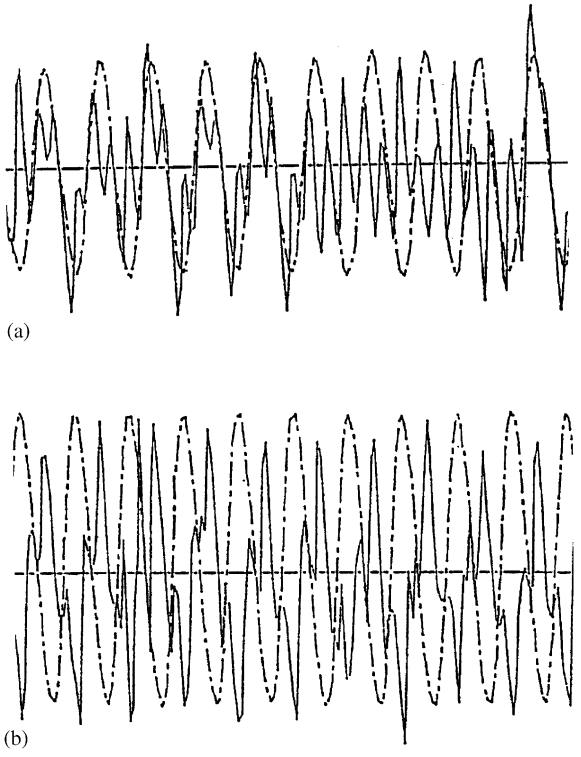

Fig. 8. Force (full line) and displacement (broken line) time series: (a) self-excited, in-line spring-supported, $V_r = 5.93$; (b) forced, in-line spring-supported, $V_r = 5.93$. The sample data show that perfect synchronization is not 'perfect' and 10% variation in peak amplitudes of force (in both forced and self-excited oscillations) is quite common (Moe and Wu, 1990).

8.2. Amplitude and phase modulations

The immediate ramifications of the facts noted above are that (a) the response amplitude given by Eq. (9a) or (9b) becomes increasingly more approximate as the amplitude and phase modulations increase; (b) the second-order fluctuations affect the frequency ratio (Eq. (8)) and the amplitude (Eq. (9a)) differently, and (c) the appearance of m^* and ζ as $m^*\zeta$ in Eq. (9a) does not mean that $m^*\zeta$ is a universal parameter of VIV for all ranges of m^* and ζ for a number of reasons. The parameter $m^*\zeta$ is based on a set of linear equations whereas the oscillations are affected by the start-up effects, history effects, and transitional second-order changes, separation excursions, correlation length fluctuations, pressure distribution, to name just a few of the governing and influencing parameters. The imposed amplitude and frequency drive the forced oscillations whereas the free oscillations are driven by the past and the prevailing state of the motion and the forces arising from it. This is particularly significant when transient phenomena take place at certain frequencies in both the idealized experiments (at low Reynolds numbers) and in practical applications (pipes and cables) at larger Reynolds numbers undergoing both in-line and transverse vibrations.

The relative amplitude of the *forced sinusoidal* oscillations can be accurately represented by

$$y_r = (A/D)\sin 2\pi f_{ex} t, \tag{6-R}$$

where f_{ex} is the driving frequency. However, the representation of the fluid-force coefficient C_y by a linearized equation, such as

$$C_y = (C_L \cos\varphi)\sin(2\pi f_{ex} t) + (C_L \sin\varphi)\cos(2\pi f_{ex} t), \tag{7b-R}$$

may be valid only for small A/D values for the following reasons. The so-called Keulegan–Carpenter number $\mathrm{K} = 2\pi A/D$ for a cylinder subjected to oscillations transverse to a uniform stream varies in the approximate range of $1.25 < \mathrm{K} < 10$. Extensive investigations of sinusoidal flow about a cylinder (Sarpkaya, 1976a, 1977a, b, 1986a, b) have shown that the drag and inertia coefficients in the MOJS equation vary

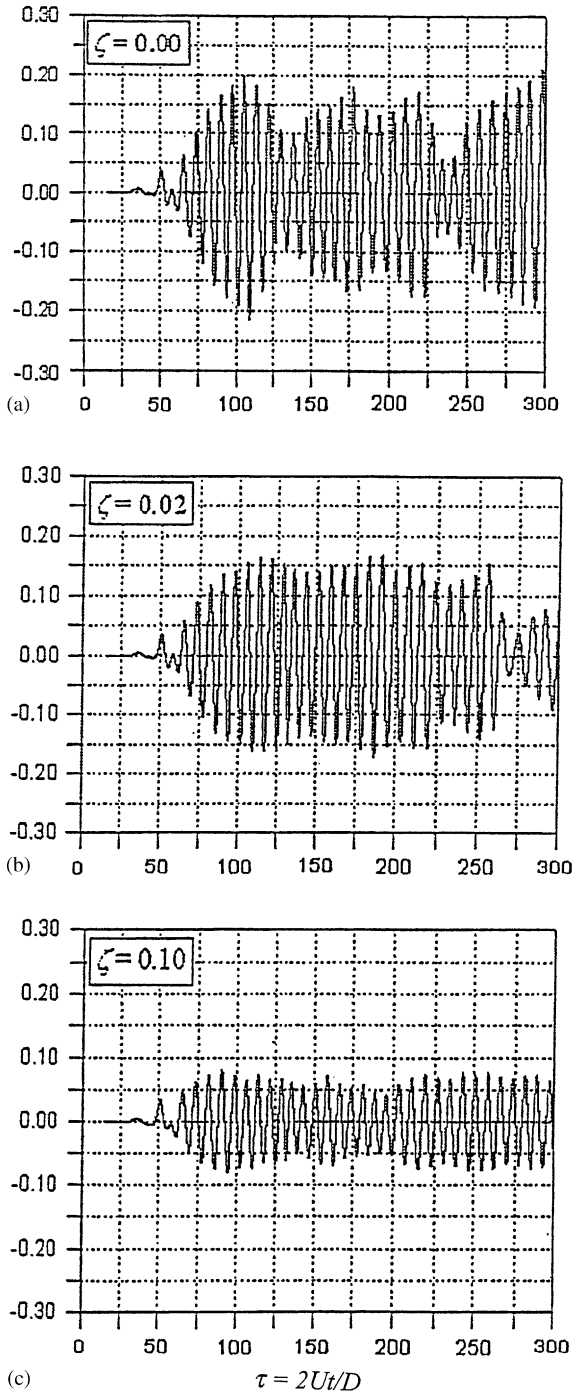

Fig. 9. Example showing that the computed lift (after sufficient transition time $\tau = 2Ut/D$) exhibits "quite large variability" (all for $m^* = 7.85$, $f_{vac} = 0.14$): (a) damping $\zeta = 0.0$; (b) $\zeta = 0.02$; (c) $\zeta = 0.10$ (Al-Jamal and Dalton, 2002).

with both Re and K. In the range of K values noted above, the variation of the added mass coefficient is particularly strong for K larger than about 7. This is primarily due to the changes in the structure of the wake on both sides of the cylinder. In the case of a circular cylinder subjected to transverse oscillations there are additional complications and major differences: the direction of the ambient flow relative to

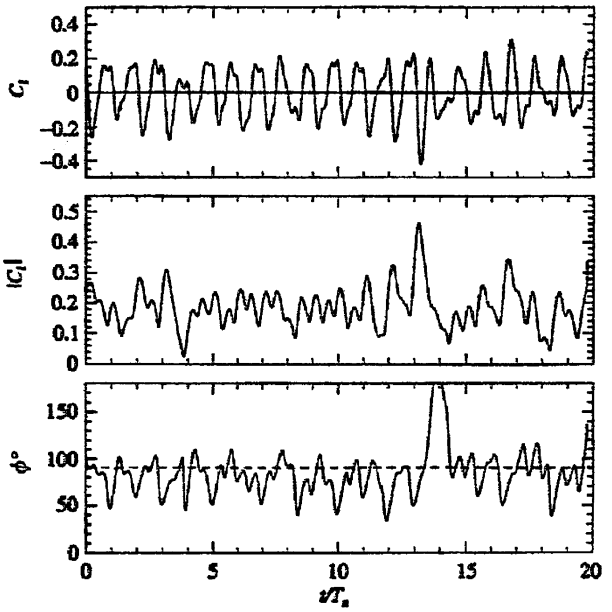

Fig. 10. Time-series of lift (top), its instantaneous magnitude (middle) and phase angle (bottom) in relation to cross-flow displacement for the three-dimensional simulations (Re = 1250, StV_r = 1.33) (Blackburn et al., 2001).

the cylinder changes with time, the oscillations are in the cross-flow direction but the ambient flow is normal to it and the wakes of the two cases are not even similar. However, one can easily surmise that both the added mass and velocity-square-dependent lift force are even more complex than that for the pure sinusoidal oscillations in a fluid otherwise at rest. This has already been shown by Sarpkaya (1978) in his forced oscillation experiments. The larger the amplitude of VIV oscillations, *the more nonlinear is the dependence of the lift and inertial forces on A/D*, *particularly at mode changes*, *phase jumps*, *hysteresis*, *and intermittent switching*. In other words, Eqs. (6) and (7b) must be replaced by a nonlinear force equation to enhance its accuracy if it is to be compared with self-excited vibrations. The only such equation (other than the addition of higher order terms with either arbitrary or Fourier-averaged coefficients) is Morison's equation. It is easy to show that it reduces to (Keulegan and Carpenter, 1958; Sarpkaya, 1977a)

$$C_y = C_d \frac{3\pi}{8} |\cos \omega t| \cos \omega t - C_a \sin \omega t. \tag{21a}$$

The maximum force occurs at $\omega t = \theta_m$, where

$$\theta_m = \sin^{-1}\left(-\frac{4}{3\pi}\frac{C_a}{C_d}\right). \tag{21b}$$

It is interesting to note that $|C_d/C_a|$ must be larger than $4/3\pi$. Using Eq. (21b) one can determine the phase angle with respect to displacement, velocity, or acceleration.

As noted above, the relative amplitude of self-excited vibrations is not constant and the motion is not a pure sinusoidal oscillation. Separation points, pressure distributions and correlation lengths are history dependent and thus the instantaneous states in forced and self-excited cases at the same amplitude and average frequency do not necessarily give rise to instantaneous similar correlation lengths, pressure distributions and sectional or total forces. The character of every cycle is determined by the cumulative effect of the prevailing conditions (Basset effect) and by the Schewe parameters. Every change in amplitude indicates a change in the lift force, which in turn, is a reflection of a mismatch between the vortex shedding frequency and the body frequency, leading to fluctuations in the shedding of vorticity. One can find better force and amplitude representations by accounting for the additional harmonics or by resigning to the use of time-averaged values. At present, there are no analytical models that would suggest the form of the nonlinearity likely to be contributing to the dynamics of VIV. In recent years new methods of multivariate and especially spacio-temporal time series analyses have been developed. Thus, the amplitude may be represented with sufficient accuracy

through the use of one of these approximate methods such as (a) the *harmonic analysis*; (b) *proper orthogonal decomposition* (POD, also known as the Karhunen–Loève decomposition); (c) *force-state mapping* (Masri and Caughey, 1979; Meskell et al., 2001); or (d) *complex demodulation analysis* in dealing with nonexact periodic series (Bloomfield, 2000). The POD is an optimal expansion scheme to discretize a random process (Loève, 1977) and has been used, e.g., by Cazemier (1997), Lenarts et al. (2001), Sarkar and Païdoussis (2003), and Cohen et al. (2003). Evangelinos and Karniadakis (1999) have successfully used the *complex demodulation analysis* in connection with their work on the VIV of a cable. If none of the above methods is used, it is suggested that Fourier-averaged force-transfer coefficients be calculated using sufficiently large number of oscillations (experimental or numerical) and incorporated into Eq. (12) to create a model to predict the force as a function of time. Such a force equation should produce, for similar normalized parameters, the lift and phase, or the drag and the added-mass coefficients obtained from the forced oscillations.

The question is not whether the two fairly idealized VIVs (forced and free, with minimum Re larger than about 15 000) are exactly alike or not, but rather whether they are sufficiently alike to extract reliable information from each for purposes of comparison toward a physics-based understanding of VIV. The final decision regarding the applicability of the fixed-body data to the prediction of the characteristics of a freely oscillating body will depend on many more experiments (forced and self-excited) with other rigid and flexible bodies at much higher Reynolds numbers.

The comparison of the flow kinematics (often of DPIV pictures at low Re) of two in-line constrained cylinders (one self-excited, one forced to oscillate) under highly idealized circumstances (in-line constrained rigid cylinder, small L/D, better correlation, small Re, uniform flow with relatively small turbulence) is far from sufficient to draw scientific and/or industrially significant conclusions regarding the dynamic similarity of self-excited and forced oscillations. The unconstrained rigid or elastic bodies (long cables or pipes with varying degrees of bending and *support* stiffness) often subjected to omni-directional waves, currents, and shear at much higher Reynolds numbers present highly complex problems. What may be true for the physics of the simplest cases may not at all hold true for the more realistic circumstances.

9. Experiments with forced oscillations

9.1. A brief summary of the existing contributions

Following the pioneering experiments of Bishop and Hassan (1964) with cylinders subjected to forced oscillations in uniform flow, Protos et al. (1968), Toebes (1969), Jones et al. (1969), Mercier (1973), Stansby (1976), Sarpkaya (1978, 1979), Chen and Jendrzejczyk (1979), Staubli (1983), Moe and Wu (1990), Cheng and Moretti (1991), Gopalkrishnan (1993), Moe et al. (1994), Sarpkaya (1995), Carberry (2002), and Carberry et al. (2002) conducted experiments using forced oscillations.

Bishop and Hassan (1964) reported their lift and drag forces in arbitrary units and assumed the added mass coefficient to be equal to its ideal value of $C_a = 1$. This invalidated their force measurements and, for the same reason, those of Protos et al. (1968) and Toebes (1969). However, Protos et al. and Toebes were the first to point out the importance of the phase angle φ in the determination of the direction of the power transfer between the fluid and the cylinder. Bishop and Hassan have identified two critical frequencies ($f_{com}/f_{st} = 0.86$ and 0.95 at $\mathrm{Re} = 6000$ and $A/D = 0.25$) delineating a hysteresis loop. The phase angle φ (between the displacement and the excitation) started with a negative value and increased gradually to a positive value of about 90° at the lower critical frequency. Then the motion became unstable and the phase angle jumped from 90° to about 180°, with no intermediate values. However, when f_{com}/f_{st} was increased, from the lower to higher values, the branch of $\varphi \cong 170°$ was followed until the upper critical frequency was reached. Then the phase angle changed abruptly by 180°. In other words, there was no gradual phase change in the interval $0.86 < f_{com}/f_{st} < 0.95$. Many years later, Krishnamoorthy et al. (2001) noted, "... the phase switch does not occur abruptly. Instead, over several cycles of cylinder oscillations, both 'in-phase' and 'out-of-phase' vortex shedding occurs during the transition." Our high-speed photographic recording (at a rate of 500 frames/s) of the forced oscillations of smooth as well as roughened cylinders have shown that the phase changes do in fact occur over several cycles.

Jones et al. (1969) forced a large cylinder to vibrate at small amplitudes, at very large $\mathrm{Re} = 1.9 \times 10^7$. Their lift coefficients were very similar to those reported at relatively low Reynolds numbers. Mercier (1973) conducted forced in-line and transverse oscillations in the range $4000 < \mathrm{Re} < 8000$ and reported a variety of figures for mean and oscillatory drag coefficients as well as drag and inertia components of the lift force, as functions of the reduced velocity and A/D. Stansby (1976) conducted forced vibration experiments with a circular cylinder, and he too observed that the

phase angle jumped about 180° in the lock-in range for decreasing f_{com}/f_{st} and increasing A/D. The switch occurred at $f_{com}/f_{st}=0.86$ (as in the case of Bishop and Hassan) at Re = 3600 and $A/D=0.25$. Stansby associated his observations with the wake width being greater for f_{com}/f_{st} below critical, to being smaller for f_{com}/f_{st} above critical. This reduced the question to what makes the relative wake width vary. Bearman and Currie (1979), working with a circular cylinder at much higher Reynolds numbers ($Re=2.4\times10^4$), reported no evidence of hysteretic behavior.

Carberry (2002) and Carberry et al. (2002) subjected circular cylinders to controlled sinusoidal oscillations transverse to a uniform flow at $Re<10^4$. They observed many of the well-known characteristics of the forces and transitions as the frequency of oscillation passes through the Strouhal frequency. They have called them a 'transition' between the "*low- and high-frequency states*" although the frequency changes only slightly during the said transition. As noted earlier, it is a "phase transition" where the 'jump' in phase could indeed be very large. Carberry (2002), in an attempt to compare her data with those obtained previously, defined a "transition frequency" f_t at which sharp changes occur in the phase and amplitude of the lift force. Obviously, f_t differed from one data set to another. Thus, using f_{ex}/f_t rather than f_{ex}/f_{st}, she was able to bring into closer agreement the phase (φ_{lift}) and C_L data of Mercier (1973), Sarpkaya (1978), Staubli (1983), Gopalkrishnan (1993), and Carberry (2002), as shown in Fig. 11. All the data have been obtained at subcritical Reynolds numbers, ranging from as low as 2300 to as high as 6×10^4, over the past 24 years. The Re values of Carberry (2002) are within the said range (Re = 2300, 4400, and 9100), but her data exhibit notable differences from the mean of the others even in a plot pulled closer by f_{ex}/f_t. This appears to be partly due to the fact that her Reynolds numbers are considerably smaller than that required for the transition in the free shear layers to mature and partly due to the fact that a 'transition frequency' f_t does not uniquely characterize a VIV event. Fig. 12 shows $C_{Lvortex}$ data of Carberry et al. (2002) for a range of A/D at Re = 2300 and for a range of Re (2300–9100) at $A/D=0.5$ as a function of f_{ex}/f_t. Their additional data at $A/D=0.25$, 0.40, and 0.60 depict equally large variations with Re and A/D probably partly due to amplitude and frequency modulations, and the increase of the instability in the free shear layers with increasing Re, and partly due to the effects of a number of secondary parameters noted earlier. Carberry et al. (2002) have also noted that small differences in the motion of the cylinder can result in significant changes in the energy transfer.

Sarpkaya (1977a, b, 1978) carried out systematic measurements of forces acting on a rigid cylinder vibrating sinusoidally transverse to a uniform water flow ($Re=6\times10^3$ to 3.5×10^4) and expressed the transverse-force coefficient in a manner consistent with the force decomposition discussed earlier (see Eqs. (14–15)). For an ambient velocity of $U=U_m\cos\omega_{com}t$, it was reduced to

$$C_a=-C_L\cos\varphi \quad \text{and} \quad C_d=C_L\sin\varphi \tag{14-R}$$

and to

$$\varphi=\tan^{-1}(-C_d/C_a)=\tan^{-1}\left(2\zeta\frac{f_{vac}f_{com}}{f_{vac}^2-f_{com}^2}\right). \tag{16-R}$$

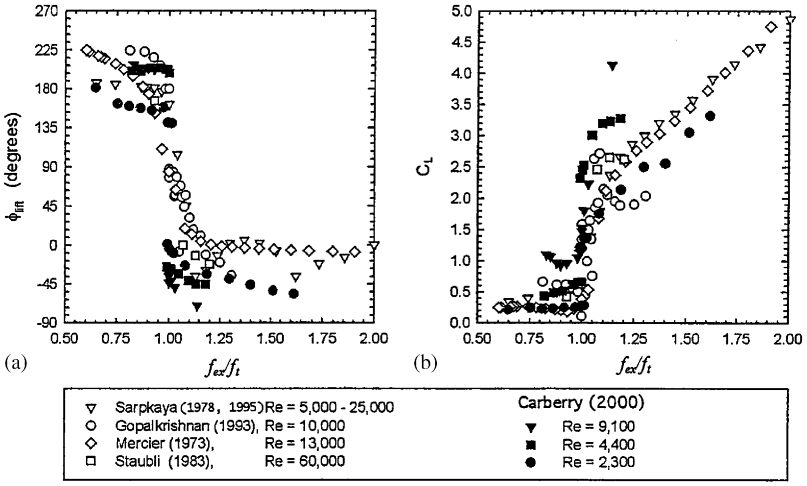

Fig. 11. (a) and (b) show the phase angle (φ_{lift}) and the lift coefficient C_L in terms of f_{ex}/f_{tr}. Apparently, the data for Re less than about $10^4-1.5\times10^4$ differ most from the rest even in a plot pulled together by f_{ex}/f_t. This suggests that the average position of the transition from a disturbed-laminar state to a turbulent state has not yet fully migrated upstream in the free shear layers (Carberry, 2000).

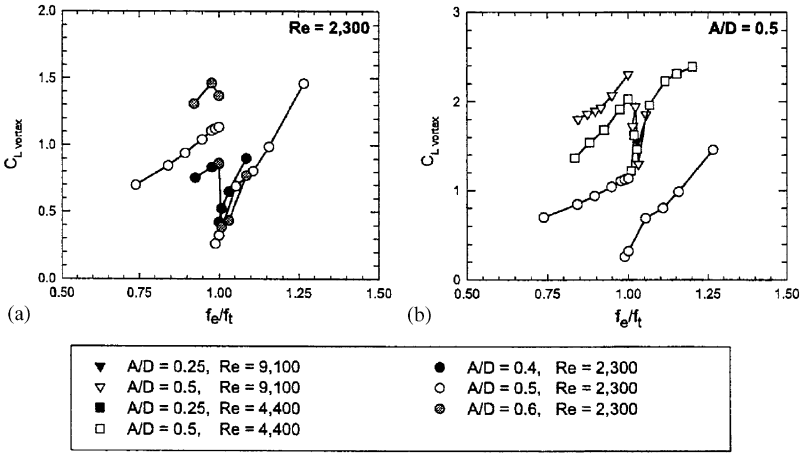

Fig. 12. Carberry et al. (2002) data show that $C_{L\,\mathrm{vortex}}$ increases with A/D for a given Re, and with Re for a given A/D in the range of Reynolds numbers from 2300 to 9100.

Sarpkaya (1978) presented the inertia or added-mass coefficient (component of lift in phase with the cylinder acceleration) and drag coefficient (component of lift in phase with the cylinder velocity) for various values of A/D in the range $6\times10^3<\mathrm{Re}<3.5\times10^4$. He then used the data in a linear equation of motion to predict the amplitudes of oscillation of an elastically mounted self-excited cylinder. His predictions were in good agreement with the experimental data of Griffin and Koopmann (1977).

Staubli (1983) measured the fluid forces acting on a transversely oscillating circular cylinder in a towing tank. His work was essentially similar to that of Sarpkaya (1978), but at a higher Reynolds number ($\mathrm{Re}\approx60\,000$). Staubli predicted the vibrations of a freely oscillating cylinder [by Feng (1968)] using the results of his measurements. In general, he found good agreement with the experimental data. He has shown that hysteresis effects, which are observed in experiments with elastically mounted cylinders of certain damping and mass ratios, are caused by the nonlinear relation between the fluid force and the amplitude of oscillation. Staubli did not present drag and inertia coefficients. However, they can be derived from his lift force and phase data and vice versa as shown in the present paper.

Moe and Wu (1990) have undertaken a major effort to conduct both free and forced oscillation experiments using the same apparatus. The cylinders were suspended such that they were (a) free in both the in-line and transverse directions; (b) clamped in the in-line direction, free in the transverse direction; (c) clamped in-line, forced in the transverse direction; and (d) free in the in-line direction and forced to vibrate in the transverse direction. Moe and Wu (1990) have obtained a number of important results: (i) the use of the true or prevailing oscillation frequency (our f_{com}) results in very similar lock-in ranges for both the forced and free oscillations; (ii) large self-excited cross-flow motions occur for a wider range of the reduced velocity if the cylinders are free to execute figure-eight motions than if they are restrained in the in-line direction; (iii) the lift force is irregular for all test cases, and most so for the self-excited case; and (iv) relatively large random effects exist in the lift force of the cylinder undergoing self-excited or forced vibrations as seen in Figs. 9(a) and (b). These effects are *stronger* for the in-line fixed cases than for the in-line spring-supported ones.

Gopalkrishnan (1993) carried out forced oscillation experiments in a towing tank ($\mathrm{Re}=10^4$) and produced extensive plots of the lift force and phase. He measured the reaction force only at one end of the test cylinder (suspended at both ends) but performed the data reduction by assuming a uniformly distributed load. Thus, the effects of three-dimensional conditions (e.g., the spanwise variations of the flow) in a nominally two-dimensional flow were not accounted for. His data, as well as those obtained by Sarpkaya (1978) and Moe and Wu (1990), were compared by Sarpkaya (1995) by plotting the in-phase and out-of-phase components of the lift force (for $A/D=0.25$, 0.50, and 0.75) as a function of $V_r\mathrm{St}=(U/Df_{ex})(f_{st}D/U)=f_{st}/f_{ex}$ in order to account for the variations in Strouhal number (and the Reynolds number) among the three experiments. The level of agreement between the three sets of data suggested to Blevins (1999) that the drag and inertia coefficients obtained by Mercier (1973), Sarpkaya (1978), Staubli (1983), Wu (1989), Deep Oil Technology (1992), and Gopalkrishnan (1993) may be combined in a single database and represented with semi-empirical correlations for design purposes only.

The test cylinders in the experiments noted above were constrained to remain in the transverse plane. As noted earlier, Moe and Wu (1990) carried out additional, but limited, tests with cylinders not-constrained in the in-line direction (using suitable springs). Interestingly enough, the random variations in the lift force turned out to be smaller for the in-line-unrestrained cases than for the in-line-restrained cases. Clearly, the data obtained with in-line-restrained rigid cylinders may be of limited use under certain circumstances, particularly when the natural frequency of the cylinder in the in-line direction is made or becomes increasingly larger than that in the transverse direction. Thus, the exploration of the biharmonic motion of a cylinder elastically supported in both directions becomes an issue even more important than that of an in-line restrained cylinder subjected to amplitude-modulated beating motions. Gopalkrishnan et al. (1992) subjected rigid cylinders, restrained in the in-line direction, to amplitude-modulated (beating) motions and expressed the transverse force in terms of an "equivalent lift coefficient."

9.2. Detailed discussion of more recent experiments

Sarpkaya (2004) repeated his 1978 experiments in a new water tunnel (with no free surface) at seven Reynolds numbers (2.5×10^3, 7.5×10^3, 12.5×10^3, 15×10^3, 20×10^3 and 45×10^3) with two 50-mm diameter cylinders with $L/D=7$ and $A/D=0.50$ (using a fast data acquisition system and an 'infinitely better' computer rather than several hundred punch cards for every data point as during the 1975–1978 period). One of the cylinders was polished to make it as smooth as possible and the other was specially modified for the exploration of VIV suppression. The velocity at the test section (356 mm × 510 mm) ranged from 0.04 to 0.92 m/s and the ambient turbulence at the lowest Re was 0.8% and at the highest Re was 1.2%. Experiments for each Reynolds number were repeated at different weeks. The objectives of the rather ambitious program were: (a) to obtain reliable data at Reynolds numbers higher than that encountered in the 1978 experiments; and, more importantly, (b) to determine the dependence of the key quantifiable parameters (phase angle and the in-phase and out-of phase components of the transverse force) on the Reynolds number at discrete values of Re in the range $2.5\times10^3<\mathrm{Re}<45\times10^3$ using the same facility, experimental procedures, and test cylinder. Only the most important findings will be described in this review. The results and their detailed discussion will appear elsewhere (Sarpkaya, 2004).

We will first describe the results for $\mathrm{Re}=45\times10^3$. The mean lines passing through the new C_a, C_d, and phase data for $A/D=0.5$ for $\mathrm{Re}=45\times10^3$ are shown in Figs. 13 and 14 as a function of f_{ex}/f_{st} and V_r, respectively. The C_a, C_d, and φ data obtained at different weeks fell within respective error bands of 4%. These figures substantiate many of the observations made earlier by Sarpkaya (1978, 1979, 1995) and others since then [e.g., Staubli (1983), Gopalkrishnan (1993)]. Evidently, important variations occur in both C_a and C_d in the range $0.80<f_{ex}/f_{st}<0.90$ and the positive values of C_d are the regions of primary and secondary synchronizations, which signify power transfer *from the fluid to the cylinder*.

The phase angle decreases rapidly from a value of about 180° to little above zero at $f_{ex}/f_{st}\approx1.5$. In addition, important variations occur in all three parameters outside the primary f_{ex}/f_{st} range noted above. Fig. 14 shows the same data as a function of $V_r=U/Df_{ex}$ where, for a given U and D, the forcing frequency decreases along the V_r axis but the Reynolds number *remains constant* at $\mathrm{Re}=45\times10^3$. The data reveal that C_a decreases sharply from about 3.9 to about −0.6, as the reduced velocity increases from $V_r\approx3.5$ to 5.90. C_a then rises slowly to about −0.4 as V_r increases toward 10. This phenomenon occurs for a wide range of A/D values with different C_a values (Sarpkaya, 1978). The changes in C_a may be interpreted in a number of interesting ways using Eqs. (3d) or (3e), i.e., $(1+C_a/m^*)=(f_{\mathrm{vac}}/f_{ex})^2$ or the virtual mass $=(m^*+C_a)=m^*(f_{\mathrm{vac}}/f_{ex})^2$. The decrease of C_a from large positive values toward zero, as V_r approaches 5.85, shows that f_{ex} is rising toward f_{vac} (i.e., the virtual mass of the body is decreasing). At $f_{\mathrm{vac}}/f_{ex}=1$, $C_a=0$, $V_r\approx5.85$ and the virtual mass of the body becomes equal to the actual mass of the body. Subsequently, C_a becomes negative and acquires its minimum value of about −0.6 (for $A/D=0.5$) at about $V_r\approx5.90$. At that point, the body's apparent mass is the smallest it will ever be and f_{ex} is the largest it will ever get for this particular amplitude ($A/D=0.5$). In short, f_{ex} increases up to about $V_r=5.90$ and then decreases gradually while remaining larger than f_{vac}.

Fig. 14 also shows that the drag coefficient C_d (the normalized out-of-phase component of the total instantaneous transverse force) rises sharply for V_r values from about 5 to 5.90, i.e., the drag is in phase with the direction of motion of the cylinder and helps to magnify the oscillations (positive energy transfer). It is positive also in the ranges $3.2<V_r<4.4$ and $5.90<V_r<10$. The foregoing substantiates the fact already noted by Sarpkaya (1978) that "synchronization or lock-in is manifested by a rapid decrease in inertial force and a rapid increase in the absolute value of the drag force" and that "lock-in is a phase transformer." Sarpkaya (1978) further noted that "The data also show that the use of an inertia or added-mass coefficient equal to unity, as determined by oscillating the cylinder in a fluid otherwise at rest, is not correct for modeling the vortex-induced oscillations." Obviously, this fact has nothing to do with the shifting of the

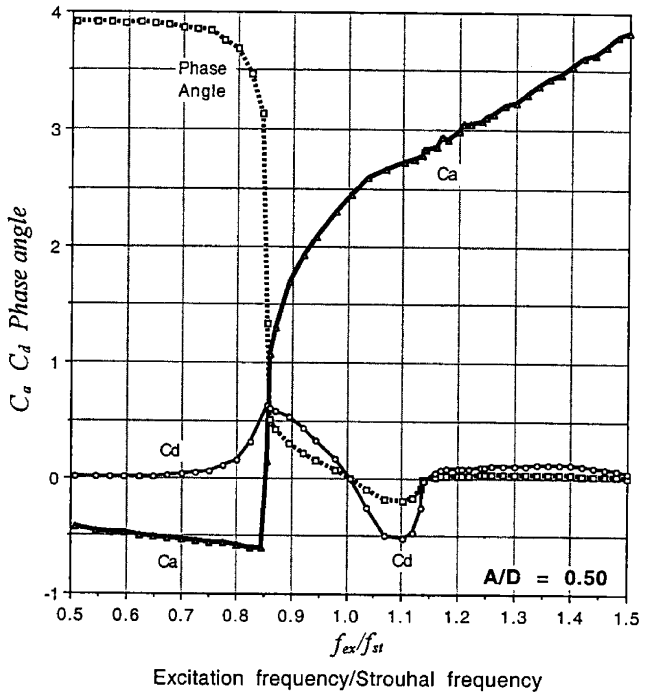

Fig. 13. Inertia and drag coefficients (or the in-phase and out-of phase components of the lift force) and the phase angle as a function of f_{ex}/f_{st} ($A/D = 0.50$, Re = 45 000, $L/D = 7$, smooth cylinder) (from author's experiments). Perfect synchronization is seen to occur at $f_{ex}/f_{st} \approx 0.85$, accompanied by rapid changes in phase and force-transfer coefficients. (Sarpkaya, 2004).

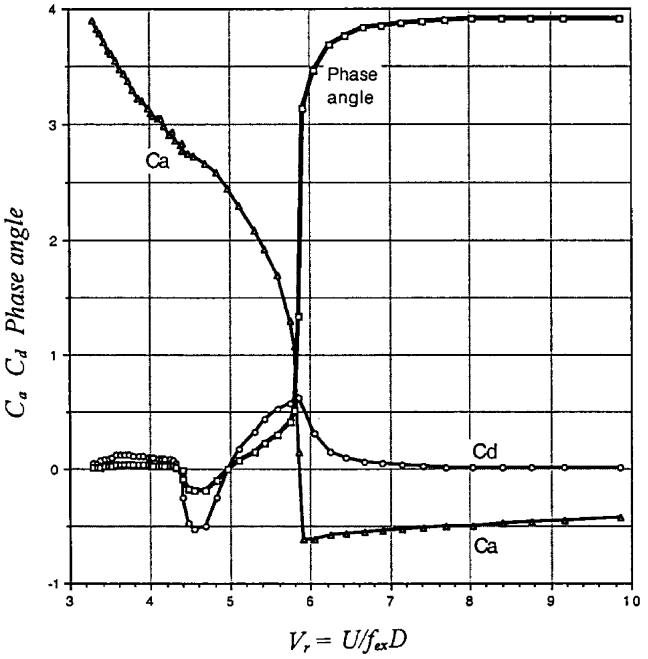

Fig. 14. Inertia and drag coefficients (or the in-phase and out-of phase components of the lift force) and the phase angle as a function of $V_r = U/f_{ex}D$ ($A/D = 0.50$, Re = 45 000, $L/D = 7$, smooth cylinder) (from author's experiments). Perfect synchronization is seen to occur at $V_r = 5.80$–5.85, accompanied by rapid changes in phase and force-transfer coefficients (same as Fig. 13 except that the horizontal axis is changed to V_r).

ideal added mass to the left side of the equation of motion and dealing only with the so-called 'vortex-induced forces,' as long as the *actual added mass* (Δm), and *not its ideal value*, *is used in calculating the prevailing body frequency*, i.e., $f_{ex}=(1/2\pi)(k/(m+\Delta m)^{1/2}$. Clearly, high m^* values diminish the contribution of C_a/m^* or $\Delta m/m$ to the virtual mass. Conversely, very small values of m^* magnify the contribution of C_a/m^* (for positive values of C_a) and lead to lock-in at very small excitation frequencies, as per Eq. (3d). Furthermore, the range of synchronization increases because the variation of $f_{\rm vac}/f_{ex}$ with respect to C_a/m^* decreases according to $(1+C_a/m^*)^{-1/2}$ and $f_{\rm vac}/f_{ex}$ loses its ability to delineate sharper frequency boundaries.

It has been noted a number of times that the added mass coefficient C_a can be negative with far-reaching consequences for freely vibrating cylinders. At first this appears paradoxical. However, further thought shows that C_a is the cycle-averaged value of the sum of the masses transported during the periods of acceleration (cylinder moving toward the mean position, i.e., $y\to 0$) and deceleration (cylinder moving toward its maximum amplitude, i.e., $y\to|A|$). Thus, (cycle-averaged) negative added mass means that the drift mass during the deceleration periods is larger than that during the acceleration periods. The basic difference between the kinematics of the two cases is that, during the deceleration periods, the velocity vector relative to the cylinder is oriented toward the axis of the wake, whereas during the periods of acceleration the said net velocity is toward the shear layer from which the cylinder is coming. Undoubtedly, this is a consequence of the particular behavior of the wake vortices during the said periods and the forces they exert on the cylinder (awaiting a Direct Numerical Simulation of VIV at high Reynolds numbers, say $\mathrm{Re}>15\,000$). Similar "negative" added mass has been previously discussed by Keulegan and Carpenter (1958) and by Sarpkaya (1976a, b) in connection with the sinusoidal motion of flow relative to smooth and roughened cylinders. Subsequently, it has been discussed by numerous investigators [see, e.g., Vandiver (1993), Gopalkrishnan (1993), Vikestad et al. (2000)]. According to Vandiver (1993), "a negative added mass simply reflects the sign of the fluid force on the cylinder being in phase with the acceleration." In self-excited oscillations, the occurrence of amplitude and frequency modulations is accompanied by corresponding changes in the added mass. For example, a change of $\Delta(f_{\rm vac}/f_{\rm com})$ leads to a change of $\Delta(C_a/m^*)=2(f_{\rm vac}/f_{\rm com})\Delta(f_{\rm vac}/f_{\rm com})$, which could be very large when $f_{\rm com}$ is relatively small as in the case of small m^*.

The second objective of our experiments (Sarpkaya, 2004) was to determine the dependence of the phase angle and the in-phase and out-of phase components of the transverse force on the Reynolds number at seven discrete values of Re in the range $2.5\times10^3<\mathrm{Re}<45\times10^3$, using the same facility, experimental procedures, and test cylinder. This was prompted by the well-known fact that the Gerrard–Bloor transition waves in the free shear layers disappear in the range of Reynolds numbers from about $\mathrm{Re}\simeq2\times10^4$ to 5×10^4 in steady flow about a stationary cylinder. Bloor (1964) measured the frequency of transition waves within $1.3\times10^3<\mathrm{Re}<4.5\times10^4$ [see also Bloor and Gerrard (1966), Gerrard (1978), Wei and Smith (1986), Ünal and Rockwell (1988), Ahmed and Wagner (2003), Zdravkovich (1997, 2003), Norberg (2003)]. When the Reynolds number reaches about 2×10^4, the near wake becomes highly three dimensional, and the eddy formation length does not move closer to the separation point. Unfortunately, there are no comparable *direct* observations and measurements with cylinders subjected to VIV. Thus, the critical value of Re_{sl}, at which the cycle-averaged eddy formation length remains nearly stationary, is not yet known. Furthermore, direct measurements to gather such data appear to be prohibitively difficult. Owing to these facts, we have chosen the three parameters noted above (C_a, C_d, φ) to deduce *indirect* information about the effect of the evolution of the unsteady free shear layers, knowing fully well that the variations observed from one Re to another at the same A/D are not exclusively due to the variations in the shear layers. However, it is not too difficult to assume that the shear layers will certainly have a predominant effect on what happens to the generation of vorticity, shedding of vortices, phase angle and the force components.

The data obtained at different weeks at each Reynolds number were compared with each other as well as with those at consecutive Reynolds numbers (2.5×10^3, 7.5×10^3, 12.5×10^3, 15×10^3, 20×10^3, and 45×10^3, all with $A/D=0.5$). For smaller values of Re (2.5×10^3 and 7.5×10^3), the differences between the force coefficients were indeed as large as those encountered by Carberry et al. (2002) with $A/D=0.5$ and $\mathrm{Re}=2.3\times10^3$, 4.4×10^3, and 9.1×10^3, as shown in Fig. 12. However, when the Reynolds number was increased to 12.5×10^3, the variations in data relative to $\mathrm{Re}=7.5\times10^3$ became smaller but certainly larger than the usual scatter in the data. The phase angle exhibited the largest difference, particularly for $f_{ex}/f_{st}>0.9$. When Re was increased to 15×10^3 and then to 20×10^3, the differences between the tracing parameters reduced to the level of the scatter observed in each experiment. The comparison of the data for $\mathrm{Re}=20\times10^3$ and $\mathrm{Re}=45\times10^3$ confirmed the conclusion that all three 'identification parameters' stabilize and do not materially depend on the Reynolds number, at least in the range $15\times10^3<\mathrm{Re}<45\times10^3$. It is tempting to assume that this conclusion will remain true for all Re in the lower subcritical range of Reynolds numbers for smooth uniform flows about smooth circular cylinders, at least for $A/D=0.5$. Obviously, experiments at larger A/D values and Reynolds numbers are desirable.

10. The wake and VIV

The most appropriate place for a brief review of the structures in the wake of a body undergoing VIV at relatively low Reynolds numbers appeared to be between the discussions of the forced and self-excited oscillations. Enormous progress in computers, and in flow visualization and measurement devices, led to the description and classification of the wake states of the simplest bodies, albeit at relatively small Reynolds numbers, and reduced the fundamental questions of VIV from: (a) under what circumstances do the various types of VIV occur; and (b) what are the controlling and influencing parameters in all ranges of $m^*\zeta$; to: (i) why do the vortices in the wake shed as two vortex pairs per cycle under certain conditions and as two single vortices in a cycle (as Karman vortices) under other circumstances; and (ii) what is the role of vortices in the cause and effect relationship between their motion, hysteresis, and the controlling and influencing parameters?

Angrilli et al. (1972) pioneered a number of experiments to establish a relationship between the vortex shedding and the cylinder displacement. They were the first to introduce the concept of 'time of vortex origin' and to suggest that VIV should be called a 'self-controlled' or 'self-regulated' phenomenon rather than a 'self-excited' one since the alternating lift force is not initiated and maintained by the body motion to exist or to persist like galloping. They have carried out experiments with a self-excited cylinder in the range of Reynolds numbers from 2500 to 7000. Fig. 15 shows the successive positions of the vortices. Angrilli et al. (1972) have found that "as long as the oscillation is small, as in Fig. 15(a), vortex trails are not very different from those produced by a stationary bluff body, but for larger oscillations, as in Figs. 15(b–c), the two vortex trajectories must cross each other twice to reach a stable configuration in the wake." Fig. 15(d) shows an unstable configuration.

Zdravkovich (1982, 1990, 1996) was the first to compare the flow visualizations of others about circular cylinders subjected to forced or free vibrations. He suggested that the phase change (about π) in the unsteady lift force near synchronization is connected to a switch in the timing of vortex shedding. This has subsequently been confirmed by Gu et al. (1994) at a relatively low amplitude ($A/D = 0.2$) and by Lu and Dalton (1996) through numerical simulations (Fig. 16). Based on the flow visualization studies of Den Hartog (1934), Meier-Windhorst (1939), Angrilli et al. (1972), Griffin and Ramberg (1974), Zdravkovich (1982) pointed out that two modes of drastically different vortex shedding occur in the lock-in range. At the beginning of the said range, the vortex formed on one side of the cylinder is shed when the cylinder is near the maximum displacement on the opposite side. However, toward the end of the lock-in range, the vortex is shed when the cylinder is near its maximum displacement on the same side. Zdravkovich (1982) also observed that the limit between these two modes is at the reduced velocity at which the maximum amplitude occurs. Öngören and Rockwell (1988a, b), using hydrogen bubbles and hot film, have observed finer details of the vortical structures on either side of the phase shift of π.

Williamson and Roshko (1988, hereafter referred to as W–R) addressed the questions "Why does the vortex formation change its character through synchronization, and why does it change so suddenly at a critical wavelength?" They drove a vertical cylinder along a sinusoidal path ($300 < \mathrm{Re} < 1000$) in a fluid otherwise at rest and photographed the path of suspended aluminum particles on the free surface of the tank. They asserted that the dynamics of the vortices in the near wake is basically inviscid over the said Reynolds number range. As noted earlier, the shear layers could not have yet developed instabilities in the said Re range toward transition and turbulence. Thus, the observations, however ingenious, *may not be relevant to higher Reynolds numbers*. Furthermore, the surfactants (suspended, nondissolvable aluminum particles) are known to affect strongly the position and strength of vortices and vorticity distribution at and near the free surface, particularly at small Reynolds numbers (Sarpkaya, 1996b). They have mentioned that the aluminum-particle technique "has been used in conjunction with a dye method beneath the surface to show that the vortex patterns are similar." However, the results of the dye technique have never been reported (Williamson, 2003).

W–R (1988) described, in the range ($300 < \mathrm{Re} < 1000$), the emergence of various regimes (see Fig. 17) in a map of A/D versus f_{st}/f_{ex} (as well as $\lambda/D = U/f_{ex}D$), where λ is the wavelength. For $U/f_{ex}D$ (or f_{ex}/f_{st}) larger than a critical value, the wake manifests itself *as long attached shear layers*. Two counter-rotating vortex pairs are shed per cycle in the so-called 2P mode, as shown in Fig. 18(a), [from Brika and Laneville (1993)]. The 2P mode is associated with the splitting of a region of vorticity in each half-cycle. The DPIV measurements of G–W (2000) have shown that the vortices of the 2P mode "convect laterally outwards from the wake centerline, causing a downstream oriented jet type flow close to the cylinder, which in turn results in a 'double-wake' type velocity profile." The 2S mode, depicted in Fig. 18(b), represents the alternate shedding of vortices in the classical Karman mode. Fig. 19 is a plot by K–W (1999) of their data ($\mathrm{Re} \approx 3700$) on the map shown in Fig. 17 showing that the Lower-branch regime (see Figs. 2(b) and (c) for definitions) collapses well when plotted against f_{st}/f_{ex}.

The region delineated by $0 < A/D < 0.8$ and $0.40 < f_{ex}/f_{st} < 1.80$ in Fig. 17 has been replotted in Fig. 20(b) in terms of increasing excitation frequency to relate the various modes relative to the changes in the added mass, the

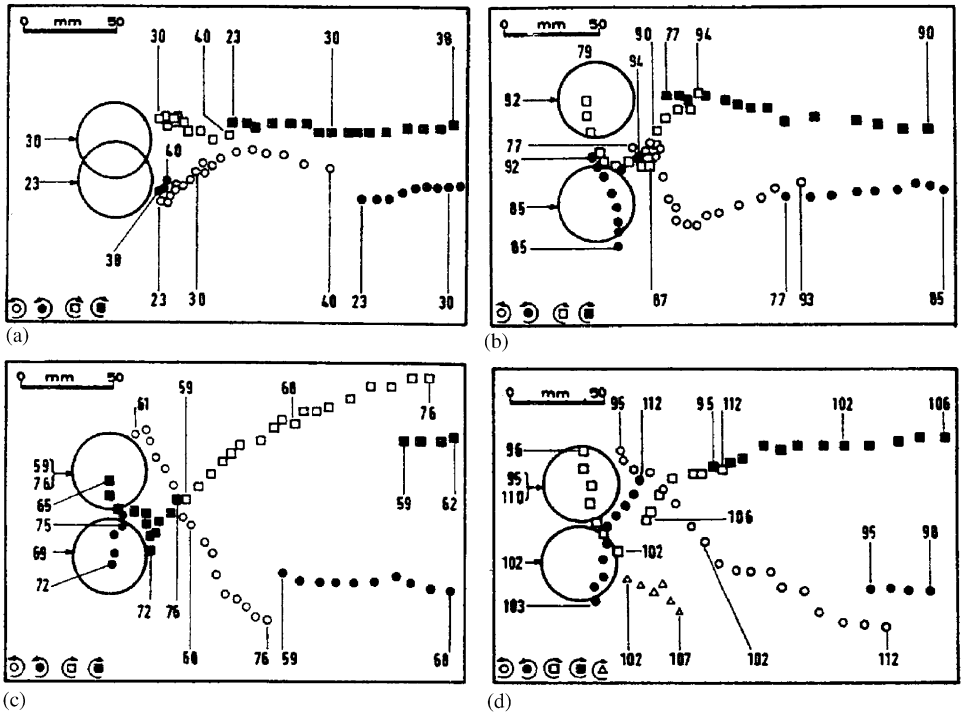

Fig. 15. Correlation between the vortex patterns and the oscillation of an elastically mounted cylinder in the range of Reynolds numbers from 2500 to 7000. The symbols represent the successive positions of the apparent center of vortices: (a) for $f_{ex}/f_{wtr} < 1$, the vortex trails are not very different from those produced by a stationary cylinder; (b) at $f_{ex}/f_{wtr} = 1$, the vortex trajectories cross each other (twice) to reach a stable configuration in the wake; (c) at $f_{ex}/f_{wtr} \approx 1$, the amplitude becomes maximum; and (d) for $f_{ex}/f_{wtr} > 1$, the vortex configuration becomes unstable (Angrilli et al., 1972).

out-of-phase component of the force, and the phase angle in our data (see Figs. 14 and 20(a)), notwithstanding the large differences between the Reynolds numbers of W–R (1988): ($300 < \mathrm{Re} < 1000$), and ours: $\mathrm{Re} = 45\,000$.

Near the left boundary of the 2P mode, in the W–R map, the out-of-phase component of the lift force (energy input to the cylinder) is small and the phase angle is large (about π) as seen in Fig. 20(a). As one approaches the critical curve along a constant A/D line (say, 0.5), the phase angle decreases rapidly, the out-of-phase component of the lift increases towards its maximum (i.e., more energy transfer from the fluid to the cylinder), and the added mass coefficient approaches its minimum value while remaining negative (i.e., the virtual mass of the oscillating system achieves its minimum value for the specific amplitude). On the critical curve, the 2P mode changes rather abruptly to the 2S mode, shown in Fig. 20(b), but only for A/D values smaller than about 0.75. The 2S mode is characterized by the shedding of a single vortex in each half cycle, like Karman vortex shedding, and by rapid increases in $C_L \sin\varphi$, phase angle and the added mass coefficient. In fact, the well-known recirculation bubble of the mean velocity field of the wake of a *stationary* cylinder manifests its presence in the 2S mode, showing that the 2S-mode of shedding, coupled with the cylinder motion, may lead to even more dynamic and organized motion. In particular, the coefficient of lift, enhanced by improved correlation, becomes *even larger than that for a fixed circular cylinder in steady flow*, emphasizing the fact that the use of all active and passive means to prevent the wake from shifting to the 2S mode is most desirable for all practical purposes.

The rate at which the velocity step is increased changes the vorticity generated on the cylinder boundary. The increased vortex strength might precipitate an earlier hysteretic jump in A/D. For small increments, the vorticity generated is small and diffuses faster without making an impact on the strength of vortices or on the energy transferred to the cylinder. The critical value of f_{ex}/f_{st} is an important example. For $A/D = 0.50$, it is seen to be about 0.85 in Figs. 14 and 20(a). According to Carberry et al. (2002), the transition occurs in the range of $f_{ex}/f_{st} = 0.84$–0.87 (for $\mathrm{Re} = 2300$). However, according to W–R (1988), the critical value is at $f_{ex}/f_{st} \approx 0.94$ for $A/D = 0.50$, as seen in Figs. 17 and 20(b). The difference between this value and those noted above may be due to the use of relatively low Reynolds numbers ($300 < \mathrm{Re} < 1000$), as noted above. Even though in the said Re range, and up to about $\mathrm{Re} = 10^4$, the Strouhal number

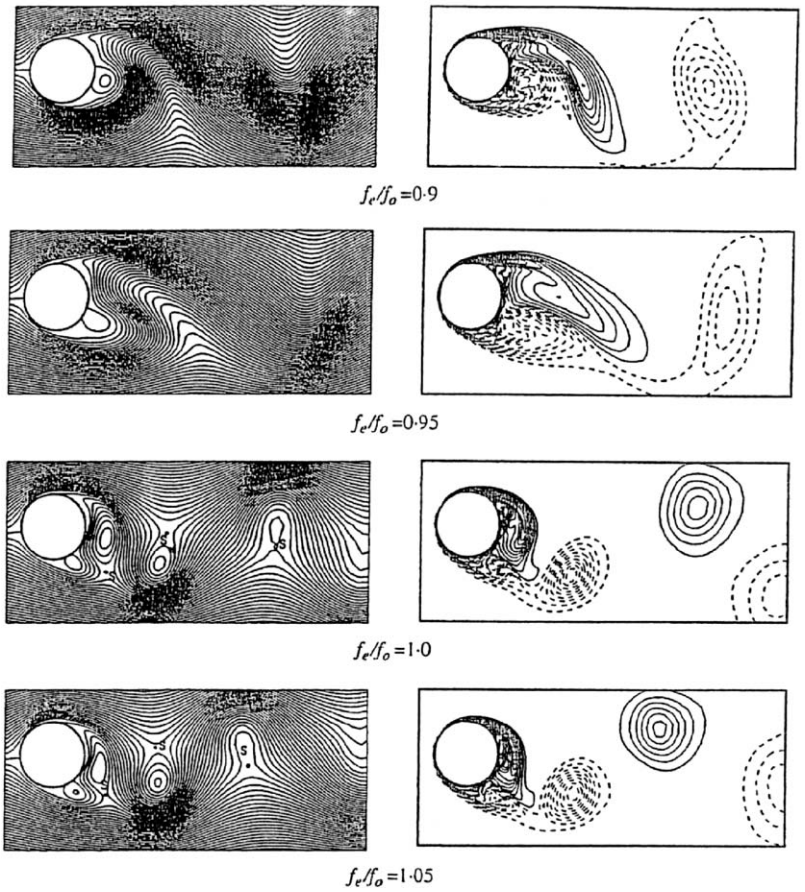

Fig. 16. Instantaneous streamlines (left) and vorticity contours (right) for various f_{ex}/f_{st} ($A/D = 0.4$, Re = 1000). In all cases, the location of the cylinder is at its extreme upper position. At $f_{ex}/f_{st} = 0.95$, a new vortex is being shed from the upper surface. However, at $f_{ex}/f_{st} = 1.0$, the shedding has switched to the lower surface (Lu and Dalton, 1996).

for a stationary cylinder remains nearly constant, the all-the-more important shear layer transition to turbulence for VIV (coherence length and separation angle) occurs at Reynolds number well above 10^3. Apparently, on the basis of what has been said so far, the critical line in Fig. 20(b) needs to be shifted to the left (to the right in the original plot of W–R, Figs. 17 and 20(b) by an amount $\Delta(f_{ex}/f_{st}) \approx 0.10$ at the level of $A/D = 0.5$. Other values of A/D and Re may require different amounts of shift. This will improve the agreement between their map and the data by Brika and Laneville (1993), K–W (1999), and G–W (2000). Finally, it is worth noting that accurate numerical solutions at relatively low Reynolds numbers [e.g., Blackburn and Henderson (1999) at Re = 500] do not find the 2P mode. Evangelinos and Karniadakis (1999) at Re = 1000 found multiple vorticity concentrations and transient mixtures of (P + S) and 2P modes in the near wake and general wake instability further downstream. The repeat of the W–R (1988) experiments in a closed system at Reynolds numbers larger than 1.5×10^4, without the use of surfactants, is most desirable in both the forced and self-excited oscillations. Rodriguez and Pruvost (2000) used a vertical tank, a slightly heated metal cylinder, spanning the width of the test section, and the schlieren technique (based on variations of the liquid refraction index with temperature). Experiments were conducted at a Reynolds number of 700, at eight different amplitudes ranging from $A/D = 0.125$ to $A/D = 1$. The vortex-shedding phase was defined with respect to the cylinder position y/A at the time of shedding. A vortex is considered shed when it is cut from its feeding sheet in a manner similar to that introduced by Sarpkaya and Shoaff (1979) in their discrete vortex simulation of flow-induced vibrations. Rodriguez and Pruvost (2000) spanned the synchronization region by varying the cylinder oscillation frequency (f_{ex}) in small steps while holding the amplitude A/D constant at one of the desired values. They have measured the prevailing vortex shedding frequency f_{vs} *in the wake*, as previously done by Cheng and Moretti (1991). They have presented extensive data and photographs (see Fig. 21) for a large number of subharmonics. Their methods of identifying the

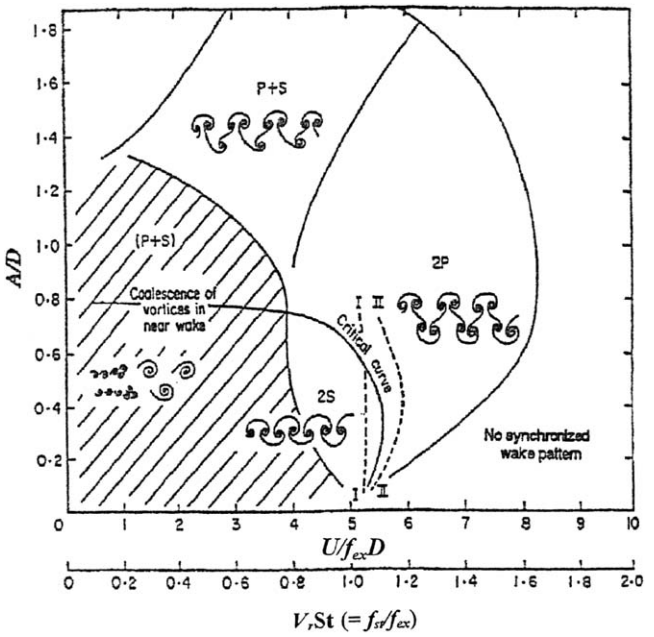

Fig. 17. Map of vortex patterns of a vertical cylinder forced to move along a sinusoidal path in the Re range of $300 < \mathrm{Re} < 1000$. The critical curve marks the transition from one mode of vortex shedding to another (Williamson and Roshko, 1988).

various phenomena and their use of significantly different notations (e.g., L and U for the vortices shed from the lower and upper sides of the cylinder) made their results somewhat difficult to interpret. Nevertheless, Rodriguez and Pruvost (2000) have substantiated the fact previously noted by Blevins (1990) that the maximum lift coincides with the shedding of the L-vortices and the minimum lift with that of the U-vortices. This is because the shedding of an L-vortex causes the separation point on the upper surface to move *downstream*. This, in turn, accelerates the flow on the top surface and increases the lift. Rodriguez and Pruvost (2000) have also noted that the motion of a cable (their primary objective) is directly related to the nature of the coupling of the numerous synchronization ranges and therefore it is important to assess whether such coupling can occur in the range of $0 < A/D < 1$ and, how and when the transition from one mode to another occurs if the velocity in the far-field varies with time.

It has been known since the 1960s that the transition, the wake states on either side of the transition, and the way in which they occur depend on the governing parameters and the Schewe parameters given by Eqs. (2) and (17). The singling out of a frame or two in the high- or low-phase regions of the oscillation is not too meaningful because the inertial forces called into action prevent an abrupt rupture of the prevailing conditions where there can be almost seamlessly incremental transitions from cycle to cycle. As noted earlier, Krishnamoorthy et al. (2001) have observed that "the phase switch does not occur abruptly. Instead, over several cycles of cylinder oscillations, both 'in-phase' and 'out-of-phase' vortex shedding occur during the transition." Other work dealing with the comparison of the wake states of free and forced oscillations is deferred to the next section for reasons which will become clear later.

11. Self-excited vibrations

Numerous contributions have been made toward the understanding of the kinematics and dynamics of self-excited vibrations of mostly circular cylinders: Marris and Brown (1963), Koopmann (1967b), Feng (1968), Di Silvio (1969), Angrilli et al. (1972), Griffin (1972), Griffin and Ramberg (1974), Gowda (1975), Di Silvio et al. (1975), Stansby (1976), Griffin and Koopmann (1977), Dean et al. (1977), Zdravkovich (1982, 1990, 1996), Williamson and Roshko (1988), Brika and Laneville (1993), Vandiver (1993), Moe et al. (1994), Sarpkaya (1995), Skop and Balasubramanian (1997), Hover et al. (1997), Hover et al. (1998), Atsavapranee et al. (1998), Zhou et al. (1999), Khalak and Williamson (1999), Govardhan and Williamson (2000), Pesce and Fujarra (2000), Davis et al. (2001), Laguë and Laneville (2002), Voorhees and Wei (2002), and on numerical simulations of long flexible cables by Newman and Karniadakis (1997), Bartran et al.

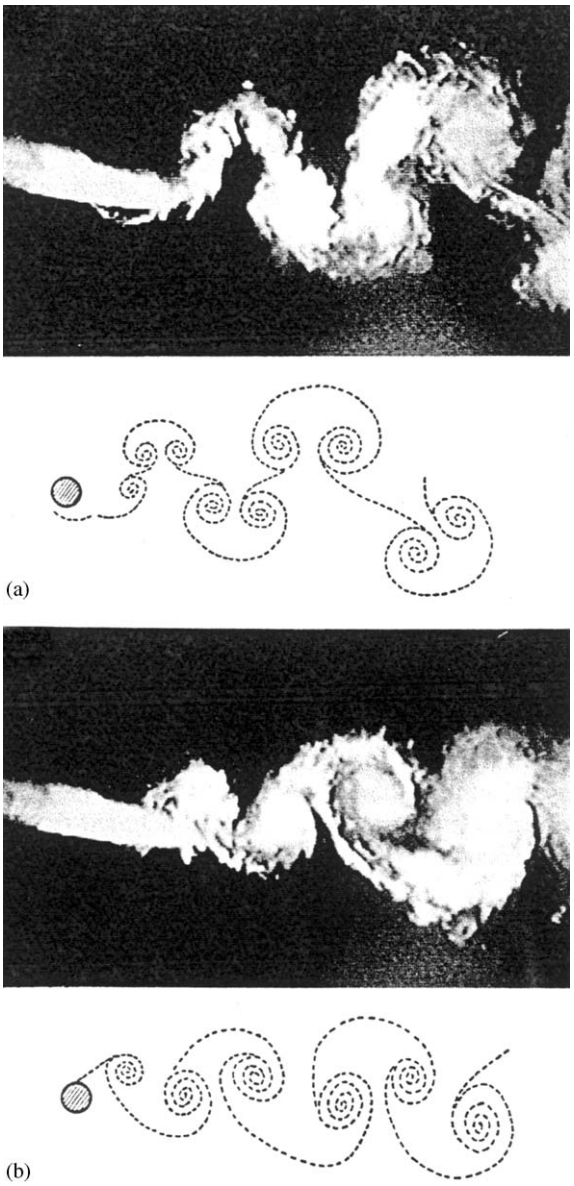

Fig. 18. Photographs and sketches showing the two near-wake patterns responsible for the hysteresis loop ($V_{rb} = 0.93$, Re = 7350). (a) 2P mode ($A/D = 0.40$); (b) 2S mode ($A/D = 0.27$). Both photographs are taken at maximum negative displacement of the cylinder (Brika and Laneville, 1993).

(1999), Evangelinos and Karniadakis (1999), Triantafyllou et al. (2003). Here only a few of these contributions will be discussed in some detail.

As noted earlier, the most interesting phenomena in VIV are hysteresis and lock-in/lock-out. For a given system, the occurrence of hysteresis depends on the approach to the resonance range—the rate of change of the velocity (with small or large increments or decrements) from a low or from a high velocity. The jump condition (double amplitude response) originates in the fluid system, and not, as once thought, in the cylinder elastic system.

Marris and Brown (1963) were interested with the elastic response of Pitot tubes under normal operating conditions. Each tube was cantilevered (in its plane of motion) to one of the walls of a water channel and subjected to uniform flow in the range ($1000 < \mathrm{Re} < 2000$). Marris and Brown were able to change the length of the tube and hence its frequency. They have determined two lengths (and hence two frequencies) one of which was 35% larger than f_{st} and the other,

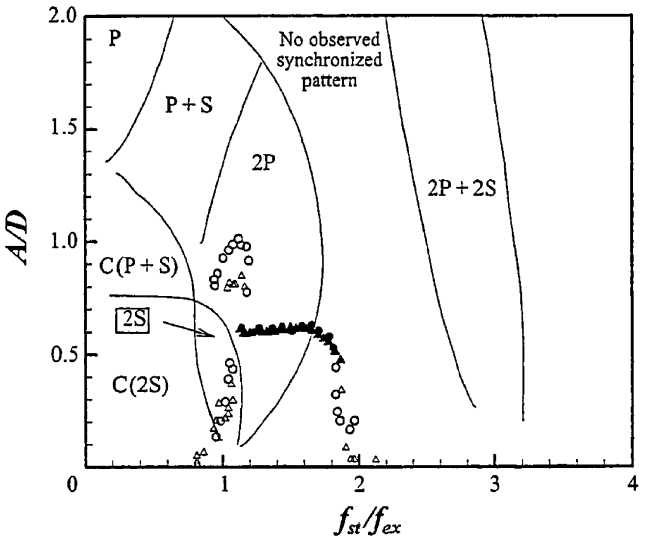

Fig. 19. A/D for Re $\approx$ 3700 and two m^* values, plotted in the Williamson-Roshko (1988) map: ○, $m^* = 1.19$ and $(m^* + C_A)\zeta = 0.011$; △$m^* = 8.63$ and $(m^* + C_A)\zeta = 0.0145$. Solid symbols indicate the Lower-branch regimes (Khalak and Williamson, 1999; Govardhan and Williamson, 2000).

about 35% lower than f_{st}. Thus, they were able to bracket the synchronization range of the tubes. To the best of our knowledge, no one has ever varied the frequency of the test beam by changing its length (and, of course, mass and damping ratios), except in industrial applications to avoid synchronization.

Feng (1968), inspired by Professor G.V. Parkinson, made one of the more widely known contributions to VIV. Experiments were carried out in a wind tunnel with a single-degree-of-freedom flexible cylinder with $m^* = 248$, $\zeta = 0.00103$ and $m^*\zeta = 0.255$, as shown in Figs. 1 and 2(a). Feng measured f_{ex}, f_{st}, A/D, and the phase angle φ for three types of experiments: (a) the cylinder started from rest at a prescribed velocity U; (b) the velocity was increased by small increments while the cylinder was oscillating at a steady state amplitude; and (c) the velocity was decreased by small increments while the cylinder oscillated at a steady-state amplitude. His phase and A/D data were presented as a function of $V_r = U/f_{\text{vac}}D$. For the first type of experiments, Feng found that for V_r less than about 5, A/D is very small (the inception phase of oscillations) and the frequency of excitation of the cylinder, f_{ex} is smaller than f_{vac} and f_{vs}. For V_{r} larger than about 5, f_{vs} and f_{ex} became one and the same or, what we prefer to call, the common frequency f_{com}, i.e., the lock-in occurred. The amplitude smoothly rose to a maximum value of $A/D = 0.32$ at about $V_r = 6$. However, at $V_r \approx 7$, lock-out occurred, i.e., the vortices returned to their Strouhal relationship and the cylinder, to a frequency very close to f_{vac}, and, with further increases in velocity, the amplitude dropped to negligible values near $V_r = 8.6$.

For the second type experiments (velocity increased by small increments while the cylinder was oscillating), the amplitude reached a much higher value ($A/D = 0.53$) at about the same V_r (≈ 6) where the maximum of ($A/D = 0.32$) occurred in the previous case. However, when V_r reached a value of about 6.4, A/D dropped sharply to the value that was reached from rest at the same wind speed. This drop was accompanied by a change of about 35° in phase and, most certainly, by a change in the wake structure. When the speed was decreased, the amplitude data followed the 'steady flow' case up to a special V_r value of 5.9 at which a second 'smaller' jump back to the higher values occurred. This resulted in a *clockwise oscillation hysteresis loop*, as shown in Fig. 1. This jump was accompanied by a phase change of about 60° and a *counter-clockwise phase-hysteresis loop*, signaling very interesting changes in the shedding mode of vortices.

There are a number of similarities as well as differences (e.g., the synchronization and hysteresis covered by the velocity range, jumps in the phase) between the data obtained by Bishop and Hassan (1964), Feng (1968), and Brika and Laneville (1993), and for a flexible cylinder by Wu (1989), Saltara et al. (1998), and Pesce and Fujarra (2000), probably due to the differences in A/D, Re, m^*, ζ, the test bodies (cable and rigid cylinders), and the Schewe parameters.

Brika and Laneville (1993, hereafter referred to as B–L) performed a series of very thorough and well-documented experiments in a wind tunnel with a *flexible circular tube* ($m^* = 2054$) in the range of relatively low Reynolds numbers (from 3.4×10^3 to 11.8×10^3) and small damping ratios (from $\zeta = 0.83 \times 10^{-4}$ for small amplitudes to $\zeta = 2 \times 10^{-4}$ for

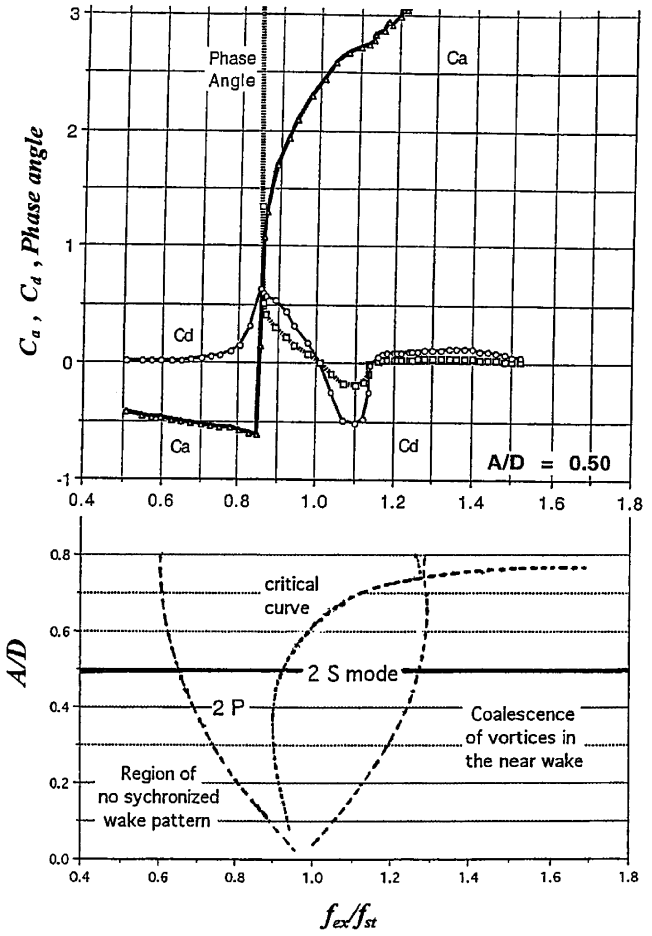

Fig. 20. Top half: Sarpkaya's data shown in Fig. 13, Re = 45 000; bottom half: a replot of Williamson-Roshko (1988) map ($300 < \mathrm{Re} < 1000$).

higher amplitudes, up to a maximum of $A/D = 0.52$). A flexible cylinder was to simulate half of the wavelength of a vibrating cable and to eliminate the end effects. B–L (1993) have performed tests in two regimes: PR: the 'progressive regime' in which the velocity of air was either (a) increased or (b) decreased *at small increments* while the cylinder was oscillating at its steady state amplitude; and, IR: the 'impulsive regime' in which the velocity of air was fixed and the cylinder was either (a) released from rest, or (b) externally excited by a shaker, at an amplitude A/D of the order of 0.85, and then released. Furthermore, as an additional experiment, the regime of PR-a was repeated using a velocity step *twice as large* as the original small step. Fig. 22 shows a comparison of the data obtained in the impulsive regimes with those obtained in the progressive regime as a function of $V_{rb} = (V_r/2\pi) = U/2\pi f_{ex}D$. It should be noted that B–L (1993) have plotted their data using f_{ex} in defining V_r rather than f_{vac} (the so-called undamped natural frequency). However, the two frequencies in their in-air experiments do not differ much.

The obvious and striking features of the data shown in Fig. 22 are their similarity to those obtained by Feng (1968). The hysteresis emphasizes once again the fact that 'one can go a little further if one goes slower and then jumps to where one should be' or 'one jumps sooner, a little higher, if one goes faster, and then ends up at the same A/D'. The phase angle (not shown here) follows the jumps in A/D quite faithfully. In the regime PR-a, (small increments in velocity), A/D increases and reaches 0.53 at $V_{rb} = 1$. The next step (at $V_r \approx 1.01$) is into an abyss that reduces A/D to 0.38 (i.e., onto the data for PR-b, the small decrement line) and increases φ by about 70°. Subsequently, A/D decreases to very small values at $V_r \approx 1.31$. If the regime PR-a is repeated with a larger step, as noted above, the amplitude data follows the PR-a (small increment data) up to $A/D = 0.13$ ($V_r \approx 0.87$) and then jumps to $A/D = 0.40$ and then continues to decrease as in the case of PR-a (small increment). Obviously, it takes a sufficiently large velocity increment (at the right

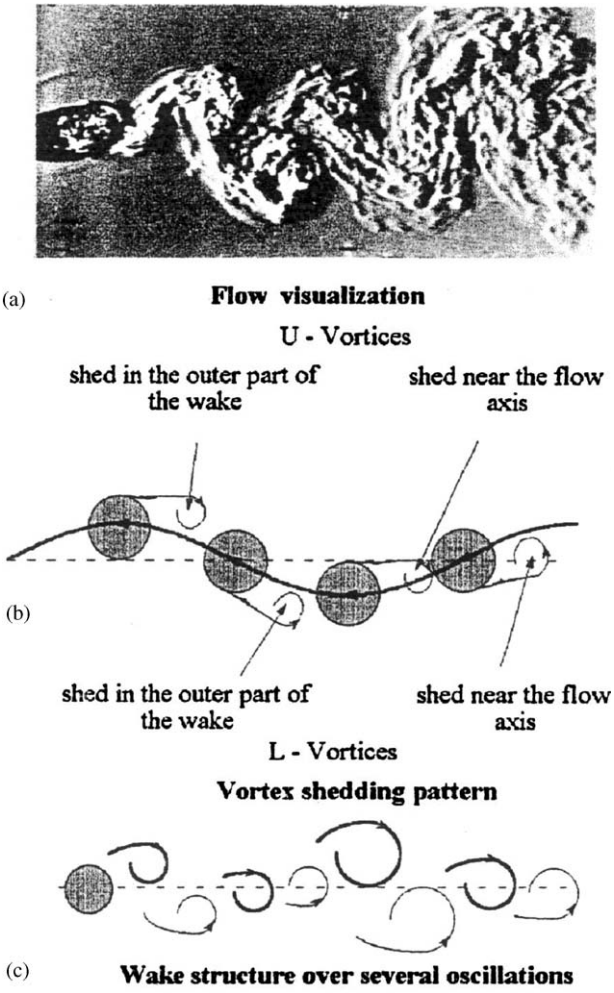

Fig. 21. Wake vortex structure over several oscillations of a heated cylinder for $f_{ex}D/U = 0.109$, $f_{ex}/f_{vs} = 1/2$ and $A/D = 0.237$: (a) shows the flow past the transversely oscillating cylinder; (b) depicts the motion of the cylinder relative to the ambient flow and the shedding of the upper (U) vortices (at $y/A = \pm 1$) and the lower (L) vortices (at $y/A = 0$); and (c) shows that the alternate shedding of the L- and U-vortices, coupled with the direction of the half cycle, creates a wake with two vortices convected on either side of the axis, followed by two vortices convected along the axis for $f_{ex}/f_{vs} = 1/2$ (Rodriguez and Pruvost, 2000).

time) to force the vortices to change to a new configuration sooner. In the absence of a stronger impulse, a stronger velocity, arrived at gradually, serves the same purpose. However, a closer look at the data and the amplitude traces (not reproduced here) reveal that there are subtle differences between the two modes. For example, in the narrow range of $V_r = 0.88$ and 0.95, there are two possible steady state amplitudes for a given velocity as far as the pre-excitation procedure (IR-b) is concerned. B–L (1993) have pointed out that for velocities larger than the synchronization onset velocity ($V_{rb} = 0.78$) and smaller than the lower critical velocity (LCV), the recording of the amplitude build-up from rest show intriguing behavior. While the system first tends toward an *unavailable final state* on an imaginary extension of the Lower branch ($V_r < 0.88$), it suddenly departs, at a point defined by a break in the envelope curve, toward a second and available steady state of the Upper branch. Such bifurcations in the envelope curves are accompanied by an abrupt change in the phase angle and in the wake flow regime.

B–L (1993) have ascertained that the phase remains constant along the cable (a flexible tube) within $\pm 5^\circ$ and concluded that the flow mode is not affected by the variation of the vibration amplitude along the cable and that their results should be comparable with those obtained with uniform rigid cylinders. Fig. 18, presented earlier, shows their photographs as well as sketches of the two near-wake vortex patterns responsible for the hysteresis loop ($V_{rb} = 0.93$,

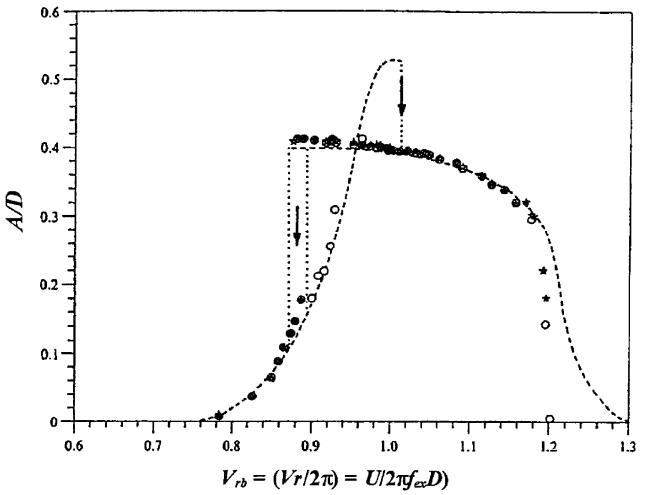

Fig. 22. The steady state vibration amplitude A/D of the impulsive regimes as a function of $V_{rb} = (Vr/2\pi) = U/(2\pi f_{ex}D)$ is compared with the results of the progressive regime: ★, from rest; ○, from a pre-excited amplitude; - - - - , progressive regime (Brika and Laneville, 1993). The similarity of their data to those obtained by Feng (1968) is quite striking (Brika and Laneville, 1993).

Re = 7350) when the cable is at $y = -A$. The upper half shows the 2P mode at $A/D = 0.40$ and the lower half the 2S mode at $A/D = 0.27$. According to Fig. 17, $V_r = 5.84$ ($V_{rb} = 0.93$) does not intersect the critical curve and the vortex shedding mode should be 2P for both cases. However, the large differences in the Reynolds numbers used by W–R (1988) and B–L (1993), amplitude variations along the cable used by Brika and Laneville, and the small or large increments or decrements of velocity imposed on the ambient flow, or the release of the cable from a pre-excited state may lead to different wake states. It appears that 2P → 2S mode jump is most sensitive to hysteresis, as intimated by B–L (1993). This may, in part, be because the 2P mode is the most precarious, and the 2S mode is the most robust of all the known modes.

Clearly, many ways exist (some yet untried) to lead a body to excitation with unimaginable jumps and hysteretic behavior, even without the effect of neighboring bodies (multiple tubes or cables). These may exhibit distinctly different excited modal shapes and hysteresis. The foregoing confirms the fact that the dynamics of the wake is very responsive to changes imposed on the kinematics of the flow and the fact (stated earlier) that $(D/U_0^2)(\mathrm{d}U/\mathrm{d}t)$ must be quantified during both the acceleration and deceleration periods for one to understand the effect of the rate of change of velocity on the inception of the transient states in both the numerical and physical experiments. Only then can one go beyond the identification of the vortex positions and types of shedding for a given experiment to further the state of the art toward prediction.

B–L (1993) compared their work with the contributions of Feng (1968) and Bishop and Hassan (1964), as shown in Fig. 23. The similarities as well as differences (the synchronization and hysteresis covered by the velocity range, jumps in phase) between the three studies are probably due to the differences in A/D, Re, mass parameter, damping, the test bodies (cable and rigid cylinders), end conditions, and the Schewe parameters. These need not be discussed here in further detail.

Sarpkaya (1995) discussed the significance of two-directional or biharmonic free oscillations (in both the in-line and transverse directions) in light of experiments undertaken for that purpose, to simulate more closely the true nature of flow-induced vibrations. His data, reproduced here as Fig. 24, have shown that the variation of A/D with V_r for the case of '*the same natural frequency in both directions*' yields about 20% larger amplitudes over a 20% larger $V_r\mathrm{St} = f_{st}/f_{ex}$ range for a Reynolds number of about 35×10^3. However, the variations of A/D for other natural frequency ratios (in-line versus transverse) are considerably more difficult, indicating dramatic changes in the wake. Moe and Wu (1990) have noted that the separation points and pressure distribution are strongly affected by the previous history of the motion and the average forces differ from the forces at the average amplitude due to the strong nonlinearity of the in-phase and out-of-phase components of the transverse force. Jong and Vandiver (1985) and, subsequently, Vandiver and Jong (1987) studied the identification of the quadratic system relating cross-flow and in-line VIVs and the relationship between the in-line and cross-flow vortex-induced oscillations of cylinders. They have concluded that a strong quadratic relationship exists between the in-line and cross-flow motions under both lock-in and non-lock-in conditions and that

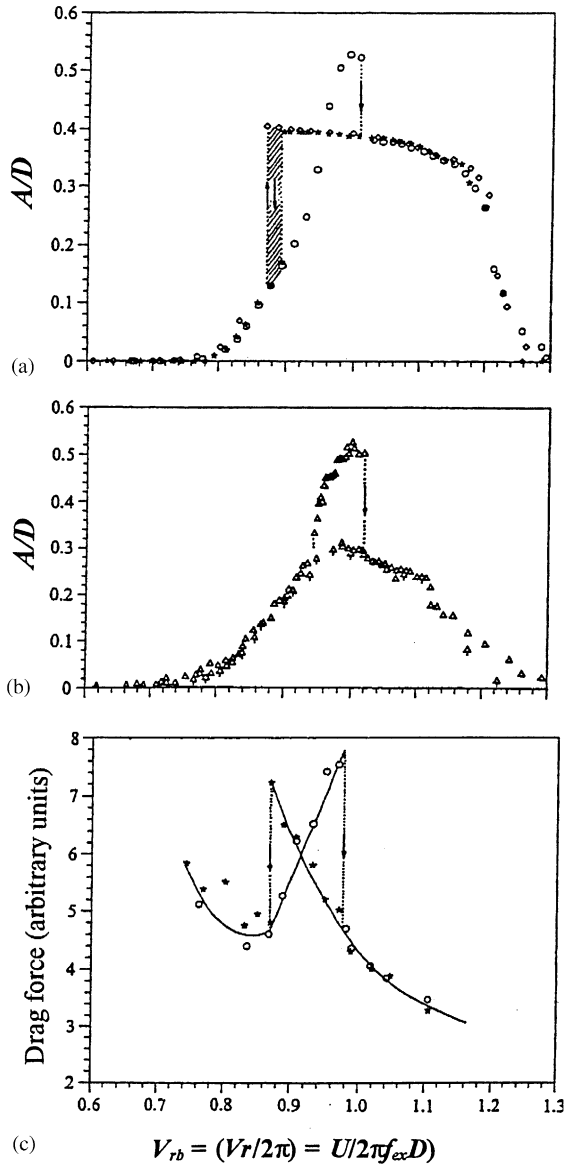

Fig. 23. Comparison of Brika and Laneville's data (1993) with those of Feng (1968) and Bishop and Hassan (1964). For symbols see Fig. 22 and Brika and Laneville (1993).

the well-known frequency doubling phenomena in the in-line response is a consequence of such a quadratic correlation. In other words, the motions in two directions are *not independent* of each other. As noted in Section 4, added mass is a function of the type of motion of the body. Thus, the added mass of a cylinder undergoing 2-dof oscillations (tracing the path of figure *eight*) is not the same as that of a cylinder constrained to move only in the transverse direction. The issue is further complicated by the differences between their dynamics (correlation length, kinetic energy imparted to the cylinder, and the phase angle). Only Jauvtis and Williamson (2002), while experimenting with a cylinder (with the same in-line and transverse natural frequency of 0.4 Hz) in two degrees of freedom, found that "the freedom to oscillate in-line with the flow affects the transverse vibration surprisingly little" and argued that the studies of the past (presumably at lower Reynolds numbers) on bodies "restrained to move only laterally to the fluid flow remain relevant and valid for the problem of VIV of a body in two degrees of freedom." In direct contradiction, Marcollo and Hinwood (2002) found, in connection with their work on 'the cross-flow and in-line responses of a long flexible cylinder subjected to

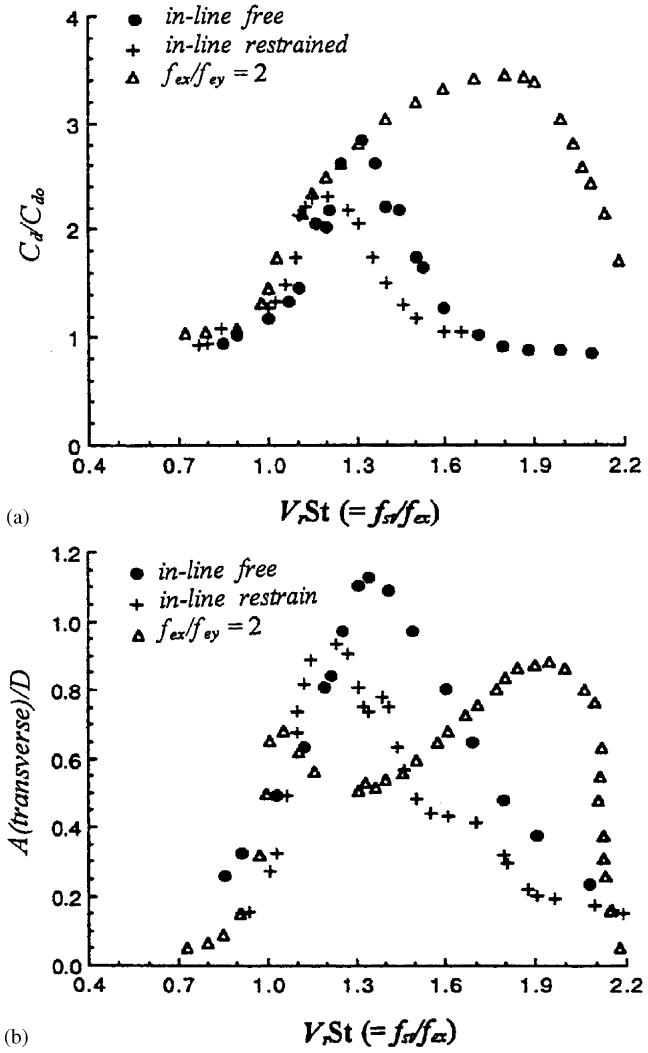

Fig. 24. (a) the normalized drag coefficient; and, (b) A/D are shown for three cases for Re = 35 000: (1) in-line free, (2) in-line restricted, and (3) $f_{ex}/f_{ey}=2$. It is seen that both C_d/C_{do} and A/D for the case of '*the same natural frequency in both directions*' yield about 20% larger values over a 20% larger V_rSt$(=f_{st}/f_{ex})$ range. However, the variations of A/D for other natural frequency ratios (in-line versus transverse) are considerably more complex (Sarpkaya, 1995).

uniform flow,' that "The in-line vibration is found to have a strong dependency on the cross-flow vibration and is forced at frequencies very different to that which would be predicted a priori." It is obvious from the foregoing and from a more careful perusal of our data shown in Fig. 24 that the interaction of cross-flow and in-line oscillations leads to substantially different results from those found at smaller Reynolds numbers. As we shall discuss later, the field data at large Reynolds numbers are in conformity with our findings.

Hover et al. (1997) pioneered a force-feedback model (FFM) for use in a laboratory environment. FFM allows modelling of complex structural dynamics, while fully accounting for the fluid–structure interaction. This is particularly significant since VIVs of cables and pipes alter the static configuration and induce additional static and large dynamic loads. The force-feedback scheme can address a range of free-vibration states, including multiple modes, traveling waves, and other nonlinearities. The use of FFM in industrial applications requires the development of appropriate hydrodynamic models. However, FFM's ability to help to sort out the differences between the single- and multi-mode cases and to understand the additional mechanisms that help to organize the wake [and possibly modify the correlation length and the mode transitions, Hover et al. (2002)] throws additional light on the intrinsic nature of VIV.

K–W (1999) and G–W (2000) conducted a series of experiments with elastically mounted rigid cylinders at relatively small Reynolds numbers (increasing with V_r from about 2000 to 10 000). Their results are briefly summarized below.

(a) There are two distinct types of system responses, depending on whether the combined mass-damping parameter ($m^*\zeta$) is high or low.

(b) At high $m^*\zeta$ (e.g., 0.255), there are only two branches: an 'Initial excitation branch' (or, a combined Initial-Upper branch), which yields the maximum amplitude for the case under consideration depicted in Figs. 1 (triangles) and 2 (diamonds), and a 'Lower branch', encountered in earlier experiments (Feng, 1968; Brika and Laneville, 1993; Saltara et al., 1998; Pesce and Fujarra, 2000). The 'Initial' and 'Lower' branches are separated by a continuous mode transition. At low $m^*\zeta$ (e.g., 0.013), there are *three* branches, as seen in Fig. 2 (black symbols): an 'Initial branch' which no longer yields the maximum amplitude, an 'Upper branch' which now yields the highest amplitude (both in the region where Re < 5000), and a 'Lower branch' which exhibits better periodicity.

(c) It has been shown by a number of investigators (Hover et al., 1998; B–L, 1993; G–W, 2000) that the 2S mode occurs in the initial (quasi-periodic) and in the initial (periodic) regions. The shedding mode changes to 2P in both the Upper and Lower branches. However, the two vortices of each pair in the Upper branch have quite unequal strengths whereas they are of about equal strength in the Lower branch. Finally, the Initial $\leftrightarrow$ Upper branch transition is hysteretic, but the Upper $\leftrightarrow$ Lower transition exhibits intermitting switching. The switch in the timing of vortex shedding is coincident with the phase jump (ϕ_{total}).

The maximum lift (r.m.s.) occurs at the transition between the Initial excitation and the Upper branch. It is indeed very low in the Lower branch. It is often stated that the phase angle in the subject transition "remains at just above 0°" (K–W, 1999). Clearly, the said phase angle must be greater than zero in order for the lift coefficient to remain finite according to our Eq. (14).

(d) G–W (2000) argued that "the range of synchronization is controlled primarily by m^* (when $m^*\zeta$ is constant), whereas the peak amplitudes are controlled principally by the product of $m^*\zeta$." Their observations at low Reynolds numbers and low-mass ratios do not refute the long-standing concerns of Sarpkaya (1978, 1979) and Zdravkovich (1990) regarding the use of a combined mass-damping parameter.

(e) G–W (2000) have shown, for two values of m^* (1.19 and 8.63) or $(m^* + C_A)\zeta$ (0.0110 and 0.0145), that the Lower-branch regimes collapse well when plotted against f_{st}/f_{ex}. Furthermore, the amplitude and the region of synchronization correlate with U/Df_{com} for a constant value of small $m^*\zeta$ (0.014, 0.017, 0.019). These empirical correlations need to be confirmed at much higher Reynolds numbers with other sets of $m^*\zeta$ for small, intermediate, and large values of $m^*\zeta$.

(f) Finally, as noted earlier, K–W (1999) and, subsequently, G–W (2000) have introduced a frequency ratio $f^* = [(m^*+C_A)/(m^*+C_a)]^{1/2}$ where "C_a is an 'effective' added-mass coefficient that includes an apparent effect due to the total transverse fluid force in phase with the body acceleration," i.e., C_a is the *added mass coefficient*, as defined in this paper. In fact, f^* is nothing more than the ratio of the oscillation frequency, based on the unknown 'prevailing' virtual mass, to the 'in still-water frequency,' obtained from pluck tests, i.e., $C_A = 1$. Thus, contrary to their assertion, f^* is not based on the equations of motion. Furthermore, numerical solutions of the 'exact' equations of motion do not need, do not depend on, and do not give rise to such arbitrary combinations of in-still-water virtual mass (m^*+C_A) and the actual virtual mass (m^*+C_a). Nevertheless, f^* has been used in the past and gives an indication of the motion in both forced and free vibration experiments. However, more recent experience has shown that the use of other normalized parameters (e.g., f_{ex}/f_{st}, f_{ex}/f_{vac}) are preferable and consistent with those used in numerical simulations.

K–W (1999) and G–W (2000) concluded, on the basis of their experiments with $m^* = 1.19$, 2.22, and 8.63, that "C_a is a constant along the Lower branch" and "it has the same constant value for all other m^*" and "$C_a = -0.54 \pm 0.02$". It is very important to note that they have assumed mass-damping ($m^*\zeta$) to be small. They have noted that "our deduced value for C_a is consistent with results from forced oscillations by Gopalkrishnan (1993), where he finds $C_a \approx -0.60$ in a large region of the (A/D versus f_{st}/f_{ex}) plane, encompassing the complete domain of the Lower branch." This is not quite true. In K–W's (1999) and G–W's (2000) experiments, the start of the Lower branch is at $f_{ex}/f_{st} = 0.87$ and the end is at $f_{ex}/f_{st} = 0.54$. In terms of Gopalkrishnan's nondimensional frequency ($f_{ex}D/U$), the said limits are at 0.104 and 0.160. It should be noted that the critical phase change in Gopalkrishnan's experiments occurs at $f_{ex}/f_{st} = 0.83$ and not at 0.87. In any case, the fact is that in the range of the limits of the Lower branch, C_a in Gopalkrishnan's plot (his original Fig. 3.16) rises from –0.3 to –0.6 as f_{ex}/f_{st} decreases from 0.83 to 0.70 and remains thereafter nearly constant at –0.60 for $A/D \leqslant 0.6$. For larger values of A/D, C_a is limited by –0.30 on either side of the boundaries of the Lower branch. The important fact is that C_a is not a constant and depends on A/D and all other parameters that determine A/D. Notwithstanding these facts, one must note that Gopalkrishnan's added mass data is rather sketchy. Sarpkaya (1978) presented detailed drag and added mass coefficients obtained by

using forced oscillations. His C_a data are reproduced here as Fig. 25 where the original $U/f_{ex}D$ axis or V_r is multiplied by 1.13 to match the Strouhal numbers at critical transitions. Thus, it is necessary to carry out detailed experiments by maintaining m^* constant (at a relatively small value) and by systematically increasing or decreasing the damping and hence the amplitude of the oscillations to investigate whether one would obtain C_a values higher or lower than –0.54.

Triantafyllou et al. (2003) have carried out experiments with a single rigid cylinder (1-dof) and a single flexible cylinder (pinned beam, 2-dof) at the 2-dof-Carriage research facility of the Massachusetts Institute of Technology, hereafter referred to as MIT. The experimental conditions were as follows: Re $=3\times10^4$, Aspect ratio $=$ 26, $m^*=3.0$, and $\zeta=0.035$, and $m^*\zeta=$ 0.105. The results are shown in Fig. 26. The amplitude A/D (1/10th highest average, treating the response as a random process) of the 1-dof rigid cylinder reaches a maximum just a little over 1.0 at $V_r\approx5.6$ and reduces to very small values after $V_r\approx11$. What is perhaps most important is the absence, rather than the presence, of some observations made at lower Reynolds numbers with low $m^*\zeta$: a hysteretic jump from the Initial excitation branch to the Upper branch (as in Fig. 2). In fact, the variation of A/D, in Fig. 26(a), from its inception to its maximum proceeds rather smoothly. This may be either due to the fact that in the experiments of Triantafyllou et al. (2003), $m^*\zeta$ ($=0.105$) is not small enough or the Reynolds number in G–W's (2000) experiments is not high enough for the Gerrard–Bloor transition waves in the free shear layers to disappear and the shear layer transition to reach its maximum upstream temporal mean position. In other words, the Initial branches observed at low $m^*\zeta$ and at low Re may be a consequence of incomplete transition in the shear layers or, in other words, a low-Reynolds number effect. Experiments are needed with $m^*\zeta<0.01$ where the minimum Re at $V_r=3$ is larger than about 15 000 to resolve the existence or absence of various regimes in the A/D versus V_r plot at industrially significant Reynolds numbers.

Fig. 26(b), for the flexible cylinder (a pinned beam with 2-dof), shows essentially the same overall behavior as that for the rigid cylinder as far as the absence of various 'branches' are concerned. However, the position of the maximum A/D is shifted to larger V_r (about 7) and to larger A/D (about 1.5). Fig. 26(c) shows the motion trajectories of the flexible cylinder. It is evident from the in-line force coefficient as well from Fig. 26(c) that the largest excursions in the drag direction occur at $V_r\approx5.5$, not at $V_r\approx7$ where the maximum amplitudes occur in the transverse direction. Clearly, the maxima of the in-line and transverse oscillations do not occur simultaneously, as seen in Figs. 26(b) and (c), the former precedes the latter. Also the larger in-line amplitudes in the range of $4<V_r<6$ suggest improved and sustained correlation conducive to in-line forces.

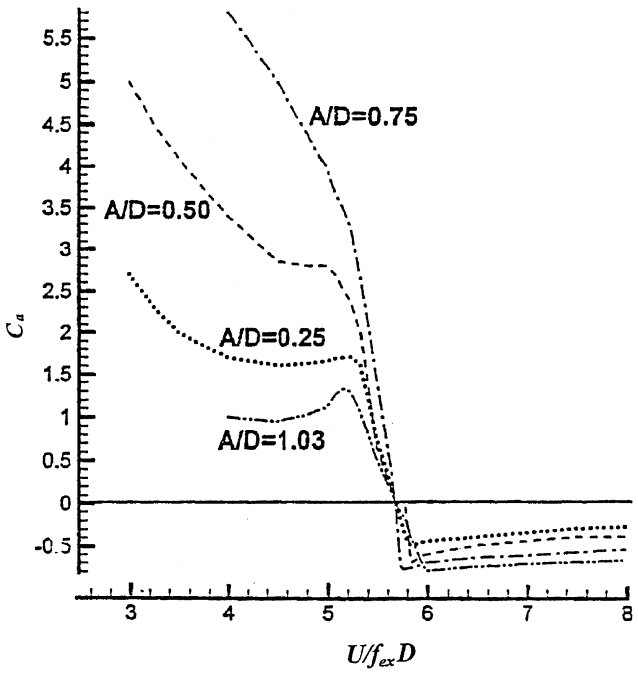

Fig. 25. Variation of the inertia coefficient C_a (in-phase component of the transverse force) with $V_r=U/f_{ex}D$ for representative values of A/D [from Sarpkaya (1978); V_r is multiplied by 1.13 to match the Strouhal numbers at critical transitions].

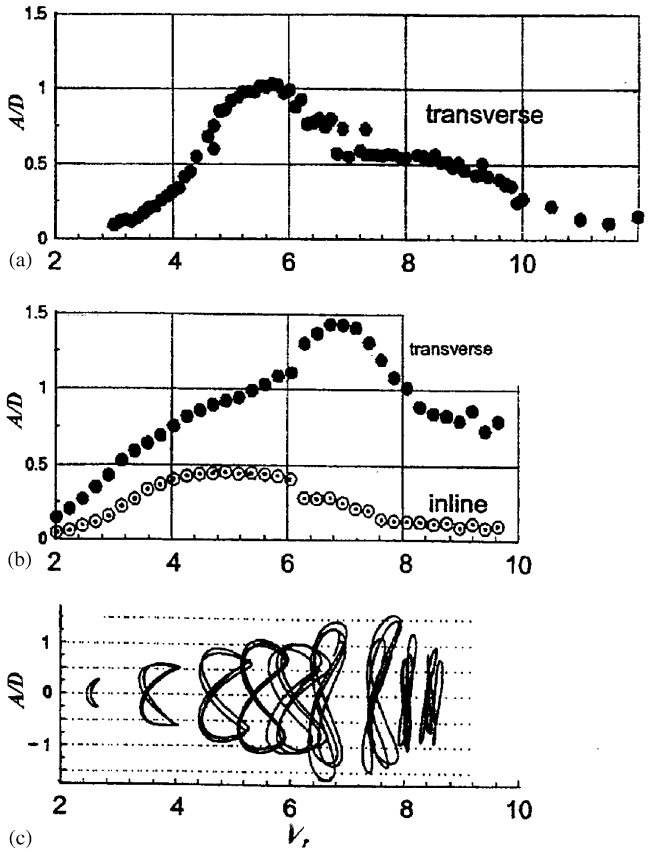

Fig. 26. (a) One degree of freedom rigid cylinder (Re = 30 000, $L/D = 26$, $m^* = 3.0$, $\zeta = 0.035$, and $m^*\zeta = 0.105$). The amplitude A/D ($\frac{1}{10}$th highest average) reaches a maximum just a little over 1.0 at $V_r \approx 5.6$. There is no upper branch, but only a smooth increase in A/D. (b) A flexible cylinder (a pinned beam with 2-dof) exhibits essentially the same overall behavior. However, the position of the maximum A/D is shifted to larger V_r (about 7) and to larger A/D (about 1.5). (c) The maxima of the in-line and transverse motion trajectories do not occur simultaneously, the former precedes the latter, see also the forces in 26(b) (Triantafyllou et al., 2003).

12. VIV at high Re: facts, extrapolations, and conjectures

In the foregoing, we have presented mostly experimental facts in the range of Reynolds numbers from about 500 to 6×10^4. These were obtained through small and medium-scale laboratory experiments under controlled conditions. Many relevant parameters such as the correlation length, pressure distribution, separation points, etc. were not measured and/or reported.

Experiments with forced and self-excited cylinders in nonsheared flows have shown that the amplitude ratio A/D, the phase angle φ, and the in-phase and out-of-phase components of the lift force depend (mostly) on the reduced velocity V_r or its various versions. These parameters are needed for the iterative design of relatively simple cables or pipes subjected to uniform flows.

However, the ocean environment is considerably more complex: lack of data, sufficient insight, and practical experience on the occurrence of VIV at critical to super-critical Reynolds numbers in omni-directional waves and currents, uniform and/or nonuniform shear, stratification, ambient turbulence, with various types of excrescencies and possible multi-modal response of structures, force the designers to continue to use relatively high safety factors. The matter is further complicated by the fact that data obtained either in the large basins around the world or in the oceans by the industry are often case-specific and proprietary. The wide dissemination of the existing ocean data would have helped to resolve many of the issues cited above for the betterment of all concerned. We do not hope to change the existing operational culture of the industrial organizations, however, we are grateful to a few who shared some information with us during the past year so that we could glean some facts from them.

12.1. Discussion of experiments

As we have noted previously, in connection with the discussion of the "Governing and influencing parameters," Humphries and Walker (1988, hereafter referred to as H–W) carried out extensive experiments with a cylinder ($D = 0.168$ m, $L/D = 33$, with a 'smooth external finish', $m^* = 1.98$, $\zeta = 0.0143$, $m^*\zeta = 0.0283$, and $f_{wtr} = 1.23$ Hz) in a deep flume in the range of Reynolds numbers from about 50 000 to 4×10^5 in both the nominally uniform flow, (U_{max}/U_{min}) = 1:1, and in linear (positive) shear with 1:1.5, 1:2, and 1:3, with the corresponding shear parameters of 0.0, 0.012. 0.02, and 0.03, respectively. The cylinder was effectively a *pinned–pinned* beam. As they have noted, "The top end of the 'pin' mounting was connected to a hydraulic ram to allow vertical movements as the vertical cylinder flexed. This prevented the introduction of axial tension, and hence changes in natural frequency, due to the model deflection."

The results of H–W are shown in Figs. 27 and 28 for the global drag coefficient and the cross-flow amplitude response, respectively. Fig. 27 shows that the drag coefficient for the uniform flow ($U_{max}/U_{min} =$ 1:1) is dramatically amplified with respect to the rigid cylinder (at rest) and that VIV in uniform flow produces the largest drag (after an initial anticipated sharp drop) in the critical regime. In the words of one of the reviewers, "this highlights an extreme sensitivity to VIV in the critical regime, and perhaps a good "flagship" example of the state of affairs in Re scaling" (at least for an effectively *pinned–pinned* beam, as noted above).

The nature of the variation of C_d is very much like that of a cylinder entering the critical transition, with C_d dropping sharply. However, when lock-in occurs (with 2-dof), C_d increases sharply, proving that VIV occurred within the zone of critical transition. Furthermore, even in the critical Re region, the occurrence of maximum C_d (at about $U_{ref}/f_{wtr}D \approx 5.6$) in Fig. 27 precedes the occurrence of maximum A/D (at $U_{ref}/f_{wtr}D \approx 6.2$) in Fig. 28, as in the case shown in Figs. 26(a) and (b), for a sub-critical flow. Furthermore, the maximum A/D for the no-shear data (about 1.5 at $U_{ref}/f_{wtr}D \approx 6.2$) corresponds quite well with that in Fig. 26(b) (about 1.5 at $U_{ref}/f_{wtr}D \approx 7$). As to the effect of shear, the data under consideration clearly show that C_d decreases with increasing shear and the lock-in occurs with smaller peaks at smaller $U_{ref}/f_{wtr}D$. Likewise, A/D maxima decrease toward unity. It is further noted that shear extends the range of the lock-in region. However, these observations and the results shown in Figs. 27 and 28 are of a global nature only since they are based on the reference velocity at mid-span. With higher shear, the character of the flow (supercritical flow, high-intensity turbulence) at the top of the pipe may be significantly different from that at the bottom (subcritical flow, lower turbulence), and there is no simple way to average out or to explain the difficult-to-quantify occurrences and transitions along the pipe. In spite of all these, shear should not necessarily instill a 'fear of the unknown' in most designs.

In recent years, several models have been developed for the prediction of VIV of slender marine structures such as risers and cables. A method for predicting approximately the static and lift responses of a flexible cylinder in a unidirectional sheared current was outlined by Patrikalakis and Chryssostomidis (1986). Their approach, based on the experimental data obtained by Sarpkaya (1978), represents the multifrequency lift response of a flexible cylinder in a

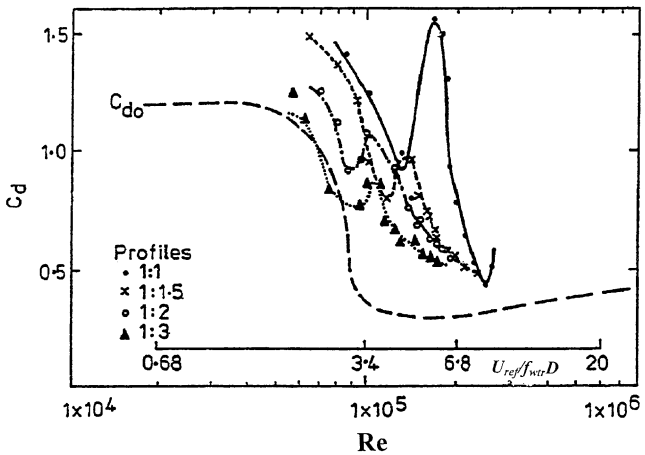

Fig. 27. (a) The nature of the variation of C_d is like that of a smooth cylinder entering the critical transition, with C_d dropping sharply. The VIV (with 2-dof) first arrests the drop in C_d and then increases it sharply, proving that VIV occurred within the zone of critical transition. The drag for the uniform flow ($U_{max}/U_{min} = 1:1$) is dramatically amplified with respect to the rigid cylinder (at rest). As to the effects of shear, the maxima of C_d decrease with increasing shear and occur at smaller $U_{ref}/f_{wtr}D$ (Humphries and Walker, 1988).

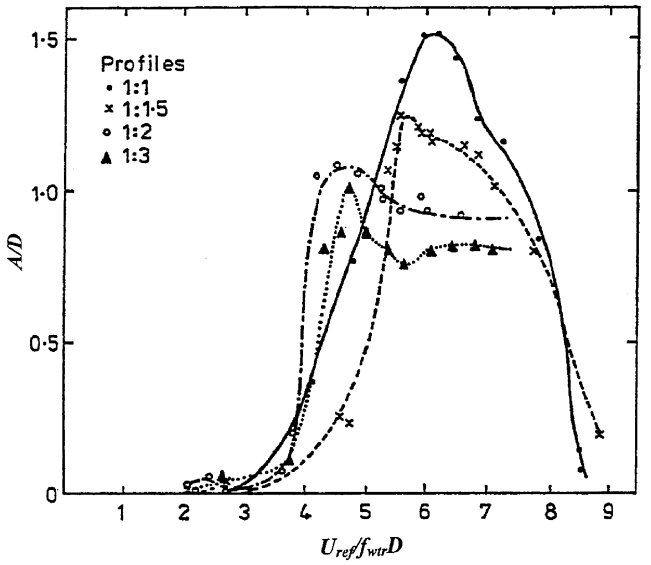

Fig. 28. The maximum A/D for the no-shear case (about 1.5 at $V_{\mathrm{ref}}/f_{\mathrm{wtr}}D \approx 6.2$) corresponds quite well with that in Fig. 26 (about 1.5 at $U_{\mathrm{ref}}/f_{\mathrm{wtr}}D \approx 7$). With shear, the maxima of A/D occur with reduced peaks at smaller $U_{\mathrm{ref}}/f_{\mathrm{wtr}}D$ and decrease towards unity. It appears that shear extends the range of the lock-in region. Even in the critical Re region, the occurrence of maximum C_d (at about $U_{\mathrm{ref}}/f_{\mathrm{wtr}}D \approx 5.6$) precedes the occurrence of maximum A/D (at $U_{\mathrm{ref}}/f_{\mathrm{wtr}}D \approx 6.2$), as in Figs. 26(a) and (b) for the sub-critical flow (Humphries and Walker, 1988).

sheared current by predicting a number of independently determined, monochromatic, multimode dynamic solutions. A numerical example assuming bimodal solutions is included to illustrate the method for the geometry of a single-tube marine riser.

Larsen and Halse (1995) provided a direct comparison and comprehensive discussion of the most commonly used models (Skomedal et al., 1989; Nedergaard et al., 1994; Triantafyllou et al., 1994; Vandiver et al., 1993; Vandiver and Li, 1994; Larsen and Bech, 1986; Lyons and Patel, 1989). Only one model was based on CFD (Skomedal et al., 1989) and only one model considered a stochastic load process (Vandiver et al., 1993).

Larsen and Halse (1995) concluded that large discrepancies exist between the predictions of the models compared and that "all aspects of VIVs are still not understood." These include, but not limited to, description of the spatial attenuation, definition of the excitation zones, the stochastic nature of vortex shedding process in time and space, the need to use experimentally determined coefficients, lack of correspondence between the experimental conditions and the application, and the use of different parameters in various data bases. Individually, each modeling group tracks the forecast skill of their model.

Future efforts may be directed towards the development of models based on VEMs (Sarpkaya, 1989; Sarpkaya and Shoaff, 1979) and on three-dimensional unsteady CFD codes, full-scale and model-scale experimental data, polyspectral methods, and nonlinear control. The objective of the second effort is to generate a database that will be used to develop and calibrate finite-degree of freedom models for design and analysis of VIV problems.

A numerical simulation tool was developed by Dalheim (1999) at Det Norske Veritas for the prediction of VIV of flexible risers in sheared currents with some promising results. The studies of large-scale model testing of deep sea risers (90 m long) in a shear current (Huse et al., 1998) have produced a number of important results: (a) VIVs may cause resonant *axial* vibrations in a deep-sea steel riser whether it is pinned at both ends or free at one end and pinned at the other; (b) such axial vibrations may lead to excessive stresses in the risers, significantly larger than the bending fatigue stresses, normally considered to be the main problem of VIV; and (c) reducing or eliminating the lateral as well as the axial excitation by employing the most suitable VIV suppression devices goes a long way toward reducing the high axial stresses.

It is evident from the foregoing that the end conditions of the test pipe, that is, the freedom allowed to the ends to move cyclically in the axial direction, emerges as an important parameter, particularly in the field tests. If both ends of a pipe (say, pinned–pinned) are constrained to extensional motion, the A/D will be smaller than if one or both ends were free to move in the axial direction, as in the case of tests by Humphries and Walker (1988). In a long pipeline,

every span is elastically connected to each other. This serves as a strong damper and increases the stiffness of the line, which, in turn, reduces the amplitude of VIV. The amount of reduction in A/D is not, however, easy to quantify because of its dependence on several other parameters (e.g., m^*, ζ, L_{span}/D, stiffness, shearing strains, temperature and its gradients, friction, time-dependent roughness, etc.). It is also clear from the foregoing, as well as from other sources, that high-Re data are not significantly different from those seen at subcritical Reynolds numbers above 20 000.

Bruschi et al. (1982) described two experimental investigations at high Reynolds numbers. The first was conducted in a wind tunnel with a model cylinder to quantify the wall-proximity effects. The second was carried out with a full-scale pipeline span (with various types of roughness) immersed in a tidal current ($1.7\times10^5 < \mathrm{Re} < 2.2\times10^5$). Bruschi et al. (1982) have not presented any graphical or numerical results but made the following observations: (a) the oscillations at the center of the span reached $0.8D$ at $\mathrm{Re}=1.7\times10^5$ for a pipe of $D=0.15$ m, and $A=2D$ at $\mathrm{Re}=2.4\times10^5$ for a pipe of $D=0.51$ m; and (b) the flow was in the critical transition region at the lower Re and in the supercritical region at the upper Re. They have conducted engineering tests with helical ropes and other 'damping' devices.

Allen and Henning (1997) performed experiments with two flexible as well as nonflexible circular cylinders in the critical/supercritical Reynolds number range ($D_1\approx0.088$ m, $k/D_1=1.37\times10^{-4}$, in the Re range of $2\times10^5<\mathrm{Re}<6\times10^5$; and $D_2\approx0.14$ m, $k/D_2=9.94\times10^{-5}$, in the Re range of $6\times10^5<\mathrm{Re}<1.5\times10^6$). Varying degrees of difficulty were encountered with the end conditions, alignment, Froude numbers exceeding unity (in the test basin) and the duration of the data-acquisition period. Their stationary nonflexible cylinder experiments tended to agree with the well-known results of Roshko (1961), Schewe (1983), and Shih et al. (1992) at similar k/D values. The results have once again illustrated the fact that the case of a smooth cylinder is a pathological case and the lightly roughened cylinder becomes the canonical bluff body, particularly at supercritical Reynolds numbers, for both stationary and vibrating cylinders.

For the smaller cylinder undergoing VIV, the drag coefficient decreased from about 1.2 to 0.6, the in-line r.m.s. displacement remained nearly constant at about $A/D=0.1$, and the amplitude of the transverse oscillations leveled off at $A/D=0.4$ for Re larger than about 3.2×10^5. For the larger cylinder undergoing VIV, the drag coefficient increased from 0.45 (at $\mathrm{Re}=7\times10^5$) to a maximum of 0.7 (at $\mathrm{Re}=1.3\times10^6$) and then decreased to about 0.6 at $\mathrm{Re}=1.5\times10^6$. The in-line r.m.s. displacement remained nearly constant at about $A/D=0.05$, except at a single point ($\mathrm{Re}=1.05\times10^6$) at which it jumped to about 0.13. It was not clear whether this singular event was a Reynolds number effect or, more likely, the effect of the Froude number exceeding unity. The r.m.s. amplitude of the transverse oscillations increased almost linearly from zero (at $\mathrm{Re}=7\times10^5$) to $A/D=0.44$ (at $\mathrm{Re}=1.3\times1.3\times10^6$) and then decreased linearly to about 0.3 at the highest Reynolds number encountered ($\mathrm{Re}=1.5\times10^6$).

12.2. Tentative conclusions

Our numerous conversations with enlightened representatives of several large petroleum concerns have helped us to deduce the following tentative conclusions, which will be presented here without empirical verification proof (i.e., *caveat emptor*!):

1. It is a well-known fact that as the Reynolds number increases from about 4×10^5 to about 10^6, the Strouhal number is undefinable for a steady flow past a 'smooth' cylinder. However, for a cylinder subjected to VIV, the *Strouhal number becomes definable in the said* Re *range* and smoothly transitions from about 0.18 to 0.24, due to the enhanced correlation. The wake width decreases from about D to $0.7D$, and the drag coefficient decreases accordingly.

2. The limited data show that the case of a "smooth" cylinder is a pathological case and the lightly roughened cylinder becomes the canonical bluff body at high Reynolds numbers [see, e.g., Achenbach (1971), Schewe (1983), Shih et al. (1992), Okajima et al. (1999)]. Cylinders of relatively small roughness exhibit relatively small A/D in the usual range of reduced velocities. However, with a roughness of about 1 mm (for instance, over a cylinder of one foot in diameter), one may expect a maximum A/D ratio of about 0.95. The same cylinder subjected to forced oscillations yields results very similar to those obtained with self-excited oscillations. The foregoing results are mostly for cylinders constrained in the in-line direction.

3. Experiments with 2-dof (both in-line and transverse oscillations) at very high Reynolds numbers show that *the results are indeed nearly identical to those reported by* Sarpkaya (1995) (see Fig. 24), as we have noted earlier. The 2-dof case produced 10–20% larger A/D values reaching about $A/D=1$ over a wider range of reduced velocities (from about 4–13). The maximum A/D values occur in the range of reduced velocities from 8–10. In the case of the constrained or 1-dof cylinders, the maximum A/D is somewhat smaller (about 0.85) in the range of reduced velocities from about 5–6, as would be expected. These results require further confirmation, hopefully, in the very near future.

4. The effect of shear is more difficult to account for in terms of various transitions and axial variations in the flow states. However, the experiments of Humphries and Walker (1988) provide strong guidance for design. Currently, strip

theory, based on forced cylinder data and correlation models, is used in spite of its obvious shortcomings (e.g., phase and amplitude differences between the segments, directional changes in velocity and/or shear).

5. None of the high Reynolds number experiments ($Re > 20\,000$) show such phenomena as "Initial branch" (seen only at Reynolds numbers smaller than about 5000). The vortex modes of 2P, 2S, and others have been mapped only at Reynolds numbers below 1000. Blackburn and Henderson (1999) did not find the 2P mode at $Re = 500$. Evangelinos and Karniadakis (1999) at $Re = 1000$ found multiple vorticity concentrations and transient mixtures of (P + S) and 2P modes in the near wake and general wake instability further downstream. Brika and Laneville (1993) found 2P and 2S modes in the range of Reynolds numbers from 3.4×10^3 to 11.8×10^3. As we have noted earlier, the mean position of the line of transition to turbulence does not reach upstream enough for Re less than about 15×10^3 to 20×10^3. Lastly, it should be noted that at Re larger than about 20 000, it may not be possible to photograph coherent vortex structures in the wake.

6. In free oscillations at sufficiently large Re, the oscillations are not sinusoidal, as evidenced by many experiments and numerical simulations. Consequently, the flow does not become fully established, say "periodic," because the amplitude, added-mass, frequency, phase angle, vortex structures, shear layers never become fully established. Each cycle is affected by the character of the previous cycle. Consequently, the ever-changing topology of the flow prevents it from exhibiting sharp changes (as branches) in the A/D versus V_r plots at high Re.

7. It may be stated with little reservation that high-Re data (A/D and force-transfer coefficients, such as lift and added-mass) with smooth and reasonably roughened, nontapered cylinders exhibit essentially the same results as those the research community has produced in the laboratories during the past 15 years in the range of Reynolds numbers from about 20 000 to 60 000 (except, as noted above, with regard to the smooth transition in Strouhal numbers and drag coefficients in the critical to supercritical regimes). Thus the issue is not the discovery of great surprises at high Re, but rather how to refine the high Re data to reduce the error to less than 10%, how to deal better with shear, how to quantify and to translate the effects of the end conditions (axial motion) for single-span laboratory experiments versus continuous pipes, how to account for and quantify multi-modes and mode interference, how to suppress VIV at any Re without drag penalty, and how to reduce the safety factors.

8. The wide dissemination of the large-scale data will improve their interpretation and the planning of future experiments. It will also enrich the science and technology of VIV and help to resolve many of the issues cited above for the betterment of all concerned.

13. Numerical simulations

The numerical simulation of flow past a circular cylinder undergoing VIV at relatively small Reynolds numbers (particularly in the range $Re = 100$–1000) is complicated by some of the most difficult problems of fluid mechanics such as separation excursions, incomplete transition in the shear layers, and the coherence length based on a yet unexplained coupling mechanism between the dynamics of the near-wake and that of the structure. Most of the disparity between the experiments and numerical simulations is attributable to the fact the mean position of the line of transition to turbulence does not reach upstream enough for Re less than about 15 000 to 20 000, even though VIV with 2-dof may precipitate the instability somewhat sooner.

Many models of turbulence, for every occasion, are described in numerous papers. However, DNS does not require 'modeling.' It deals only and purely with the numerical problem of solving the time-dependent Navier–Stokes equations, albeit at relatively small Reynolds numbers. LESs appeared to be a compromise. However, as Grinstein and Karniadakis (2002) noted recently: "After more than 30 years of intense research on LESs of turbulent flows based on eddy-viscosity subfilter models (Deardroff, 1970), there is now consensus that such an approach is subject to fundamental limitations. It has been demonstrated for a number of different flows that the shear stress and strain tensors involved in subfilter eddy-viscosity models have different topological features rendering scalar eddy-viscosity models inaccurate." Recently, Michelassi et al. (2003) expressed a more optimistic point of view in connection with their work on flow around low-pressure turbine blades at Reynolds numbers 5.18×10^4 and 2×10^5: "Direct numerical simulation and LES are able to provide a much deeper insight in the wake-boundary-layer interaction mechanism as compared to two-dimensional unsteady RANS simulations."

Other computational methods include the discrete-vortex method (DVM), the use of RANS, or the combination of a number of them. We will not dwell on simulations at Reynolds numbers smaller than 1000. They may be of interest in assessing a given numerical scheme at a given Re, but not necessarily to predict VIV at more realistic Reynolds numbers.

The discrete vortex model was first used by Sarpkaya and Shoaff (1979) with reasonable success after judicious selection of the controlling parameters (Sarpkaya, 1989, 1994). Meneghini et al. (2002) used DVM to calculate the

behavior of cylinders ($m^* = 3.3$, $m^*\zeta = 0.013$, and $L/D = 94.5$, 480, 4600) subjected to currents and shear (Re = 10 000). Their simulation did not yield an 'Upper branch.' The case of a cantilever yielded similar results. Their single riser simulations provided the expected vibration modes and the comparisons with the quasi-steady analysis were quite encouraging.

Evangelinos and Karniadakis (1999) and, subsequently, Evangelinos et al. (2000), Lucor and Karniadakis (2002), and the references cited therein, dealt with the predictability and uncertainty in flow-structure interactions and with the dynamics of flow structures in the wake of rigid and flexible cylinders subjected to VIV. Recently, Lucor et al. (2003) extended their DNS model to Re = 3000 (by increasing the lateral spacing of the mesh size), but not without some difficulties. Guilmineau and Queutey (2001) used a two-dimensional finite volume analysis in conjunction with RANS and a K–ω model for turbulence to simulate the 1-dof response of a cylinder in the range of Re from 900 to 15×10^3 and compared their predictions with those of K–W (1999) at Re $\approx$3700. Three initial conditions were used in the simulations: a cylinder starting from a state of rest, increasing velocity, and decreasing velocity. For the conditions of 'from rest' and 'decreasing velocity' they have predicted only the Lower branch. With 'increasing' velocity, on the other hand, the maximum amplitude corresponded to the experimental value, but the Upper branch did not match the experiments (Fig. 29). The use of a fully developed turbulence model, (K–ω) for a two-dimensional finite volume analysis, in the range of *transitional* Reynolds numbers (for the shear layers) makes it difficult to discern the reasons for the differences between the experiments and their numerical simulations.

Notwithstanding the concerns expressed by Grinstein and Karniadakis (2002), LES has been used by a number of investigators. Saltara et al. (1998) used DVM and LES for a 1-dof VIV at Re = 1000. Tutar and Holdo (2000) used LES in conjunction with the finite element method at Re = 2.4×10^4 for a cylinder subjected to forced oscillations and found that three-dimensional representation was necessary to obtain accurate enough results. This follows from the fact that two-dimensional representations naturally yield perfect correlations. VIV enhances the correlation but it does not make it perfect. As we have noted earlier, the degree of correlation, related to all other parameters, plays a major role in all aspects of VIV. As noted by Al-Jamal and Dalton (2004), "An LES model, either 2-D or 3-D, is not capable of calculating the full flow past a stationary cylinder, much less an oscillating one." DNS is Re—limited for the foreseeable future.

Zhang and Dalton (1996) performed a two-dimensional LES study for a transversely oscillating cylinder at Re = 13 000. Their results exhibited the same trends as the experimental results of Feng (1968). Lu and Dalton (1996)

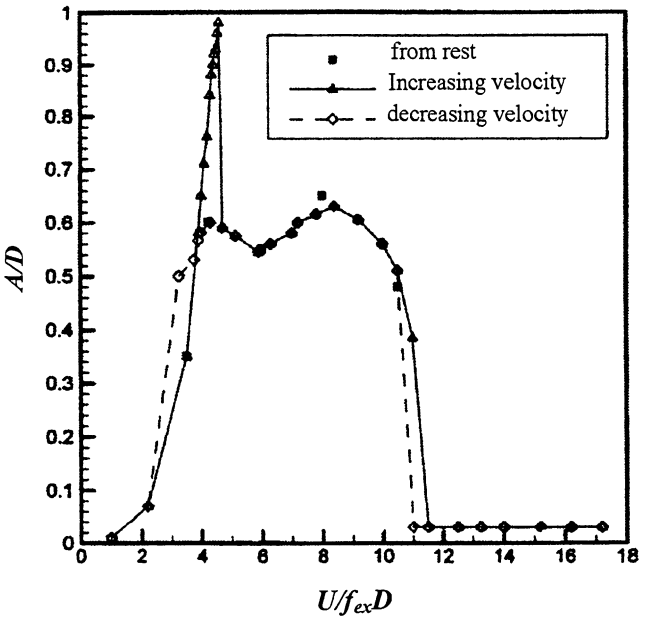

Fig. 29. A two-dimensional finite volume analysis, RANS equations, and a K–ω model for turbulence are used to simulate the 1-dof response of a cylinder in the range of Re from 900 to 15 000 with $m^* = 2.4$ and $m^*\zeta = 0.013$. Three initial conditions were used: cylinder starting from a state of rest, increasing velocity, and decreasing velocity. For the conditions of 'from the rest' and 'decreasing velocity' only the lower branch was predicted. With 'increasing' velocity, on the other hand, the maximum amplitude corresponded to the experimental value, but the upper branch did not match the experiments (Guilminaeu and Queutey, 2001).

examined the VIV problem for a two-dimensional viscous flow at Re = 200 and two-dimensional turbulent flow at Re = 855. They found good agreement with the results of Öngören and Rockwell (1988a, b) and reasonably good agreement with the results of Lecointe and Piquet (1989). However, the lift calculations of Lecointe and Piquet were about 35% larger at Re = 855 than those of Zhang and Dalton because they had not used a turbulence model. More recently, Al-Jamal and Dalton (2004) have performed two-dimensional LES calculations of the self-excited response of a cylinder at Re = 8000 for a range of damping ratios and natural frequencies. In spite of the shortcomings of a two-dimensional simplification, their results predicted the expected vibratory response in the range $0.72 < f_{com}/f_{st} < 1.26$. Decreasing material damping increased the lock-in range. A beating behavior was observed in the oscillations, which decreased with increasing damping (see Fig. 9). Clearly, one does not expect the two-dimensional LES to represent the inception and growth of the instabilities accurately, let alone the transition to turbulence, in unsteady shear layers. It appears that the question of the three-dimensional numerical simulation of VIV even for a smooth circular cylinder in the range of Reynolds numbers from a few thousand to over a million will remain unresolved indefinitely. Higher order modes caused by secondary instabilities resulting from the changes in phase and amplitude in self-excited oscillations will certainly complicate the simulations with any turbulence model in any indirect numerical simulation.

At present, none of the methods discussed above ensures sufficient generality in a large parameter space as far as VIV is concerned. Thus, all one can hope for is the prediction of some aspects of VIV through the use of RANS (with suitable turbulence models) and LES (with suitable subgrid models) under the safeguiding as well as safeguarding eyes of high-quality experiments in suitable ranges of Reynolds number. Large-scale benchmark experiments at large Reynolds numbers coupled with three-dimensional numerical simulations using RANS (employing several turbulence models) and LES may allow one to develop industrial codes that may be used (after many calibrations) for design purposes in small domains of the controlling parameters.

14. Conclusions and recommendations

The modest objective of this paper has been to review the VIVs in a few specific fundamental cases, as in 1979. However, the difficulty of this review has been materially increased by the enormous growth of the size and number of conferences and publications during the past 25 years. Those who desire a more comprehensive or utilitarian treatment of VIV will find the references cited in the text and hundreds of other papers which appeared in the proceedings of numerous conferences, to be most helpful. Obviously, much remains to be done, and we will record here only a few cautious suggestions for consideration, rather than a competent glance into the future:

1. Carry out intricate experiments in the range of Re from about 3000 to 50 000 on the evolution of instability on unsteady shear layers emanating from a rigid cylinder undergoing synchronized (free/forced) oscillations.

As noted in the Introduction, Re in our on-going experiments is kept constant at a specified value by maintaining U, D, L/D, k, ζ, ρ_f and ν constant and varying only m in $\rho_m = 4m/(\pi LD^2)$ in small increments and hence f_{vac} in $V_r = U/f_{vac}D$ or in f_{ex}/f_{vac}. Subsequently, Re is changed to a new value for a new set of experiments with varying m. The data will define a three-dimensional space showing A/D versus f_{ex}/f_{vac} in each plane of constant Re. We intend to continue this study with further data inter-comparisons and hope that the results will complement other contributions dealing directly with the evolution of instability on unsteady shear layers and with the DNS, LES, or RANS simulations of VIV at a given Re.

2. Obtain a new set of data (at $Re > 2 \times 10^4$) for all values of S_G (for rigid cylinders and cables with proper end conditions) using refined methods, instrumentation, and proper damping (in air) partly for practical purposes and partly, and most importantly, for determining the regions and the reasons where S_G *alone* correlates the data and the regions where m^* and ζ operate as independent parameters. This will help to separate the regions of applicability of the simple linear-motion analysis of VIV, from which the S_G emanates, from the nonlinear range of the system response.

3. Determine the character and magnitude of the self-limiting behavior of VIV of the cylinders and cables at large Re and L/D as S_G approaches zero.

4. Perform a whole new set of careful experiments with forced and self-excited cylinders at $Re > 20\,000$ in a facility without free surface or surfactants (dissolvable or nondissolvable) to delineate the vortex shedding modes as a function of f_{ex}/f_{st} in the entire range of synchronization. It has already been emphasized a number of times that the Reynolds number effects in all VIV experiments and numerical simulations remain an unresolved practical as well as fundamental problem of major significance.

5. Perform a numerical simulation of the motion of two parallel shear layers subjected to sinusoidal transverse motion in a uniform steady flow [*à la* Abernathy and Kronauer (1962)]. Even though one may not be

able to connect all the links of the chain, the parts that can be connected might provide a better understanding of vortex shedding modes.

6. Systematically investigate (at $Re > 20\,000$) the role of the amplitude modulations in free oscillations on the differences between the free and forced oscillations. The rate of increase or decrease of the ambient velocity and the intensity and integral length scale of turbulence must be quantified for each experiment.

7. Find the means (numerically or experimentally) to interfere with the coupling mechanisms between the near-wake dynamics and the structure dynamics to change the phase difference.

8. Control the mode: all active and passive means to prevent the wake from shifting to a 2S mode.

9. Introduce additional frequencies into the motion of a flexible body (cable) to cancel some others and diffuse the energy between various frequencies.

10. Produce cables and structures with smart materials [see, e.g., Zhang et al. (2003), Chopra (2002) and the references cited therein] that increase their (material) damping when subjected to cyclic motion, stiffen their supports, and reduce the correlation length (interfering with the boundary layers and shear layers).

11. Carry out extensive measurements and numerical simulations to enhance the understanding of the effects of body proximity, vortex shedding from, and VIV of three-dimensional bodies.

12. Perform extensive measurements and numerical simulations to enhance the understanding and prediction of the effect of ambient turbulence on shear layer instability, separation excursions, and VIV.

13. Find more elegant means to suppress VIV and to control (decrease) the correlation length throughout the cycle (ropes are so noningenious).

14. Determine the mutual interaction of low frequency *ocean* waves, uniform (or sheared) collinear currents and VIV at $Re > 20\,000$. 'Young turbulence', as defined by Evangelinos and Karniadakis (1999), at $Re \cong 1000$ is commendable, but not enough.

15. Make great strides to enhance the power of computers, numerical methods, and approximate models (the existing as well as new ones) to enhance the prediction of VIV. There are, at present, large Re gaps between the computable, measurable, and industrially significant ranges of VIV. Evangelinos et al. (2000) noted that the DNS simulations "are currently prohibitively expensive to be used in the engineering design of VIV." They have also suggested that "the answer could be provided by dynamical systems modeling, given the low dimensionality of the wake." Clearly, the subject will remain exciting for generations to come not only because turbulence remains poorly understood but also because it needs simulations at a level that could be used for industrial design explorations and ingenious VIV suppression devices at any Re, in any environment. As noted earlier, a better way may be developing robust codes based on various versions of RANS and LES, suitable turbulence models, and benchmark experiments at large Reynolds numbers, and establishing code banks for validation and verification.

Acknowledgements

I am indebted to a large number of people on whose work I have so extensively drawn to produce this review. Many colleagues have responded generously to my requests for advice, references, advance copies of papers, reports, and theses, and/or originals of some figures. I am particularly indebted to Professor Charles Dalton, Professor Geir Moe, Dr Owen H. Oakley, Professor Michael S. Triantafyllou, and Professor J. Kim Vandiver for stimulating discussions, references, and encouragement. I am grateful to the reviewers whose comments have improved the clarity of the manuscript. My heartfelt thanks go to Mrs Irma L. Fink and Mr Jeff N. Rothal of the NPS library who did the endless search for references and always managed to find them. My thanks also go to the Cambridge University Press and Elsevier Science Ltd. who permitted reproductions from earlier publications. Generous support of the Naval Postgraduate School is gratefully acknowledged. Partial support was provided by ONR through (N00014-02-WR-20109).

References

Abernathy, F.H., Kronauer, R.E., 1962. The formation of vortex streets. Journal of Fluid Mechanics 13, 1–20.

Achenbach, E., 1971. Influence of surface roughness on the cross-flow around a circular cylinder. Journal of Fluid Mechanics 46, 321–335.

Ahmed, N.A., Wagner, D.J., 2003. Vortex shedding and transition frequencies associated with flow around a circular cylinder. AIAA Journal 4, 542–544.

Alexander, C.M., 1981. The complex vibration and implied drag of a long oceanographic wire in cross-flow. Ocean Engineering 8, 379–406.

Al-Jamal, H., Dalton, C., 2002. Vortex induced vibrations using large eddy simulation at a moderate Reynolds number. Conference on Bluff Body Wakes and Vortex-Induced Vibrations (BBVIV3), Port Douglas, Australia.

Al-Jamal, H., Dalton, C., 2004. Vortex induced vibrations using large eddy simulation at a moderate Reynolds number. Journal of Fluids and Structures 19, 73–92.

Allen, D.W., Henning, D.L., 1997. Vortex-induced vibration tests of a flexible smooth cylinder at supercritical Reynolds numbers. In: Proceedings of the 1997 ISOPE Conference, Vol. III, Honolulu, pp. 680–685.

Angrilli, F., Di Silvio, G., Zanardo, A., 1972. Hydroelasticity study of a circular cylinder in a water stream. In: Naudascher, E. (Ed.), Flow Induced Structural Vibrations. IUTAM-IAHR Symposium, pp. 504–512.

Atsavapranee, P., Benaroya, H., Wei, T., 1998. Vortex dynamics in the near wake of a freely-oscillating cylinder. Proceedings of the FEDSM'98. ASME Fluids Engineering Division, Summer Meeting, Washington, DC, pp. 1–6.

Au-Yang, M.K., 2001. Flow-Induced Vibrations of Power and Process Plant Components—A Practical Workbook. The American Society of Mechanical Engineers, New York, NY.

Bartran, D., Kinsey, J.M., Schappelle, R., Yee, R., 1999. Flow-induced vibration of thermowells. Journal of The Science and Engineering of Measurement and Automation 38, 123–132.

Basset, A.B., 1888. On the motion of a sphere in a viscous liquid. Philosophical Transactions Royal Society of London 179, 43–63. (See also a Treatise on Hydrodynamics, Vol. 2, Deighton, Bell and Co, Cambridge. Also New York, Dover Publications).

Basu, R.I., 1985. Aerodynamic forces on structures of circular cross sections, part 1. Journal of Wind Engineering and Industrial Aerodynamics 21, 273–294.

Basu, R.I., 1986. Aerodynamic forces on structures of circular cross sections, part 2. Journal of Wind Engineering and Industrial Aerodynamics 24, 33–59.

Batchelor, G.K., 1967. An Introduction to Fluid Dynamics. Cambridge University Press, Cambridge, p. 357.

Bearman, P.W., 1984. Vortex shedding from oscillating bluff bodies. Annual Review of Fluid Mechanics 16, 195–222.

Bearman, P.W., Brankovic, M., 2002. Passive control of vortex-induced vibration. Conference on Bluff Body Wakes and Vortex-Induced Vibrations (BBVIV3), 17–20 December, Port Douglas, Australia.

Bearman, P.W., Currie, I.G., 1979. Pressure fluctuation measurements on an oscillating circular cylinder. Journal of Fluid Mechanics 91, 661–677.

Benjamin, T.B., 1986. Note on added mass and drift. Journal of Fluid Mechanics 169, 251–256.

Berger, E., Wille, R., 1972. Periodic flow phenomena. Annual Reviews of Fluid Mechanics 4, 313–340.

Bishop, R.E.D., Hassan, A.Y., 1964. The lift and drag forces on a circular cylinder in a flowing fluid. Proceedings of Royal Society of London, Series A 277, pp. 32–50, 51–75.

Blackburn, H.M., Henderson, R.D., 1999. A study of two-dimensional flow past an oscillating cylinder. Journal of Fluid Mechanics 385, 255–286.

Blackburn, H.M., Govardhan, R.N., Williamson, C.H.K., 2001. A complementary numerical and physical investigation of vortex-induced vibration. Journal of Fluids and Structures 15, 481–488.

Blevins, R.D., 1990. Flow-Induced Vibration, 2nd Edition. Van Nostrand Reinhold, New York, USA.

Blevins, R.D., 1999. On vortex-induced fluid forces on oscillating cylinders. Proceedings of the ASME Pressure Vessels and Piping Division Publication PVP 389, pp. 103–111.

Blevins, R.D., Burton, T.E., 1976. Fluid forces induced by vortex shedding. Journal of Fluids Engineering 95, 19–24.

Bloomfield, P., 2000. Fourier Analysis of Time Series—An Introduction. Wiley, Canada.

Bloor, S.M., 1964. The transition to turbulence in the wake of a circular cylinder. Journal of Fluid Mechanics 19, 290–309.

Bloor, S.M., Gerrard, J.H., 1966. Measurements on turbulent vortices in a cylinder wake. Proceedings of the Royal Society of London, Series A 294, 319–342.

Brika, D., Laneville, A., 1993. Vortex-induced vibrations of a long flexible circular cylinder. Journal of Fluid Mechanics 250, 481–508.

Bruschi, R.M., Buresti, G., Castoldi, A., Migliavacca, E., 1982. Vortex shedding oscillations for submarine pipelines: comparison between full-scale experiments and analytical models. Offshore Technology Conference OTC Number 4232.

Bublitz, P., 1972. Unsteady pressures and forces acting on an oscillating circular cylinder in transverse flow. Symposium of Flow-Induced Structural Vibrations, Karlsruhe, Germany, pp. 443–453.

Carberry, J., 2002. Wake states of a submerged oscillating cylinder and of a cylinder beneath a free-surface. Ph.D. Thesis, Monash University, Melbourne, Australia.

Carberry, J., Sheridan, J., Rockwell, D., 2002. Controlled oscillations of a cylinder: forces and wake modes, submitted for publication.

Cazemier, W., 1997. Proper orthogonal decomposition and low dimensional models for turbulent flows. Ph.D. Thesis, Rijksuniversiteit, Groningen, Sweden.

Chen, S.S., 1987. Flow-Induced Vibration of Circular Cylinder Structures. Hemisphere Publishing Corporation, Springer, Washington, DC, USA (Chapter 7).

Chen, S.S., Jendrzejczyk, J.A., 1979. Dynamic response of a circular cylinder subjected to liquid cross flow. Journal of Pressure Vessel Technology 101, 106–112.

Cheng, M., Moretti, P.M., 1991. Lock-in phenomena on a single cylinder with forced transverse oscillation. In: Au-Yang, M.K., Hara, F. (Eds.), Flow-Induced Vibration and Wear, PVP-Vol. 206, ASME, pp. 129–133.

Chopra, I., 2002. Review of state of art of smart structures and integrated systems. AIAA Journal 40, 2145–2187.
Cohen, K., Siegel, S., McLaughlin, T., Gilles, E., 2003. Feedback control of a cylinder wake low-dimensional model. AIAA Journal 4, 1389–1391.
Dalheim, J., 1999. Numerical prediction of VIV on deepwater risers subjected to shear currents and waves. Offshore Technology Conference, OTC Number 10933, Houston, TX.
Darwin, Sir Charles, 1953. Note on hydrodynamics. Proceedings of Cambridge Philosophical Society 49, 342–354.
Davies, M.E., 1976. A comparison of the wake structure of a stationary and oscillating bluff body. Using a conditional averaging technique. Journal of Fluid Mechanics 75, 209–231.
Davis, J.T., Hover, F.S., Landolt, A., Triantafyllou, M.S., 2001. Vortex-induced vibrations of cylinders in a tandem arrangement. Proceedings of the Fourth International Symposium on Cable Dynamics, May 28–30, Montreal, QC, Canada, pp. 109–120.
Dean, R.B., Milligan, R.W., Wooton, L.R., 1977. An experimental study of flow-induced vibration. E.E.C. Report 4, Atkins Research and Development, Epsom, UK.
Deardorff, J.W., 1970. A numerical study of three-dimensional turbulent channel flow at large Reynolds numbers. Journal of Fluid Mechanics 41, 453–480.
Deep Oil Technology, 1992. Joint Industry Program on Vortex-Induced Motions of Large Floating Platforms, Houston, TX, USA.
Den Hartog, J.P., 1934. The vibration problems in engineering. Proceedings of the Fourth International Congress Applied Mechanics Cambridge, pp. 34–53.
Deniz, S., Staubli, T., 1997. Oscillating rectangular and octagonal profiles: interaction of leading- and trailing-edge vortex formation. Journal of Fluids and Structures 11, 3–31.
Deniz, S., Staubli, T., 1998. Oscillating rectangular and octagonal profiles: modeling of fluid forces. Journal of Fluids and Structures 12, 859–882.
Dickens, W.R., 1979. The self-induced vibration of cylindrical structures in fluid flow. Proceedings of the Institution of Civil Engineers Part 2, 67, 13–30.
Di Silvio, G., 1969. Self controlled vibration of cylinder in fluid stream. ASCE Journal of Engineering Mechanics Division 95 (EM2), 347–361.
Di Silvio, G., Angrilli, F., Zanardo, A., 1975. Fluid elastic vibrations: mathematical model and experimental result. Meccanica 10, 269–278.
Dye, R.C.F., 1978. Photographic evidence of the mechanisms of vortex-exited vibration. Journal of Photography Science 26, 203–208.
Evangelinos, C., Karniadakis, G.E., 1999. Dynamics and flow structures in the turbulent wake of rigid and flexible cylinders subject to vortex-induced vibrations. Journal of Fluid Mechanics 400, 91–124.
Evangelinos, C., Lucor, D., Karniadakis, G.E., 2000. DNS-derived force distribution on flexible cylinders subject to vortex-induced vibration. Journal of Fluids Structures 14, 429–440.
Feng, C.-C., 1968. The measurement of vortex induced effects in flow past stationary and oscillating circular and d-section cylinders. Master's Thesis, Department of Mechanical Engineering, The University of British Columbia, Canada.
Ferguson, N., Parkinson, G.V., 1967. Surface and wake flow phenomena of vortex-excited oscillation of a circular cylinder. ASME Journal of Engineering for Industry 89, 831–838.
Fischer, P.F., Patera, A.T., 1994. Parallel simulation of viscous incompressible flows. Annual Review of Fluid Mechanics 26, 483–527.
Frédéric, L., Laneville, A., 2002. Vortex-induced vibrations of a flexible cylinder in a slowly varying flow: experimental results. Proceedings of IMECE 2002. ASME International Mechanical Engineering Congress and Exposition, November 17–22, New Orleans, Louisiana, USA.
Gerard, J.H., 1978. The wake of cylindrical bluff bodies at low Reynolds number. Philosophical Transactions A 288, 351–382.
Gopalkrishnan, R., 1993. Vortex induced forces on oscillating bluff cylinders. Ph.D. Thesis, Department of Ocean Engineering, MIT, Cambridge, MA, USA.
Gopalkrishnan, R., Grosenbaugh, M.A., Triantafyllou, M.S., 1992. Influence of amplitude modulation on the fluid forces acting on a vibrating cylinder in cross-flow. International Journal of Offshore and Polar Engineering, Transactions of the ISOPE 2(1), pp. 32–37.
Govardhan, R., Williamson, C.H.K., 2000. Modes of vortex formation and frequency response of a freely vibrating cylinder. Journal of Fluid Mechanics 420, 85–130.
Gowda, B.H.L., 1975. Some measurements on the phenomenon of vortex-shedding and induced vibrations of circular cylinders. Technical Report DLR-FB 75-01, Technische Universität, Berlin.
Griffin, O.M., 1972. Flow near self exited and forced vibrating circular cylinders. ASME Journal of Engineering for Industry 94, 539–547.
Griffin, O.M., Koopmann, G.H., 1977. The vortex-exited lift and reaction forces on resonantly vibrating cylinders. Journal of Sound Vibration 54, 435–448.
Griffin, O.M., Ramberg, S.E., 1974. The vortex-street wakes of vibrating cylinders. Journal of Fluid Mechanics 66, 553–576.
Griffin, O.M., Ramberg, S.E., 1982. Some recent studies of vortex shedding with applications to marine tubulars and risers. ASME Journal of Energy Resources Technology 104, 2–13.
Griffin, O.M., Skop, R.A., Ramberg, S.E., 1976. Modeling of the vortex-induced oscillations of cables and bluff structures. Society for Experimental Stress Analysis Spring Meeting, 9–14 May, Silver Spring, MD, USA.

Grinstein, F.F., Karniadakis, G.E., 2002. Alternative LES and hybrid RANS/LES for turbulent flows. Journal of Fluids Engineering 124, 821–822.

Gu, W., Chyu, C., Rockwell, D., 1994. Timing of vortex formation from an oscillating cylinder. Physics of Fluids 6, 3677–3682.

Guilminaeu, E., Queutey, P., 2001. Numerical simulation in vortex-induced vibrations at low mass-damping. AIAA Paper No. 2001-2852.

Halse, H.K., 1997. On vortex shedding and prediction of vortex-induced vibrations of circular cylinders. Ph.D. Thesis, Norwegian University of Science and Technology. Trondheim, Norway.

Hartlen, R.T., Baines, W.D., Currie, I.G., 1968. Vortex excited oscillations of a circular cylinder. University of Toronto Report UTME-TP 6809. Also see Hartlen, R.T., Currie, I.G., 1970. Lift oscillation model for vortex-induced vibration. ASCE Journal of Engineering Mechanics Division 96, 577–591.

Hover, F.S., Miller, S.N., Triantafyllou, M.S., 1997. Vortex-induced vibration of marine cables: experiments using force feedback. Journal of Fluids and Structures 11, 306–326.

Hover, F.S., Techet, A.H., Triantafyllou, M.S., 1998. Forces on oscillating uniform and tapered cylinders in crossflow. Journal of Fluid Mechanics 363, 97–114.

Hover, F.S., Davis, J.T., Triantafyllou, M.S., 2002. Is mode transition three-dimensional? Conference on Bluff Body Wakes and Vortex-Induced Vibrations (BBVIV3), 17–20 December, Port Douglas, Australia.

Huerre, P., 2002. Global nonlinear instabilities in wake flows. Conference on Bluff Body Wakes and Vortex-Induced Vibrations (BBVIV3), 17–20 December, Port Douglas, Australia.

Humphries, J.A., Walker, D.H., 1988. Vortex-excited response of large-scale cylinders in sheared flow. ASME Journal of Offshore Mechanics and Arctic Engineering 110, 272–277.

Huse, E., Kleiven, G., Nielsen, F.G., 1998. Large scale model testing of deep sea risers. Offshore Technology Conference, OTC Number 8701, 4–7 May, Houston, TX, USA.

Iwan, W.D., Jones, N.P., 1987. On the vortex-induced oscillations of long structural elements. ASME Journal of Energy Resources Technology 109, 161–167.

Jauvtis, N., Williamson, C.H.K., 2002. Vortex-induced vibration of a cylinder in two degrees of freedom. Conference on Bluff Body Wakes and Vortex-Induced Vibrations (BBVIV3) (4P), 17–20 December, Port Douglas, Australia.

Jones, G.W., Cincotta, J.J., Walker, R.W., 1969. Aerodynamic forces on a stationary and oscillating circular at high Reynolds numbers. Technical Report NASA R-300: N69-17304. National Aeronautics and Space Administration, Washington, DC, USA.

Jong, J.-Y., Vandiver, J.K., 1985. The identification of the quadratic system relating cross-flow and in-line vortex-induced vibration. In: Dynamic System Measurement and Control, ASME Winter Annual Meeting.

Keulegan, G.H., Carpenter, L.H., 1958. Forces on cylinders and plates in an oscillating fluid. Journal of Research of the National Bureau of Standards 60, 423–440.

Khalak, A., Williamson, C.H.K., 1999. Motions, forces and mode transitions in vortex-induced vibrations at low mass-damping. Journal of Fluids and Structures 13, 813–851.

Kim, Y.H., Vandiver, J.K., Holler, R., 1986. Vortex-induced vibration and drag coefficients of long cables subjected to sheared flow. ASME Journal of Energy Resources Technology 108, 77–83.

Koopmann, G.H., 1967a. On the wind-induced vibrations of circular cylinders. Master's Thesis, Catholic University of America, Washington, DC, USA.

Koopmann, G.H., 1967b. The vortex wakes of vibrating cylinders at low Reynolds numbers. Journal of Fluid Mechanics 28, 501–512.

Krishnamoorthy, S., Price, S.J., Païdoussis, M.P., 2001. Cross-flow past an oscillating circular cylinder: synchronization phenomena in the near wake. Journal of Fluids and Structures 15, 955–980.

Laguë, F., Laneville, A., 2002. Vortex-induced vibrations of a flexible cylinder in a slowly varying flow: experimental results. Proceedings of ASME International Mechanical Engineering Congress and Exposition, New Orleans, Louisiana, USA, pp. 1–7.

Larsen, C.M., Bech, A., 1986. Stress analysis of marine risers under lock-in condition. In: Proceedings of the Fifth International Offshore Mechanics and Arctic Engineering Symposium, Tokyo, Japan, pp. 450–457.

Larsen, C.M., Halse, K.H., 1995. Comparison of models for vortex-induced vibrations of slender marine structures. In: Bearman P.W. (Ed.), Flow-Induced Vibration. Balkema, Rotterdam, pp. 467–482, ISBN 90 5410547X.

Lecointe, Y., Piquet, J., 1989. Flow structure in the wake of an oscillating cylinder. ASME Journal of Fluids Engineering 111, 139–148.

Lenarts, V., Kerschen, G., Golival, J.C., 2001. Proper orthogonal decomposition for updating of non-linear mechanical systems. Mechanical Systems and Signal Processing 15, 31–43.

Leonard, A., Roshko, A., 2001. Aspects of flow-induced vibration. Journal of Fluids and Structures 15, 415–425.

Lighthill, M.J., 1986. Fundamentals concerning wave loading on offshore structures. Journal of Fluid Mechanics 173, 667–681.

Loève, M., 1977. Probability Theory, 4th Edition. Springer, New York.

Lotfy, A., Rockwell, D., 1993. The near wake on an oscillating trailing edge. Journal of Fluid Mechanics 251, 173–201.

Lu, X.-Y., Dalton, C., 1996. Calculation of the timing of vortex formation from an oscillating cylinder. Journal of Fluids and Structures 10, 527–541.

Lucor, D., Karniadakis, G.E., 2002. Predictability and uncertainty in flow-structure interactions. Conference on Bluff Body Wakes and Vortex-Induced Vibrations (BBVIV3), 17–20 December, Port Douglas, Australia.

Lucor, D., Foo, J., Karniadakis, G.E., 2003. Correlation length and force phasing of a rigid cylinder subject to VIV. IUTAM Symposium on Fluid–Structure Interactions, June 2003, Rutgers State University, USA.

Lyons, G.J., Patel, M.H., 1989. Application of a general technique for prediction of riser vortex-induced response in waves and current. ASME Journal of Offshore Mechanics and Arctic Engineering 111, 82–91.

Mandini, R.V., 1961. Kinematics of vortices in the early wake of vibrating circular cylinders. Master's Thesis, University of California, Berkeley, CA, USA.

Mansy, H., Yang, P.-M., Williams, D.R., 1994. Quantitative measurements of three-dimensional structures in the wake of a circular cylinder. Journal of Fluid Mechanics 270, 227–296.

Marcollo, H., Hinwood, J.B., 2002. Vortex-induced-vibration of a long flexible cylinder in uniform flow with both forcing and response. Conference on Bluff Body Wakes and Vortex-Induced-Vibrations (BBVIV3), Port Douglas, Australia.

Marris, A.W., Brown, O.G., 1963. Hydrodynamically excited vibrations of cantilever-supported probes. ASME Paper No. 62, Hyd-7.

Masri, F., Caughey, T.K., 1979. A non-parametric identification technique for non-linear dynamic problems. Journal of Applied Mechanics 46, 433–447.

Maull, D.J., Milliner, M.G., 1979. The forces on a circular cylinder having a complex periodic motion. In: Shaw, T.L. (Ed.), Mechanics of Wave-Induced Forces on Cylinders. Pitman, London, pp. 490–502.

Mei, V.C., Currie, I.G., 1969. Flow separation on a vibrating cylinder. Physics of Fluids 12, 2248–2254.

Meier-Windhorst, A., 1939. Flarterschwingungen von Zylindern in gleichmassigen Flussingkeirssrom. Mitteilungen des hydraulischen Instituts der Technischen Hochschule, München, Heft 9, 3–39.

Meneghini, J.R., Saltara, F., Fregonesi, R.A., Yamamoto, C.T., Ferrari Jr., J.A., 2002. Numerical simulations of VIV on long flexible cylinders immersed in complex flow fields. Conference on Bluff Body Wakes and Vortex-Induced Vibrations (BBVIV3), 17–20 December, Port Douglas, Australia.

Mercier, J.A., 1973. Large amplitude oscillations of a circular cylinder in a low-speed stream. Ph.D. Thesis, Stevens Institute of Technology, Hoboken, NJ, USA.

Meskell, C., Fitzpatrick, J.A., Rice, H.J., 2001. Application of force-state mapping to a non-linear fluid elastic system. Mechanical Systems and Signal Processing 15, 75–85.

Michelassi, V., Wissink, J.G., Fröhlich, J., Rodi, W., 2003. Large-eddy simulation of flow around low-pressure turbine blade with incoming wakes. AIAA Journal 41, 2143–2156.

Moe, G., Wu, Z.-J., 1990. The lift force on a cylinder vibrating in a current. ASME Journal of Offshore Mechanics and Arctic Engineering 112, 297–303.

Moe, G., Holden, K., Yttervoll, P.O., 1994. Motion of spring supported cylinders in subcritical and critical water flows. Proceedings of the Fourth International Offshore and Polar Engineering Conference 3, Osaka, Japan, pp. 468–475.

Molin, B., 2002. Hydrodynamique des Structures Offshore. Editions Technip, Paris, 2002.

Morison, J.R., O'Brien, M.P., Johnson, J.W., Schaaf, S.A., 1950. The force exerted by surface waves on piles. Petroleum Transactions. AIME 189, 149–154.

Naudascher, E., Rockwell, D., 1994. Flow-Induced Vibrations. An Engineering Guide. A.A. Balkema, Rotterdam.

Nedergaard, H., Ottesen Hansen, N.-E., Fines, S., 1994. Response of free hanging tethers. In: Proceedings of the Seventh International Conference on Behaviour of Offshore Structures, Boston, MA, pp. 315–326.

Newman, D.J., Karniadakis, G.E., 1997. Simulations of flow past a freely vibrating cable. Journal of Fluid Mechanics 344, 95–136.

Norberg, C., 2003. Fluctuating lift on a circular cylinder: review and new measurements. Journal of Fluids and Structures 17, 57–96.

Novak, M., Tanaka, H., 1975. Pressure correlations on a vibrating cylinder. In: Eaton, K.J. (Ed.), Proceedings of the Fourth International Conference on Wind Effects on Buildings and Structures. Cambridge University Press, Cambridge, pp. 227–232, 273.

Okajima, A., Nagamori, T., Matsunaga, F., Kiwata, T., 1999. Some experiments on flow-induced vibration of a circular cylinder with surface roughness. Journal of Fluids and Structures 13, 853–864.

Okajima, A., Nakamura, A., Kosugi, T., Uchida, H., 2002. Flow-induced in-line oscillation of a circular cylinder. Conference on Bluff Body Wakes and Vortex-Induced Vibrations, (BBVIV3), Port Douglas, Australia.

Olinger, D.J., Sreenivasan, K.R., 1988. Nonlinear dynamics of the wake of an oscillating cylinder. Physical Review Letters 60, 797–800.

Öngören, A., Rockwell, D., 1988a. Flow structure from an oscillating cylinder. Part 1. Mechanisms of phase shift and recovery in the near wake. Journal of Fluid Mechanics 191, 197–223.

Öngören, A., Rockwell, D., 1988b. Flow structure from an oscillating cylinder. Part 2. Mode competition in the near wake. Journal of Fluid Mechanics 191, 225–245.

Pantazopoulos, M.S., 1994. Vortex-Induced Vibration Parameters: Critical Review of the 13th International Conference on Offshore Mechanics and Arctic Engineering, Vol. 1, pp. 199–255.

Parkinson, G.V., 1974. Mathematical models of flow-induced vibrations of bluff bodies. In: Naudascher, E. (Ed.), Flow-Induced Structural Vibrations. Springer, Berlin, pp. 81–127.

Parkinson, G.V., 1989. Phenomena and modeling of flow-induced vibrations of bluff bodies. Progress in Aerospace Sciences 26, 169–224.

Patrikalakis, N.M., Chryssostomidis, C., 1986. Vortex induced response of a flexible cylinder in a sheared current. ASME Journal of Energy Resources Technology 108, 59–64.
Pesce, C.P., Fujarra, A.L.C., 2000. Vortex-induced vibrations and jump phenomenon: experiments with a clamped flexible cylinder in water. International Journal of Offshore Polar Engineering 10, 26–33.
Protos, A., Goldschmidt, V.W., Toebes, G.H., 1968. Hydroelastic forces on bluff cylinders. ASME Journal of Basic Engineering 90, 378–386.
Ramberg, S.E., Griffin, O.M., 1976. The effects of vortex coherence, spacing and circulation on the flow-induced forces on vibrating cables and bluff structures. Report 7945, Naval Research Laboratory, Washington, DC.
Raudkivi, A.J., Small, A.F., 1974. Hydroelastic excitation of cylinders. Journal of Hydraulic Research 12, 99–131.
Riecke, E., 1888. Notes on hydrodynamics. Nachrichten der Akademie der Wissenschaften in Göttingen. II, Mathematisch-Physikalische Klasse, pp. 347–450 (in German).
Rodriguez, O., Pruvost, J., 2000. Wakes of an oscillating cylinder. IUTAM Symposium, June 13–16, Marseille, France.
Roshko, A.L., 1961. Experiments on the flow past a circular cylinder at very high Reynolds number. Journal of Fluid Mechanics 10, 345–356.
Sainsbury, R.N., King, R., 1971. The flow induced oscillation of marine structures. Proceedings of the Institution of Civil Engineers 49, 269–302.
Saltara, F., Meneghini, J.R., Siqueira, C.R., Bearman, P.W., 1998. The simulation of vortex shedding from an oscillating circular cylinder with turbulence modeling. FEDSM98-5189 in CD-ROM from ASME.
Sarkar, A., Païdoussis, M.P., 2003. A compact limit-cycle oscillation model of a cantilever conveying fluid. Journal of Fluids and Structures 17, 525–539.
Sarpkaya, T., 1963. Lift, drag and added mass coefficients for a circular cylinder immersed in a time-dependent flow. Journal of Applied Mechanics 30, 13–18.
Sarpkaya, T., 1976a. Vortex shedding and resistance in harmonic flow about smooth and rough circular cylinders at high Reynolds numbers. Technical Report No: NPS-59SL76021, Naval Postgraduate School, Monterey, CA, USA.
Sarpkaya, T., 1976b. In-line and transverse forces on smooth and sand-roughened cylinders in oscillatory flow at high Reynolds number. Naval Postgraduate School Technical Report No: NPS-69L76062, Monterey, CA, USA.
Sarpkaya, T., 1977a. In-line and transverse forces on cylinders in oscillatory flow at high Reynolds numbers. Journal of Ship Research 21, 200–216.
Sarpkaya, T., 1977b. Transverse oscillations of a circular cylinder in uniform flow. Part 1. Technical Report NPS-69SL77071, Naval Postgraduate School, Monterey, CA, USA.
Sarpkaya, T., 1978. Fluid forces on oscillating cylinders. Journal of Waterway Port Coastal and Ocean Division ASCE, WW4, 104 (WW4), 275–290.
Sarpkaya, T., 1979. Vortex-induced oscillations, a selective review. Journal of Applied Mechanics 46, 241–258.
Sarpkaya, T., 1981. Morison's equation and the wave forces on offshore structures. Technical Report CR 82 008, Naval Civil Engineering Laboratory, Department of the Navy, Port Hueneme, CA, USA.
Sarpkaya, T., 1985. Past progress and outstanding problems in time-dependent flows about ocean structures. Proceedings of the International Symposium on Separated Flow Around Marine Structures, Norwegian Institute of Technology, Trondheim, Norway, pp. 1–36.
Sarpkaya, T., 1986a. In-line transverse forces on smooth and rough cylinder in oscillatory flow at high Reynolds numbers. Technical Report No. NPS-69-86-003, Naval Postgraduate School, Monterey, CA, USA.
Sarpkaya, T., 1986b. Force on a circular cylinder in viscous oscillatory flow at low Keulegan-Carpenter numbers. Journal of Fluid Mechanics 165, 61–71.
Sarpkaya, T., 1987. Oscillating flow about smooth and rough cylinders. Proceedings of the Sixth International Offshore Mechanics and Arctic Engineering Symposium, Houston, TX, USA, pp. 113–121.
Sarpkaya, T., 1989. Computational methods with vortices—the 1988 Freeman Scholar Lecture. ASME Journal of Fluids Engineering 111, 5–51.
Sarpkaya, T., 1991. Non-impulsively started steady flow about a circular cylinder. AIAA Journal 29, 1283–1289.
Sarpkaya, T., 1994. Unsteady flows: a selective review. In: Schetz, J.A. (Ed.), Handbook of Fluid Dynamics. McGraw-Hill, New York, USA.
Sarpkaya, T., 1995. Hydrodynamic damping, flow-induced oscillations, and biharmonic response. ASME Journal of Offshore Mechanics and Arctic Engineering 117, 232–238.
Sarpkaya, T., 1996a. Unsteady flows. In: Schetz, J.A., Fuhs, A.E. (Eds.), Handbook of Fluid Dynamics and Fluid Machinery, Vol. 1. Wiley, New York, pp. 697–732.
Sarpkaya, T., 1996b. Interaction of vorticity, free-surface, and surfactants. Annual Review of Fluid Mechanics 28, 83–128.
Sarpkaya, T., 1997. Discussion of "Dynamics of a hydroelastic cylinder with very low mass and damping" (by A. Khalak, C.H.K. Williamson). Journal of Fluids and Structures 11, 549–552.
Sarpkaya, T., 2000. Resistance in unsteady flow: search for an in-line force model. International Journal of Offshore and Polar Engineering 10, 249–254.
Sarpkaya, T., 2001. On the force decompositions of Lighthill and Morrison. Journal of Fluids and Structures 15, 227–233.
Sarpkaya, T., 2002. Taylor–Gortler instability and separation on a cylinder in sinusoidally oscillating flow. Proceedings of the IUTAM Symposium on Unsteady Flows, Toulouse, France.

Sarpkaya, T., 2004. Fluid forces on oscillating cylinders at various Reynolds numbers (2.5×10^3, 7.5×10^3, 12.5×10^3, 15×10^3, 20×10^3, and 45×10^3). Technical Report (in preparation).

Sarpkaya, T., Butterworth, W., 1992. Separation points on a cylinder in oscillating flow. Journal of Offshore Mechanics and Arctic Engineering 114, 28–35.

Sarpkaya, T., Shoaff, R.L., 1979. A discrete-vortex analysis of flow about stationary and transversely oscillating circular cylinders. Technical Report NPS-69SL79011, Naval Postgraduate School, Monterey, CA, USA.

Schewe, G., 1983. On the force fluctuations acting on a circular cylinder in cross-flow from subcritical up to transcritical Reynolds numbers. Journal of Fluid Mechanics 133, 265–285.

Shih, W.C.L., Wang, W.C.L., Coles, D., Roshko, A., 1992. Experiments on flow past rough circular cylinders at large Reynolds numbers. Second International Colloquium on Bluff Body Aerodynamics and Applications, December 7–10, Melbourne, Australia.

Skomedal, N.G., Teigen, P., Vada, T., 1989. Computation of vortex induced vibration and the effect of correlation on circular cylinders in oscillatory flow. In: Proceedings of the Eighth International Conference on Offshore Mechanics and Arctic Engineering, Vol. 11, The Hague, The Netherlands, pp. 327–334.

Skop, R.A., Balasubramanian, S., 1997. A new twist on an old model for vortex-exited vibrations. Journal of Fluid and Structures 11, 395–412.

Stansby, P.K., 1976. The locking-on if vortex shedding due to the cross-stream vibration of circular cylinders in uniform and shear flows. Journal of Fluid Mechanics 74, 641–665.

Staubli, T., 1983. Calculation of the vibration of an elastically mounted cylinder using experimental data from forced oscillation. ASME Journal of Fluids Engineering 105, 225–229.

Stokes, G.G., (Sir) 1851. On the effect of the internal friction of fluids on the motion of pendulums. Transactions of the Cambridge Philosophical Society 9, 8–106.

Sugimoto, T., Saito, S., Matsuda, K., Okajima, A., Kiwata, T., Kosugi, T., 2002. Water tunnel experiments on in-line oscillation of a circular cylinder with a finite span length. Conference on Bluff Body Wakes and Vortex-Induced Vibrations, (BBVIV3), Port Douglas, Australia.

Sumer, B.M., Fredsøe, J., 1988. Transverse vibrations of an elastically mounted cylinder exposed to an oscillating flow. ASME Journal of Offshore Mechanics and Arctic Engineering 110, 387–394.

Sumer, B.M., Fredsøe, J., 1997. Hydrodynamics around Cylindrical Structures. World Scientific, Singapore.

Taylor, G.I., 1928a. The energy of a body moving in an infinite fluid, with an application to airships. Proceedings of the Royal Society of London A 120, 13–20.

Taylor, G.I., 1928b. The forces on a body placed in a curved or converging stream of fluid. Proceedings of the Royal Society of London A 120, 260–283.

Toebes, G.H., 1969. The unsteady flow and wake near an oscillating cylinder. Journal of Basic Engineering 91, 493–502.

Triantafyllou, M.S., Grosenbaugh, M.A., 1995. Prediction of vortex-induced vibrations in sheared flows. In: Proceedings of the Sixth International Conference on Flow-induced Vibrations. A. A. Balkema, Rotterdam, pp. 73–82.

Triantafyllou, M.S., Gopalkrishnan, R., Grosenbaugh, M.A., 1994. Vortex-induced vibrations in a sheared flow: a new predictive method. In: Proceedings of the International Conference on Hydroelasticity in Marine Technology, Trondheim, Norway, pp. 31–34.

Triantafyllou, M.S., Techet, A.H., Hover, F.S., Yue, D.K.P., 2003. VIV of slender structures in shear flow. Presented at IUTAM Symposium on Flow-Structure Interactions, June 2003, Rutgers State University, USA.

Tutar, M., Holdo, A.E., 2000. Large eddy simulation of a smooth circular cylinder oscillating normal to a uniform flow. ASME Journal of Fluids Engineering 122, 694–702.

Ünal, F., Rockwell, D., 1988. Vortex formation from a cylinder: Part I—the initial instability, and Part II—control by wake interference. Journal of Fluid Mechanics 190, 491–512.

Vandiver, J.K., 1993. Dimensionless parameters important to the prediction of vortex-induced vibration of long, flexible cylinders in ocean currents. Journal of Fluids and Structures 7, 423–455.

Vandiver, J.K., Jong, J.-Y., 1987. The relationship between in-line and cross-flow vortex-induced vibration of cylinders. Journal of Fluids and Structures 1, 381–399.

Vandiver, J.K., Li, L., 1994. SHEAR7 Program Theoretical Manual. Department of Ocean Engineering, MIT, Cambridge, MA, USA.

Vandiver, J.K., Li, L., Venogupal, M., 1993. SHEAR Program Theoretical Manual. Department of Ocean Engineering, MIT, Cambridge, MA, USA.

Vickery, B.J., Watkins, R.D., 1962. Flow-induced vibration of cylindrical structures. Proceedings of the First Australian Conference on Hydraulics and Fluid Mechanics.

Vikestad, K., 1992. Dynamic response of risers in sheared current using cross-correlated excitation and the finite element method. Master's Thesis, University of Trondheim, Norway.

Vikestad, K., Vandiver, J.K., Larsen, C.M., 2000. Added mass and oscillation frequency for a circular cylinder subjected to vortex-induced vibrations and external disturbance. Journal of Fluids and Structures 14, 1071–1088.

Voorhees, A., Wei, T., 2002. Three-dimensionality in the wake of a surface piercing cylinder mounted as an inverted pendulum. Conference on Bluff Body Wakes and Vortex-Induced Vibration (BBV1V3), Port Douglas, Australia, 17–20 December 2002, 4pp.

Wei, T., Smith, C.R., 1986. Secondary vortices in the wake of circular cylinders. Journal of Fluid Mechanics 169, 513–533.

Williamson, C.H.K., 2003. Personal communication on 04/02/03.
Williamson, C.H.K., Roshko, A., 1988. Vortex formation in the wake of an oscillating cylinder. Journal of Fluids and Structures 2, 355–381.
Wu, Z.-J., 1989. Current induced vibrations of a flexible cylinder. Ph.D. Thesis, Civil Engineering, The Norwegian Institute of Technology, Trondheim, Norway.
Zdravkovich, M.M., 1981. Review and classification of various aerodynamic and hydrodynamic means for suppressing vortex shedding. Journal of Wind Engineering and Industrial Aerodynamics 7, 145–189.
Zdravkovich, M.M., 1982. Modification of vortex shedding in the synchronization range. ASME Journal of Fluids Engineering 104, 513–517.
Zdravkovich, M.M., 1990. On origins of hysteretic responses of a circular cylinder induced by vortex shedding. Zeitschrift für Flugwissenchaft und Weltraumforschung 14, 47–58.
Zdravkovich, M.M., 1996. Different modes of vortex shedding: an overview. Journal of Fluids and Structures 10, 427–437.
Zdravkovich, M.M., 1997. Flow Around Circular Cylinders, Vol. 1: Fundamentals. Oxford University Press, Oxford, England.
Zdravkovich, M.M., 2003. Flow Around Circular Cylinders, Vol. 2: Applications. Oxford University Press, Oxford, England.
Zhang, J., Dalton, C., 1996. Interaction of vortex-induced vibration of a circular cylinder and a steady approach flow at a Reynolds number of 13,000. Computers and Fluids 25, 283–294.
Zhang, M.M., Zhou, Y., Cheng, L., 2003. Spring-supported cylinder wake control. AIAA Journal 41 (8), 1500–1506.
Zhou, C.Y., So, R.M., Lam, K., 1999. Vortex-induced vibrations of elastic circular cylinders. Journal of Fluids and Structures 13, 165–189.
Ziada, S., Staubli, T., 2000. Flow-Induced Vibration. A.A. Balkema, Rotterdam.